ONBOARD ANTENNA SUBSYSTEM OF IITMSAT TO IITM

A THESIS
submitted by

T Rajavardhan

for the award of the degree

of

Master of Technology

DEPARTMENT OF ELECTRICAL ENGINEERING
INDIAN INSTITUTE OF TECHNOLOGY MADRAS
MAY 2014

THESIS CERTIFICATE

This is to certify that the thesis titled **ONBOARD ANTENNA SUBSYSTEM OF IITMSAT**, submitted by **T Rajavardhan**, to the Indian Institute o Technology, Madras, for the award of the degree of **Master of Technology**, is a bona fide record of the research work done by him under my supervision. The contents of this thesis, in full or in parts, have not been submitted to any other Institute of University for the award of any degree of diploma.

Dr Harishankar Ramachandran

Project Guide

Professor and Head

Dept. of Electrical Engineering

IIT-Madras

Place: Chennai - 600036

Date : $6^{th}\, May\, 2014$

Contents

List of Figures

Acknowledgments

I am fortunate and also lucky to work with Prof Harishankar Ramachandran for this project (IITMSAT). It was a very rich experience working with him. His positive approach and warmth he exudes are always inspiring and make us comfortable. I would feel happy every time I met him. There are numerous incidents where he forgived me for my mistakes. I am grateful to him for guiding through this project.

I should thank my senior Mr. Shahul Hameed Ansari, who patiently taught me to use the software Ansys HFSS and shared important information and still providing his worthful suggestions for the project.

Sincere thanks to Mr. Akshay Gulati, Project officer, IITMSAT for the encouragement he gave throughout the period. He helped me understand different subsystems of the satellite project and their effect on antenna subsystem and vice versa.

Sincer thanks Shri Mukundan KK and Shri Satyabhushan Shukla, Scientists from VSSC, Trivandrum for their kind permission and co-operation for measuring the gain patterns of the antennas. I am grateful to the technical staff at VSSC, who assisted in the process. Special mention of Mr. Suresh S, Project officer, IITMSAT and Mr. Sakthivel K for spending their valuable time in supervising the measurement process at VSSC and helping in the process.

Sincere thanks to Prof Amitava DasGupta and group for kindly giving the permission to the utilize the Ansys HFSS license. Also sincere thanks to Prof Ananthkrishan and group for kindly sharing the lincense of CST microwave studio.

Abstract

IITMSAT project requires the design for the onboard antennas. This was done by Shahul Hameed Ansari [2]. This document presents the improvized antennas designed.

The IITMSAT requires an onboard antenna system with constraints of sturctural rigidity, near omni-directional radiation pattern and minimum losses. The designed Tx antennas are 'F-antennas'. A brief picture of theretical understanding of them presented.

The design of the Rx antenna (VHF - 145 MHz) posed a challenge as the size of the satellite is less than wavelength. It was the decision of the team not to have deployable antenna as it increases the complexity of various systems. Hence a rigid antenna within the size contraints was required.

The radiation pattern of the antenna for linear polarizations were measured at VSSC, Trivandrum. Selected results are presented here.

1. Introduction

IITMSAT is a student-built nano-satellite mission of Indian Institute of Technology Madras, Chennai, India. The objective is to study the precipitation of high energy electrons and protons to 600-900 km altitude from Van-Allen radiation belt due to resonance interaction with low frequency EM waves. The unique design of IITMSAT evolves from the challenging design requirements posed by the mission and the satellite's payload, Space based Proton and Electron Energy Detector (SPEED). [3].

IITMSAT is a 15 kg satellite of a form factor of 29 x 29 x 27 cm that includes a large and heavy payload of 7kg with a volume of 27 x 27 x 13 cm.

1.1. Challenges of Antenna design for small satellites[1]

The establishment of a telecommunication uplink and downlink capability is one of the major challenges that the design team of small satellites face, due to severe restrictions on weight, power and accomodation; for these reasons, UHF and VHF bands are preferred in many applications.

The main challenges in designing antennas for small satellites include:

1. Antennas must be highly reliable, as it is not possible to replace the antennas in space.
2. Antennas must be mechanically robust, and able to survive both random vibration and shock during the launch.
3. As the antennas are fitted on a small platform, EMC and mutual coupling amongst these antennas, the payloads, and circuits need to be carefully considered.
4. The small-satellite structure should be taken into account as its size is comparable to wavelength of antenna operation. The structure can cause electromagnetic scattering and interfere with the antenna's radiation pattern.
5. The radiation pattern is also affected by adjacent antennas, cameras, booms, sun sensors, and solar panels.
6. The polarization requirements on the antennas also need be taken into account.

7. The thermal design of the antennas must be carefully evaluated. The antennas are designed to perform over a wide temperature variation, typically from $-150°$ C to $+150°$ C.

1.2. Antenna for small satellites[1]

The design of a small satellite antenna starts with the mission requirements and the link budget. The quantity of data produced by the payloads, the needs for separate telemetry, tracking and command links are investigated. The bulk of the payload data, the transmission rate, the freqency of operation along with available satellite power for communications helps to define the gain required of the antenna.For telemetry, tracking and command antennas, the key requirements are omnidirectional coverage, with associated low gain.

For small satellite without adequate attitude control systems, omnidirectional or wide coverage antennas are required. Sometimes, more than two such antennas are mounted on different sides of the satellite, to provide better coverage for the telemetry, tracking and command link, as well as redundancy.

Various monopole antennas, PIFAs, microstrip-patch antennas, helics, and patch-exicted cup antennas, have been developed for the UHF , VHF, S, C and X bands. These antennas are simple, easy to fabricate, and have wide radiation-pattern coverage; thus the satellite does not need accurate control of attitude.

Pictures of different antennas designed for small satellites can be found in [1].

Most of the cubesats have custom designed antennas. In most of the cases the antennas are monopoles or dipoles[4].

1.3. Antennas for Cubesats

Most of the cubesats have custom designed antennas. In most of the cases the antennas are monopoles or dipoles[4].

1.4. Satellite Orbit

Low Earth Orbit (LEO)

It is just above the Earth's atmosphere, where there is almost no air to cause drag on the satellite and reduce is speed. The Hubble Space Telescope, for example, operates at an altitude of about $610\,km$ with an orbital period of 97 minutes. LEO altitudes are limited by Van Allen radiation effects (sensors, integrated circuits and

solar cells can be damaged by this radiation). Satellites in these orbits have an orbital period of around (90-110) minutes.

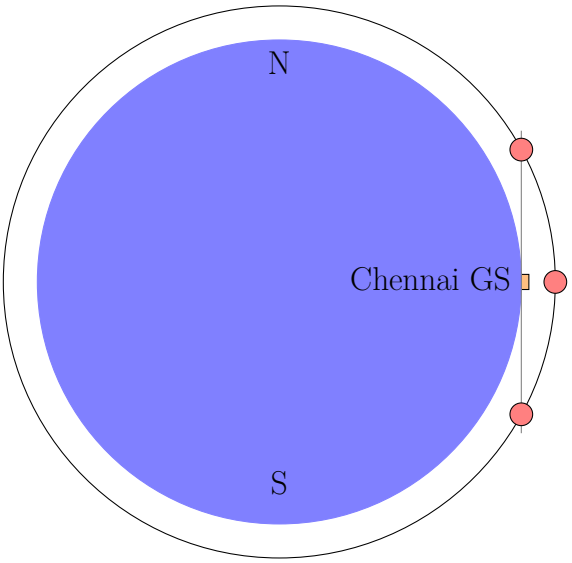

Figure 1.1.: Satellite in LEO orbit

1.5. Subsystems

IITMSAT encompasses many subsystems,

- Attitude Control System (ACS)
- Communication System (COM)
- Electrical Power System (EPS)
- Payload and related electronics
- Command and Data Management System (CDMS)
- Structure and Mechanisms (SAM)
- Thermal Control System (TCS)

Among these predominantly the ACS and SAM dictates the antenna properties.

The basic structure of the IITMSAT is a metallic cube of side $300\,mm$ approximately made of aluminium. This structure size is comparable to the wavelengths of operation given in the table.

Onboard	frequency	wavelength	Quarter wavelength
Tx	$435\,MHz$	$690\,mm$	$172.5\,mm$
Rx	$145\,MHz$	$2070\,mm$	$517.2\,mm$

Table 1.1.: Tentative Tx and Rx frequencies

Hence the structure as whole needs to be considered for the antenna design.

1.6. Constraints on Antenna Design of IITMSAT

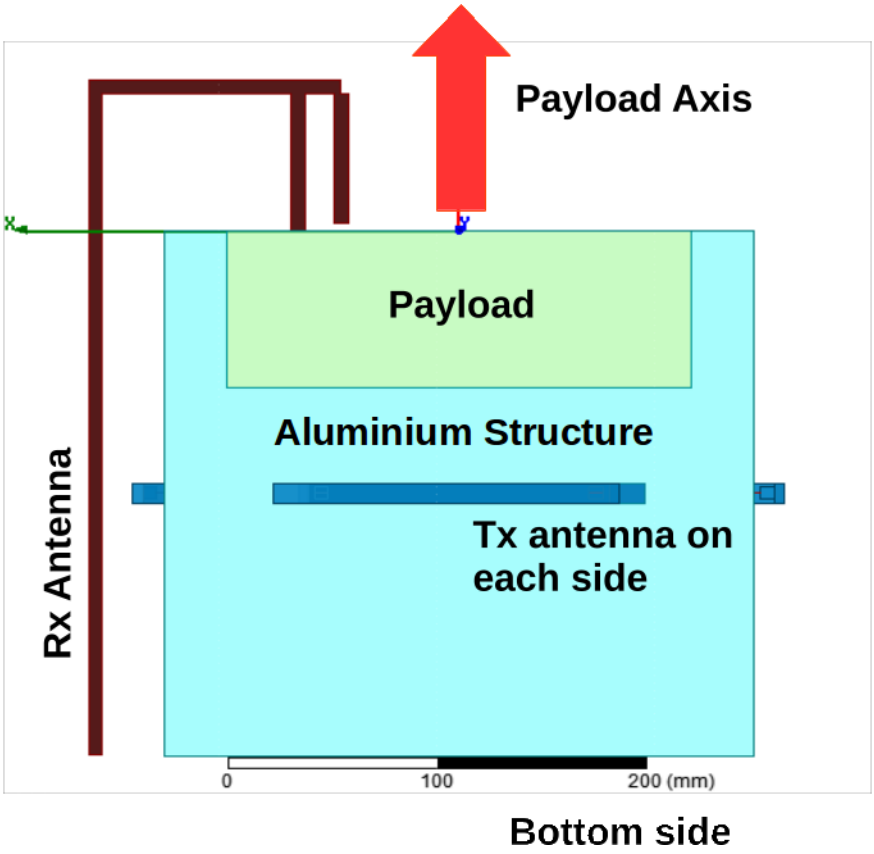

Figure 1.2.: Satellite structure description

Fig. 1.2 shows the antenna structure with the antennas. The body is an aluminium structure. The payload is considered as a dielectric. The axis perpendicular to the payload is termed as payload axis in this document.

- The ACS of thte IITMSAT is being designed to have control only along *two* axes due to power and space limitations of the satellite. The payload of the satellite, SPEED, has the requirement of its detector plane perpendicular to the magnetic field lines in the orbit Fig. 1.3.
- No metallic objects be placed near the payload, which may deter the payload's performance.
- The bottom surface of the satellite will be fixed on a mechanical adaptor of the rocket for launch. There is not room on this side of the satellite for antennas.

- The payload axis should always be along the magnetic field lines as shown in Fig. 1.3.

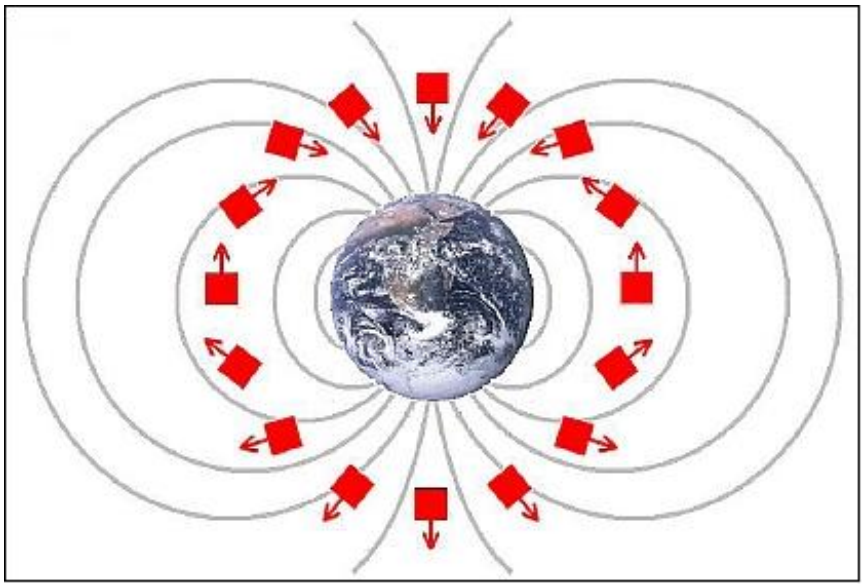

Figure 1.3.: Satellite pointing requirement

Due to this two axis attitude control the satellite is prone to rotation along the uncontrolled axis. In this case it is the axis of the payload.

These constraints lead to the requirement of omnidirectional radiation patterns for both transmitter and receiver antennas.

1.7. Gain of antenna

Gain is four π times the ratio of an antenna's radiation internsity in a given direction to the total power accepted by the antenna.

$$gain = 4\pi \frac{U}{P_{acc}}$$

where

- U is the radiation intensity in Watts per steradian in the direction specified
- $P_{acc}$is the power accepted in watts entering the antenna

The gain patterns of the antenna are presented in this thesis at different parts

1.8. Polarization Loss

1.8.1. Field Polarization in terms of LHCP and RHCP

In general field can be represented as

$\overrightarrow{E} = E_x e^{i(\phi_x - \omega t)}\hat{x} + E_y e^{i(\phi_y - \omega t)}\hat{y}$

Any wave can be decomposed into a sum of linearly polarized waves or a sum of circularly polarized waves.

$$\begin{aligned}\overrightarrow{E} &= E_x e^{i(\phi_x-\omega t)}\left(\frac{\hat{e}_R+\hat{e}_L}{\sqrt{2}}\right) + E_y e^{i(\phi_y-\omega t)}\left(\frac{\hat{e}_R-\hat{e}_L}{\sqrt{2}}\right)\\ &= \left[(E_{10}e^{i\phi_x} - iE_{20}e^{i\phi_y})\left(\frac{\hat{e}_R}{\sqrt{2}}\right) + (E_{10}e^{i\phi_x} + iE_{20}e^{i\phi_y})\left(\frac{\hat{e}_L}{\sqrt{2}}\right)\right]e^{-i\omega t}\\ &= (E_R\hat{e}_R + E_L\hat{e}_L)e^{-i\omega t}\end{aligned}$$

$$\hat{e}_{R,L} = \frac{\hat{x} \pm \hat{y}}{\sqrt{2}}$$

Cicular Polarization have properties

$$\hat{e}_L \cdot \hat{e}_R^* = 0 \text{and } \hat{e}_L \cdot \hat{e}_L^* = \hat{e}_R \cdot \hat{e}_R^* = 1$$

and where

$$\begin{aligned}E_R &= \frac{1}{\sqrt{2}}\left[E_x\cos\phi_x + E_y\sin\phi_y + i\left(E_x\sin\phi_x + E_y\cos\phi_y\right)\right]\\ &= |E_R|\, e^{i\chi_R}\end{aligned}$$

The magnitude is

$$|E_R| = \frac{1}{\sqrt{2}}\sqrt{E_x^2 + E_y^2 + 2E_xE_y\sin(\phi_y - \phi_x)}$$

and phase is

$$\tan\chi_R = \frac{E_x\sin\phi_x - E_y\cos\phi_y}{E_x\cos\phi_x + E_y\sin\phi_y}$$

similarly,

$$E_L = \frac{1}{\sqrt{2}} \left[E_x \cos\phi_x - E_y \sin\phi_y + i \left(E_x \sin\phi_x + E_y \cos\phi_y \right) \right]$$
$$= |E_R| \, e^{i\chi_R}$$

The magnitude is

$$|E_R| = \frac{1}{\sqrt{2}} \sqrt{E_x^2 + E_y^2 - 2E_x E_y \sin(\phi_y - \phi_x)}$$

and phase is

$$\tan\chi_R = \frac{E_x \sin\phi_x + E_y \cos\phi_y}{E_x \cos\phi_x - E_y \sin\phi_y}$$

1.8.2. Polarization Vector and Polarization Ratioo

- The field can be represented as

  $$\overrightarrow{E} = \hat{x} \cdot E_x + \hat{y} \cdot E_y e^{j\phi}$$

  where $\phi$is the phase difference between y and x components.

- The **polarization vector** is the normalized phasor of the electric field vector. It has direction of the electric field vector.

  $$\hat{\rho}_L = \hat{x} \cdot \frac{E_x}{E_m} + \hat{y} \cdot \frac{E_y}{E_m} e^{j\phi}$$

  where $E_m = \sqrt{E_x^2 + E_y^2}$

- **Polarization ratio** is the ratio of the complex amplitudes of the two orthogonal polarized field components. It is a complex number.

  $$r_L e^{j\phi} = \frac{E_y}{E_x} e^{j\phi}$$

- **Polarization ellipse** is the path traced by the tip of the electric field vector at a particular point in space as the wave propagates. An example of the ploarization ellipse is as shown in Fig. 1.4.

Here, the tilt angle ψ, major and minor axes can be presented as

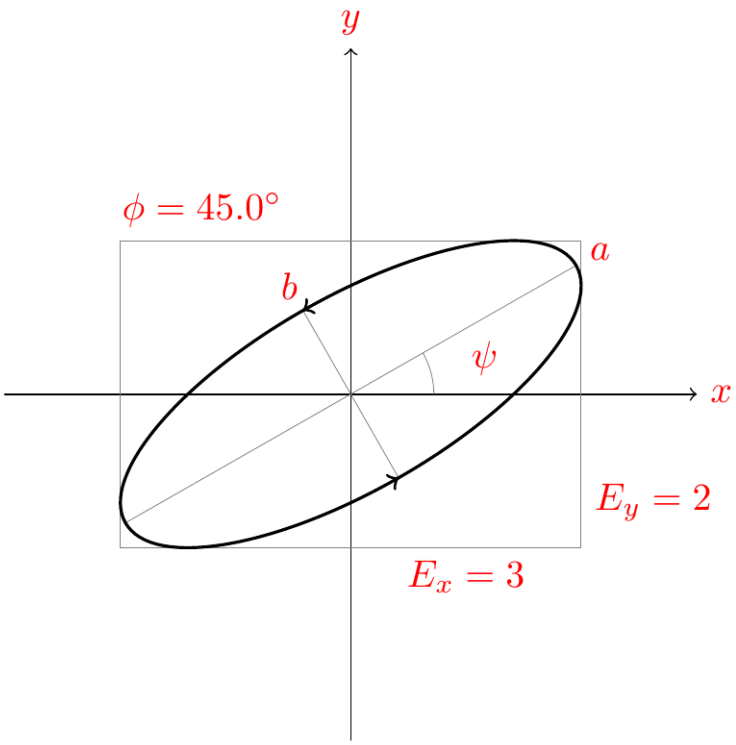

Figure 1.4.: Polarization Ellipse

$$\psi = \frac{1}{2}\arctan\left(\frac{2E_xE_y}{E_x^2 - E_y^2}\cos\phi\right)$$

$$a = 2 \times \sqrt{\frac{1}{2}\left[E_x^2 + E_y^2 + \sqrt{E_x^4 + E_y^4 + 2E_x^2E_y^2\cos(2\phi)}\right]}$$

$$b = 2 \times \sqrt{\frac{1}{2}\left[E_x^2 + E_y^2 - \sqrt{E_x^4 + E_y^4 + 2E_x^2E_y^2\cos(2\phi)}\right]}$$

- **Axial ratio** is the ratio of the major axis to the minor axis of the polarization ellipse.

$$Axial\ Ratio = \frac{a}{b}$$

1.8.3. Polarization Loss Factor

- Generally the polarization of the receiving antenna is not the same as the polarization of the incident wave. This is called polarization mismatch.
- The Polarization Loss Factor (PLF) characterizes the loss of EM power because

of polarization mismatch.$PLF = |\hat{\rho}_i \cdot \hat{\rho}_a|^2$where ρ_i represents the polarization vector of incident wave and ρ_a , the polarization vector of receiving antenna in transmitting mode.

- A transmitting antenna producing far-zone field in RHCP coupled to a receiving antenna also RHCP (in transmitting mode) do not have polarization loss.
- The Losses for LHCP and RHCP receivers for the incident wave with polarization as are

$$PLFL = 20\log_{10}\left(\left[2\left(E_x^2 + E_y^2\right)\right]^{-0.5} \times |E_x - jE_y\left(\cos\left(\phi\right) + j\sin\left(\phi\right)\right)|\right)$$

$$PLFR = 20\log_{10}\left(\left[2\left(E_x^2 + E_y^2\right)\right]^{-0.5} \times |E_x + jE_y\left(\cos\left(\phi\right) + j\sin\left(\phi\right)\right)|\right)$$

1.8.4. An example

For a wave with electric field $\overrightarrow{E} = \hat{x} \cdot 5 + \hat{y} \cdot 3\, e^{j\pi/8}$, the polarization ellipse along with the decomposed RHCP and LHCP components is shown in Fig. 1.5.

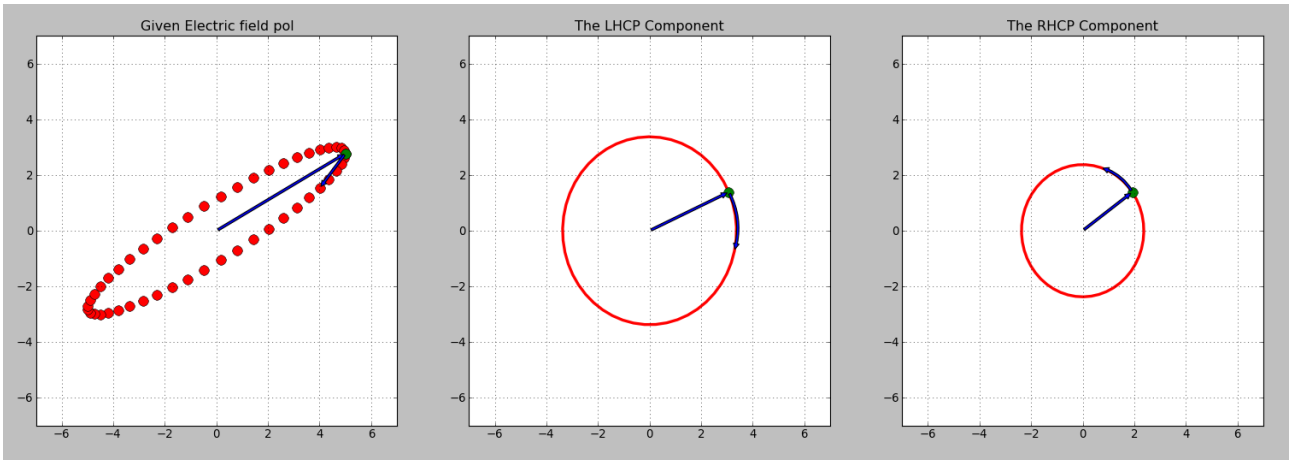

Figure 1.5.: Polarization Ellipse with LHCP and RHCP components

The polarization losses for for LHCP receiver and RHCP receiver are

$PLFL = 1.74\,dB$

$PLFR = 4.80\,dB$

$Axial\ Ratio = \frac{a}{b} = \frac{5.5}{1.92} = 2.86 = 9.1\,dB$

$Tilt\ Angle = \psi = 26.4°$

- If the incident wave is linear, then the polarization loss will be $3\,dB$ at both LHCP and RHCP receivers.

Many charts specifying the polarization losses for different combinations are available in literature [5, 6]. The Ludwig chart as in [6] with some annotations is presented in Fig. 1.6 for illustration.

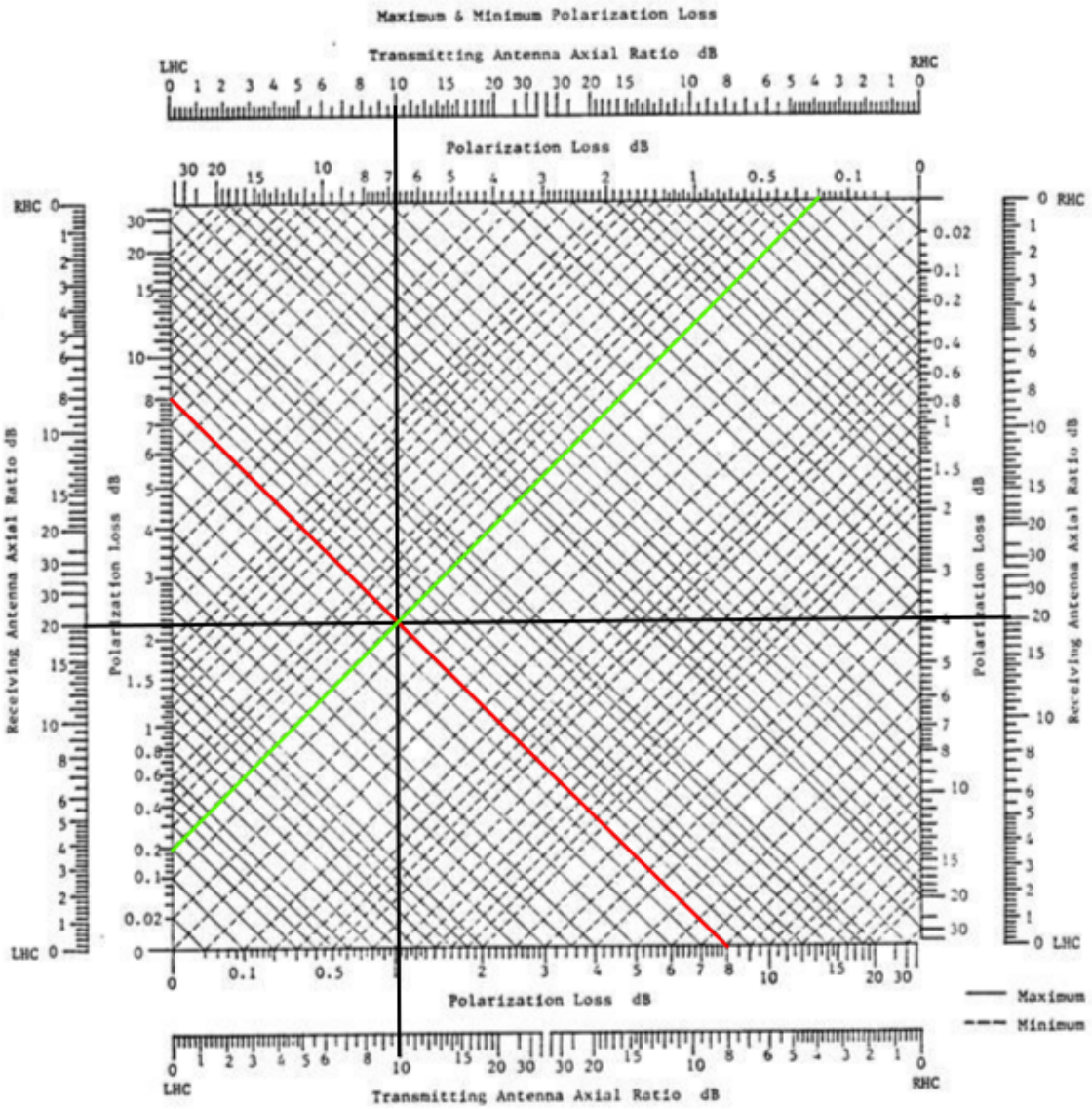

Figure 1.6.: Ludwig Chart

The annotations represent the transmitting antenna with axial ratio of $10\,dB$ and receiving antenna with axial ratio of $20\,dB$. The particular crosssection point leads to the minimum of $0.2\,dB$ and maximum of $8\,dB$ polarization losses.

2. Designed Antennas

Explain the coordinate system for radiation patterns.

2.1. Tx antennas

As per the requirement for a near omni-directional radiation pattern, four inverted F-antennas are placed on each side of the metallic structure except the top face, accomadating the payload and the bottom face as shown in Fig. 2.1, where the blue one are the Tx antennas.

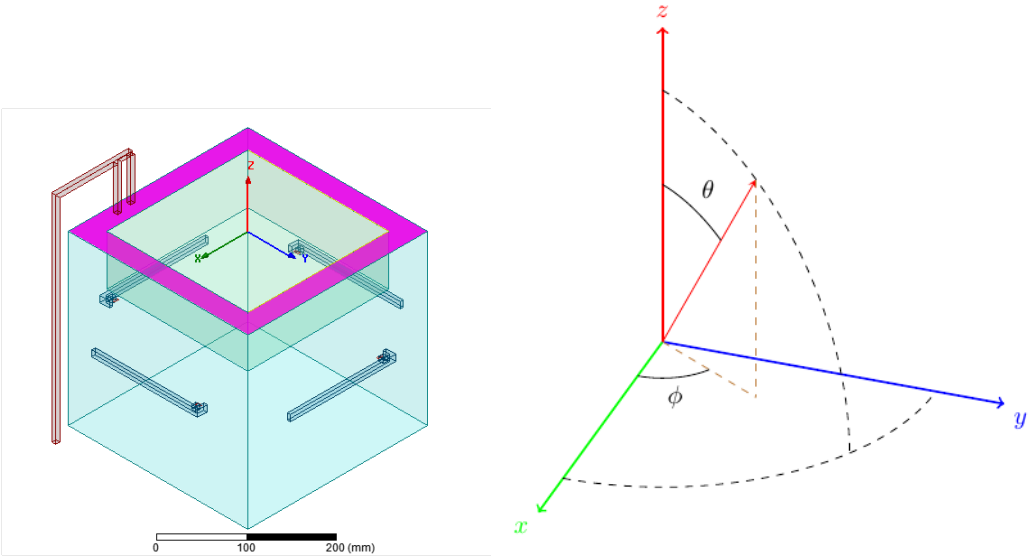

Figure 2.1.: Satellite structure with antennas in isometric view and description of the co-ordinate system

2.2. Tx antennas Return Loss Characteristics

The return loss curves of the four antennas are shown in Fig. 2.2. Though four antennas are similar, there is deviation in the return loss curves. This can be attributed to the presence of the Rx antenna in the structure.

All the four antennas have a return loss of 14 dB. This corresponds to a VSWR of 1.5 and imply that only 4% of the power is reflected back to the source.

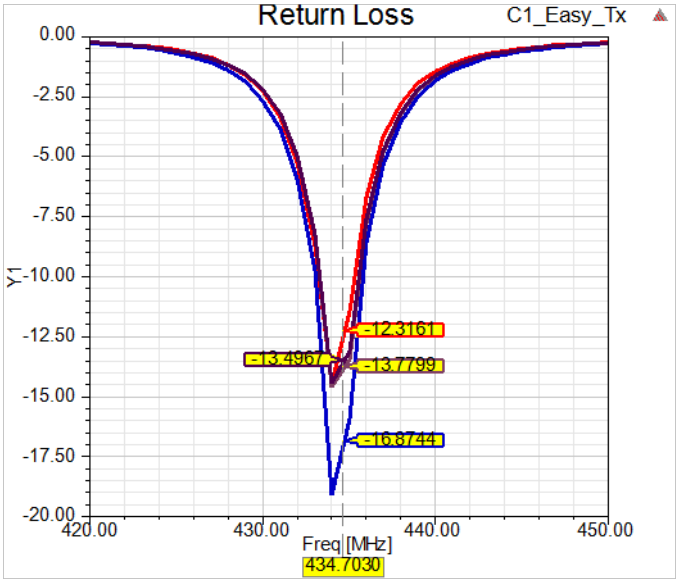

Figure 2.2.: Negative Return Loss (S_{22}) curves of 4 Tx antennas

2.3. Tx antennas gain pattern

The gain pattern of the Tx antennas is shown in Fig. 2.3.

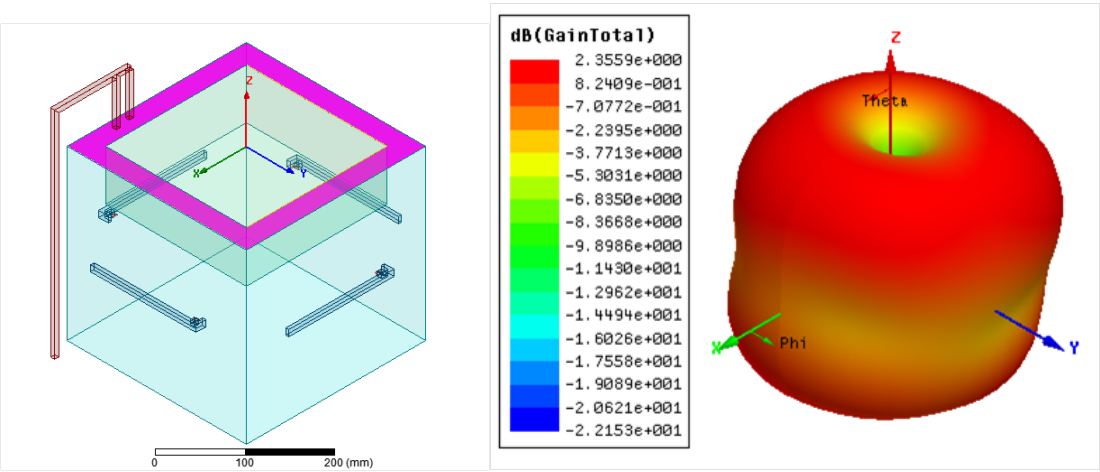

Figure 2.3.: Satellite and the Tx antenna Total_Gain pattern in isometric view

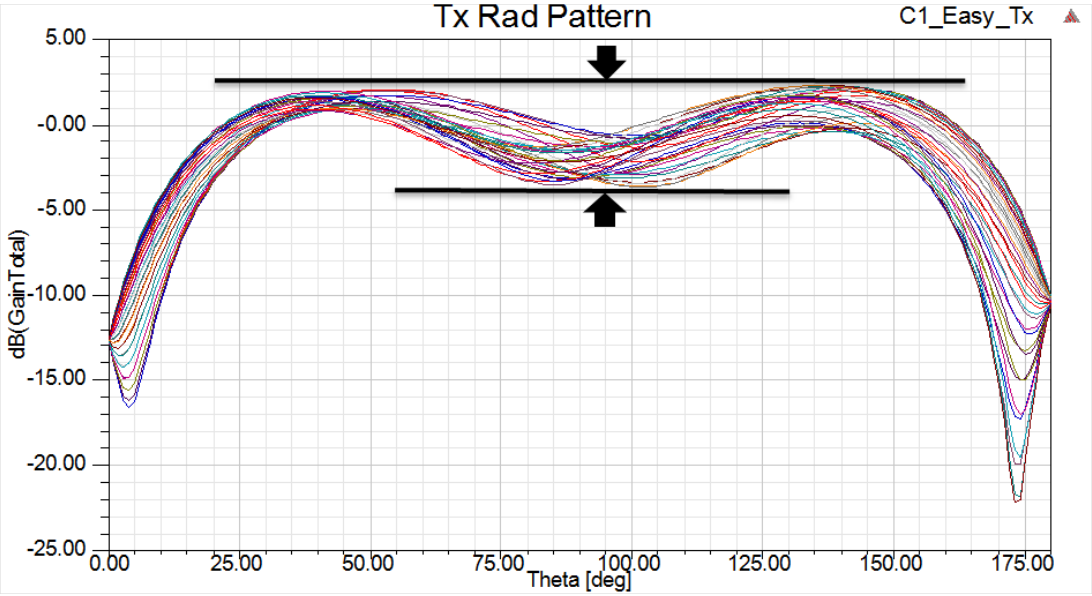

Figure 2.4.: Total_Gain pattern of the Tx antennas in rectangular plot

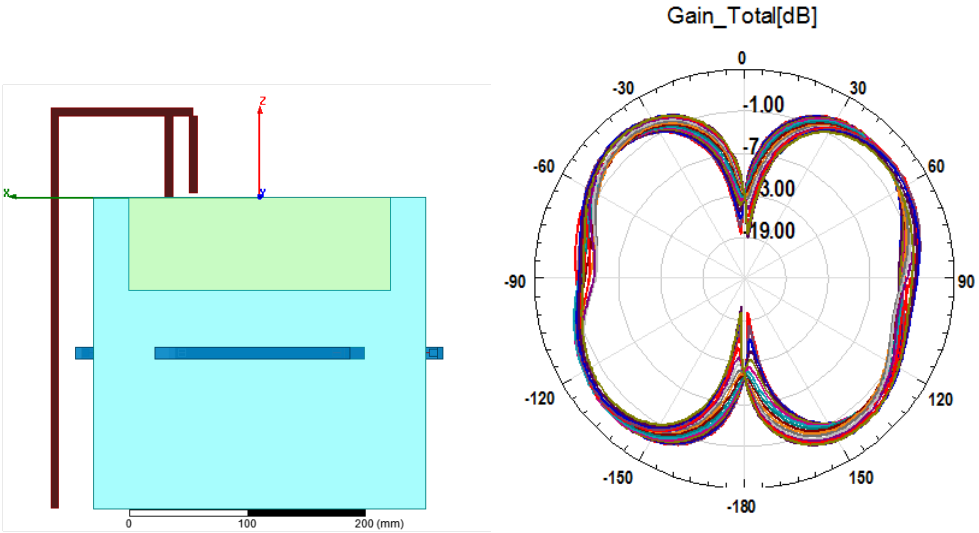

Figure 2.5.: Total_Gain pattern of the Tx antennas in polar plot

The rectangular pattern of the gain pattern is shown in Fig. 2.4 & Fig. 2.5. Each line corresponds to different ϕ in spherical co-ordinate system as shown in Fig. 2.3. These plots show the total gain pattern, and they seems to be fulfilling the requirement. But the LHCP and RHCP gain patterns lead to a different scenario as presented below.

Fig. 2.6 show that the gain pattern has different polarization in different directions, in other words a strong cross-polarization is present.

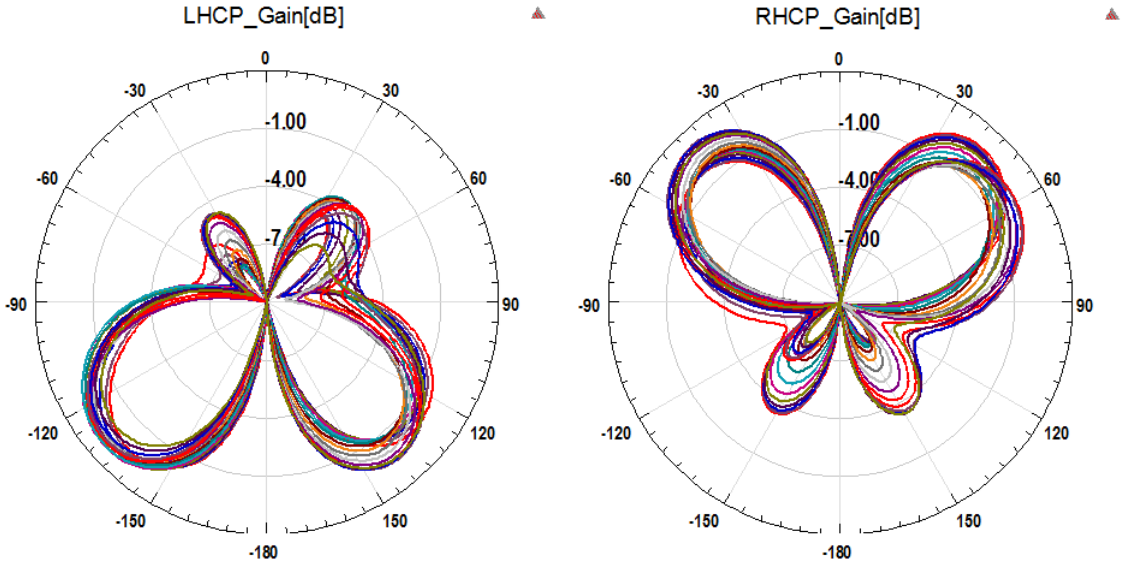

Figure 2.6.: LHCP & RHCP gain patterns of the Tx antennas in polar plot

2.3.1. Polarization Loss

The rectangular plots of the LHCP and RHCP Tx gain patterns are shown in Fig. 2.7. These plots convey the same information as that of Fig. 2.6.

The axial ratio (sec. 1.8.2) plot in Fig. 2.8 show that the gain pattern is linear arount $\theta = 90°$ and at $\theta = 0° \,\&\, 180°$. Also it tends to be elliptical in other regions. Axial ratio do not specify the sense of polarization. The actual sense of polarization is evident from Fig. 2.7. The gain pattern is lefthandedness dominated for theta 90° to 180° and lefthanded dominated for theta 0° to 90°. From these plots it is evident there is transition of polarization around $\theta = 90°$. As the sense of polarization changes along the satellite path through the ground station, Polarization Diversity System should be part of the ground station to handle this polarization change and prevent loss of communication.

Fig. 2.9 shows the polarization state at different points as the satellite passes through the ground station. Here an ideal path of the satellite with maximum elevation of 90° is chosen. The plot actually corresponds to the change in polarization in the Tx gain pattern of the satellite for θ 0° to 90° for ϕ at 90°.

Fig. 2.10 shows the polarization loss at the receiver side if antenna of same sense is employed. The maximum loss is $3\,dB$, which corresponds to linear polarization recived by circular polarized antenna.

Fig. 2.11 shows the polarization loss at the receiver side if antenna of opposite sense is employed. The minimum loss is here is $3\,dB$.

2.4. Quadrature phase inputs

The results presented in the previous sections were for the case of inputs to the four antenna were in phase. Some commercial antennas with such 4 antenna configuration are avaible which inherently provide inputs with quadrature phase inputs [7].

There can be two ways of applying the quadrature phase shifted inputs. The input types and corresponding radiation patterns are shown in Fig. 2.12Fig. 2.13. In both cases the gain patterns do not fulfill the mission requirements and hence such a configuration is not considered for IITMSAT.

2.5. Rx antenna

The VHF Rx antenna is designed to be resonant at $145\,MHz$ which corresponsds to quarter wavelength of $517\,mm$. The antenna should be compact with required radiation pattern and return loss characteristics.

After trying a many configurations, the antenna in Fig. 2.14 has been found to meet the requirements.

Here it is to be noted that, this antenna deviates from the F-antenna presented previously. The stub is on the radiating side of the antenna. This configuration gave very good return loss characteristcs.

2.6. Rx antenna gain pattern

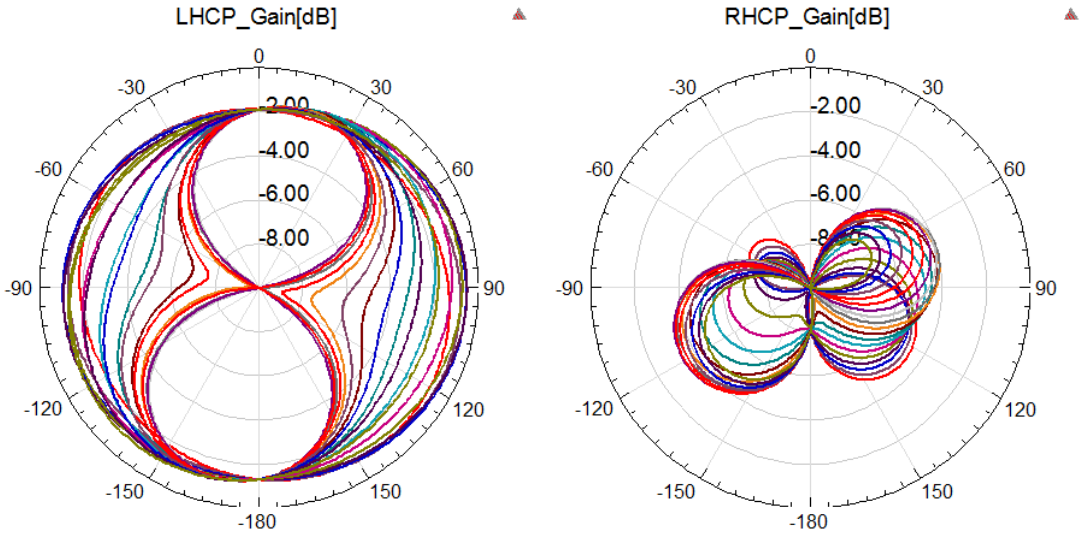

Figure 2.15.: Rx antenna LHCP and RHCP gains

The LHCP and RHCP gain patterns are shown in Fig. 2.15. These are the polar plots of the gain pattern, each line corresponds to different ϕ of spherical co-ordinate system.

It is clear from the above plots that the LHCP gain is better compared to the RHCP gain.

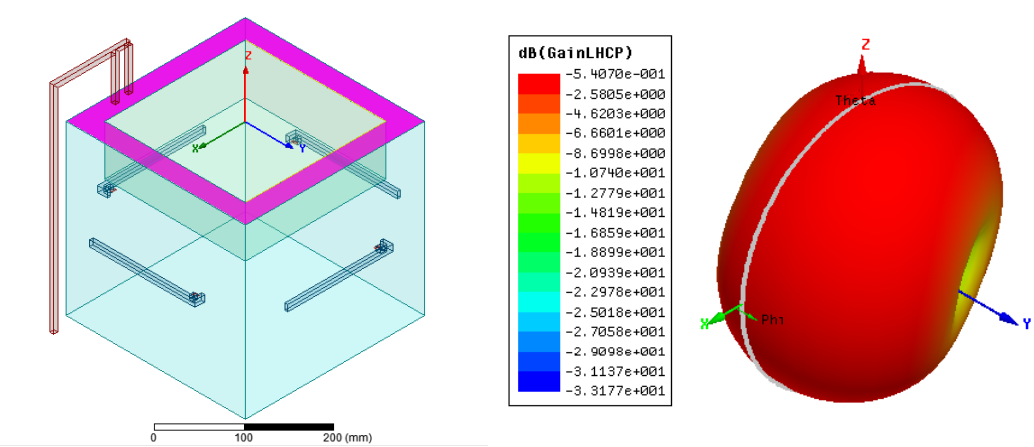

Figure 2.16.: Satellite Rx LHCP gain pattern in isometric view

The LHCP gain 3D plot along with the satellite structure is shown in Fig. 2.16.

The rectrangular plot of the LHCP gain is shown in Fig. 2.17.

2.7. Rx Return Loss characteristics

The return loss curves of the Rx antenna is shown in Fig. 2.18.

All the four antennas have a return loss of more than $25\,dB$. This corresponds to a VSWR of 1.1 and imply that only 0.3% of the power is reflected back to the source if it is used as a source.

2.8. Rx coupled to Tx

It is to be noted that when the onboard Tx communication system transmits a power of $1\,W$ $(30\,dBm)$ and Rx is bound to detect power levels of $-120\,dB$. So, there is a chance of receiver getting saturated by the power coupled from the Tx antenna to the Rx antenna.

The power that may get coupled has been arrived using HFSS and it was $16\,mW$ if $1\,W$ of power is being pumped to the Tx antennas.

This was calculated as follows. The Rx antennas was also assigned a port in the simulation for the analysis at Tx frequency of 435 MHz. From the S parameters (Rx, 4 Tx antennas), the highest being $-18\,dBm$, the power coupled would be $16\,mW$.

Fig. 2.19 shows the surface currents of the structure and antennas. The surface currents on the Rx antenna can be observed in the picture.

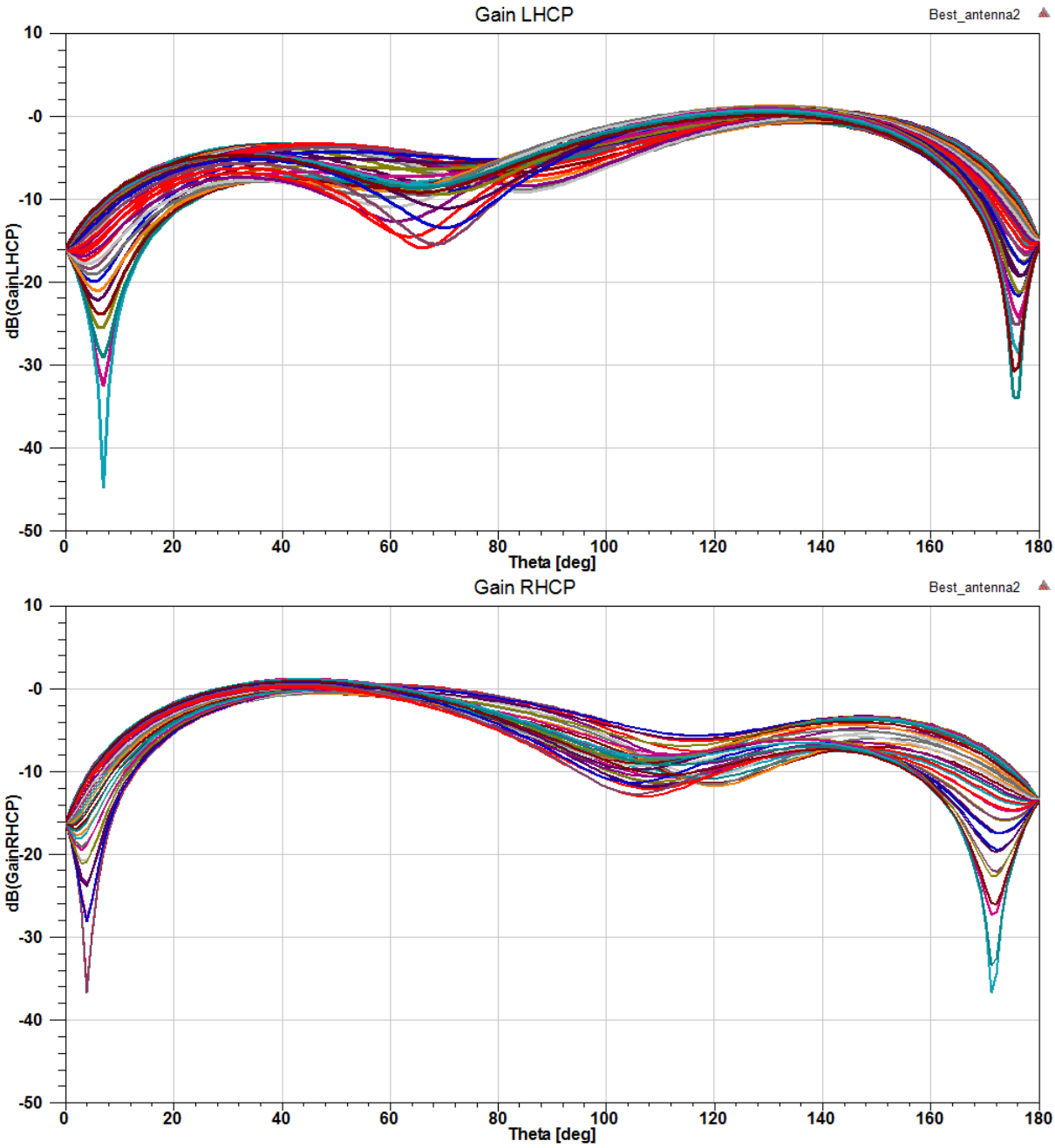

Figure 2.7.: LHCP & RHCP gain patterns of the Tx antennas in rectangular plot

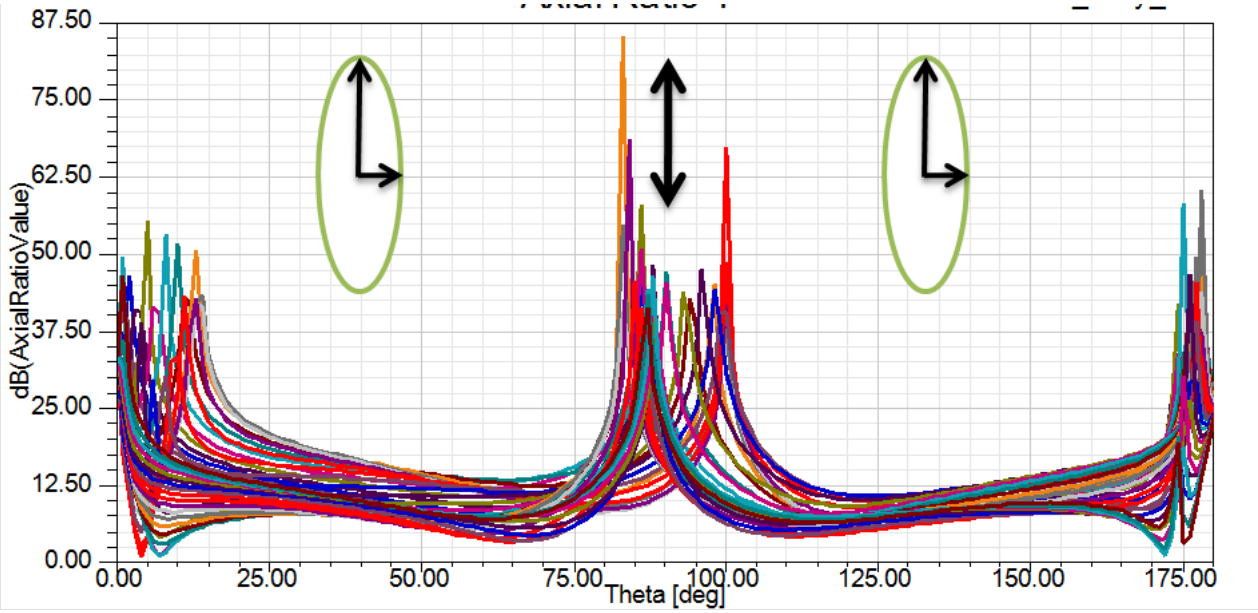

Figure 2.8.: Axial Ratio of the Tx antennas Gain pattern

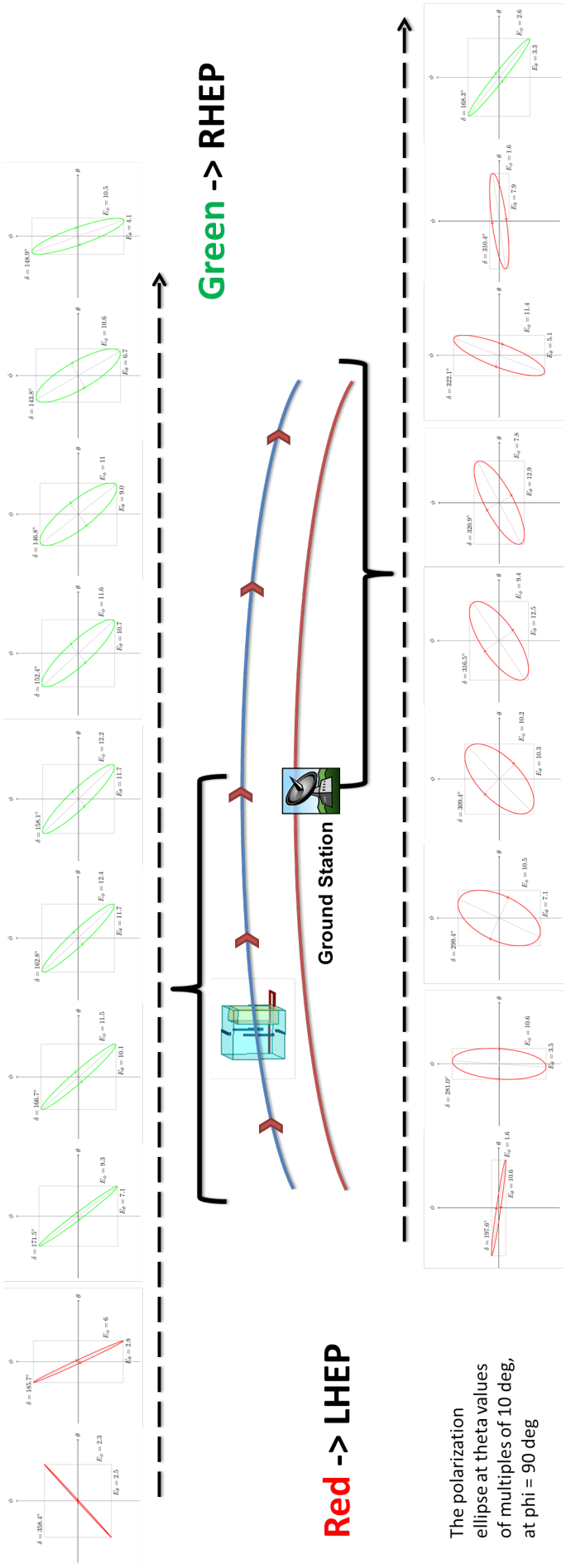

Figure 2.9.: The polarization ellipses at different points of the satellite trace across the orbit. The polarization is inhomogeneous and changes at elevation of 90°. This mandates use of polariztion diversity system.

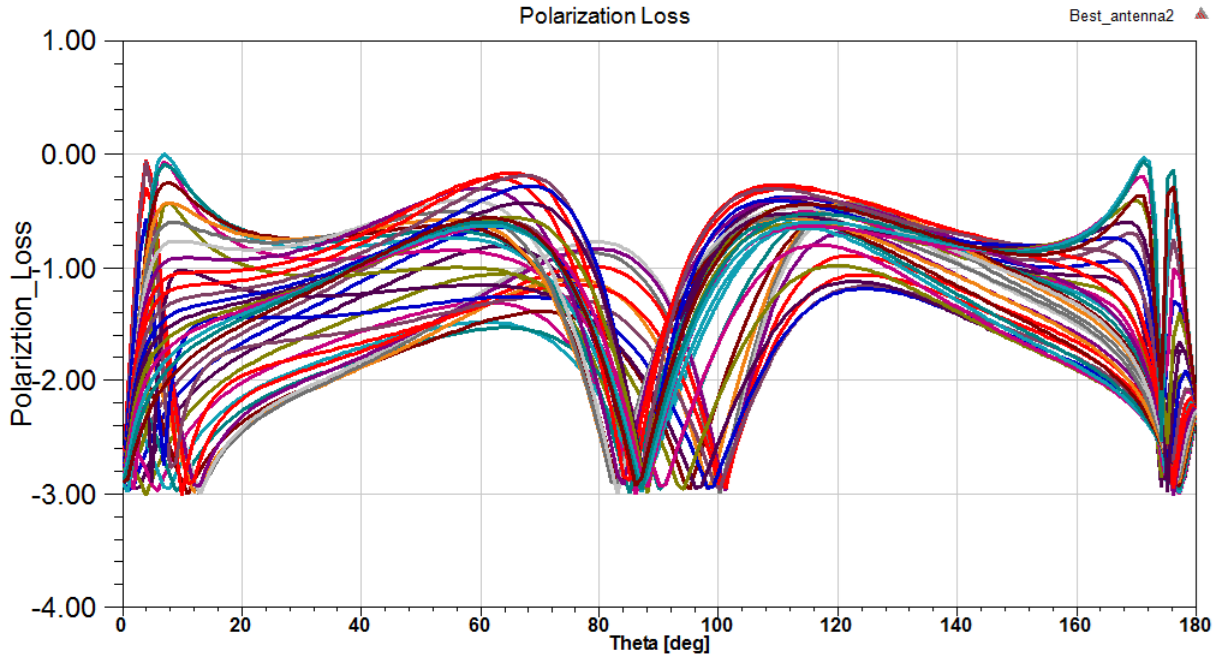

Figure 2.10.: Possible polarization loss if polarization divesity system is employed.

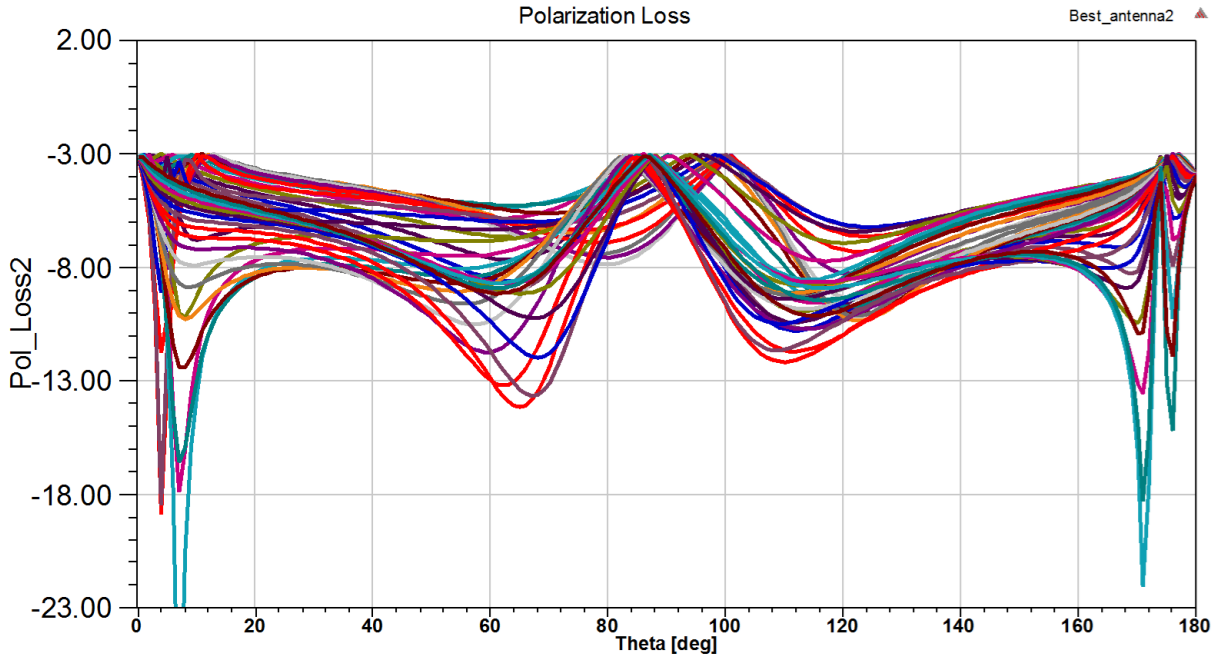

Figure 2.11.: Polarization loss if receiver antenna of opposite sense is used.

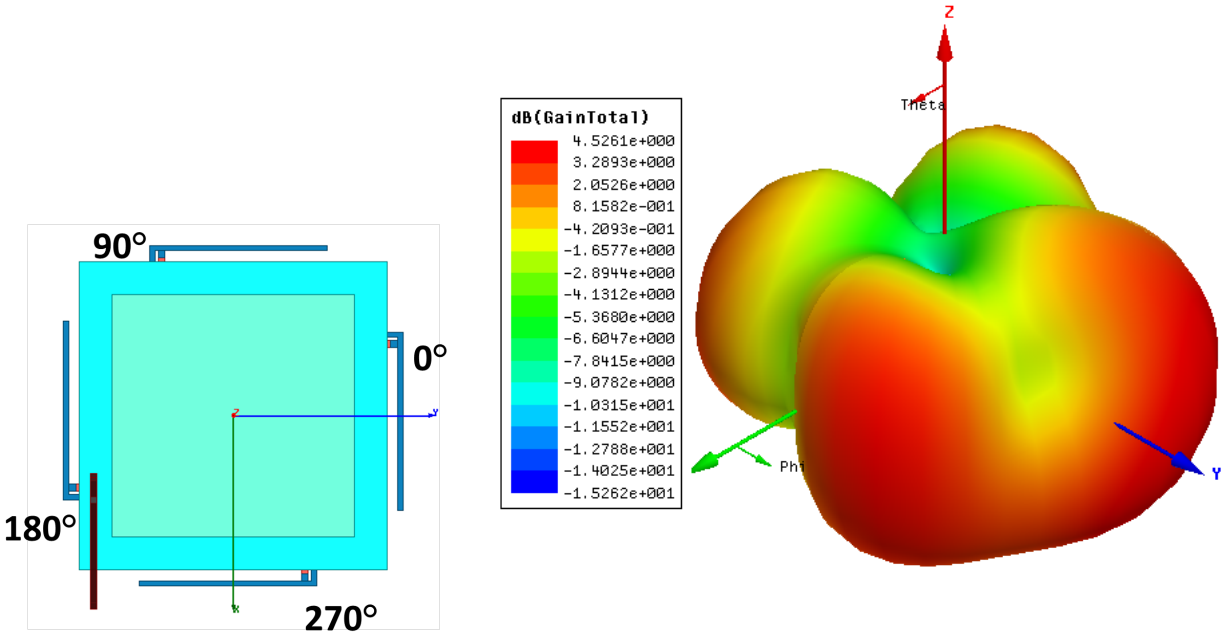

Figure 2.12.: Quadrature phase inputs 1

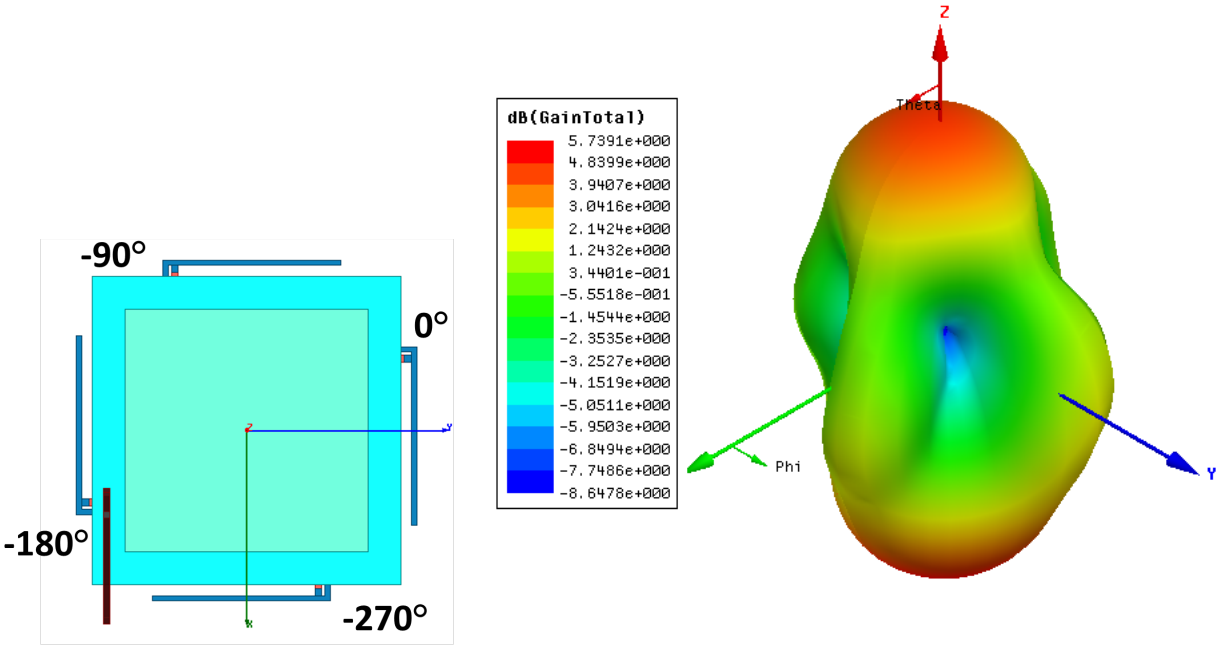

Figure 2.13.: Quadrature phase inputs 2

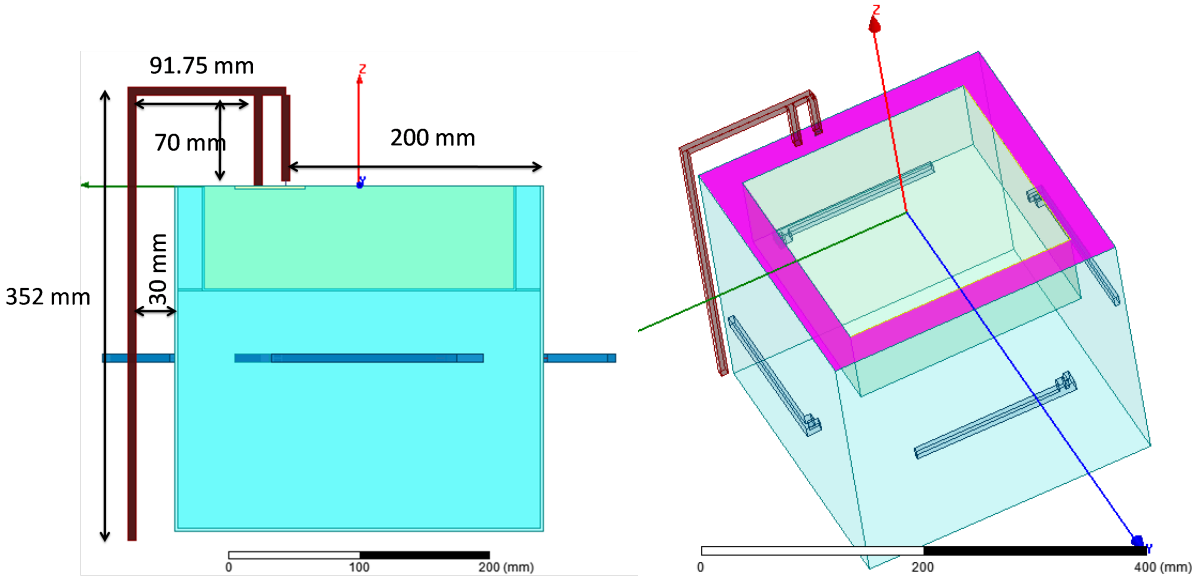

Figure 2.14.: Rx antenna with dimensions

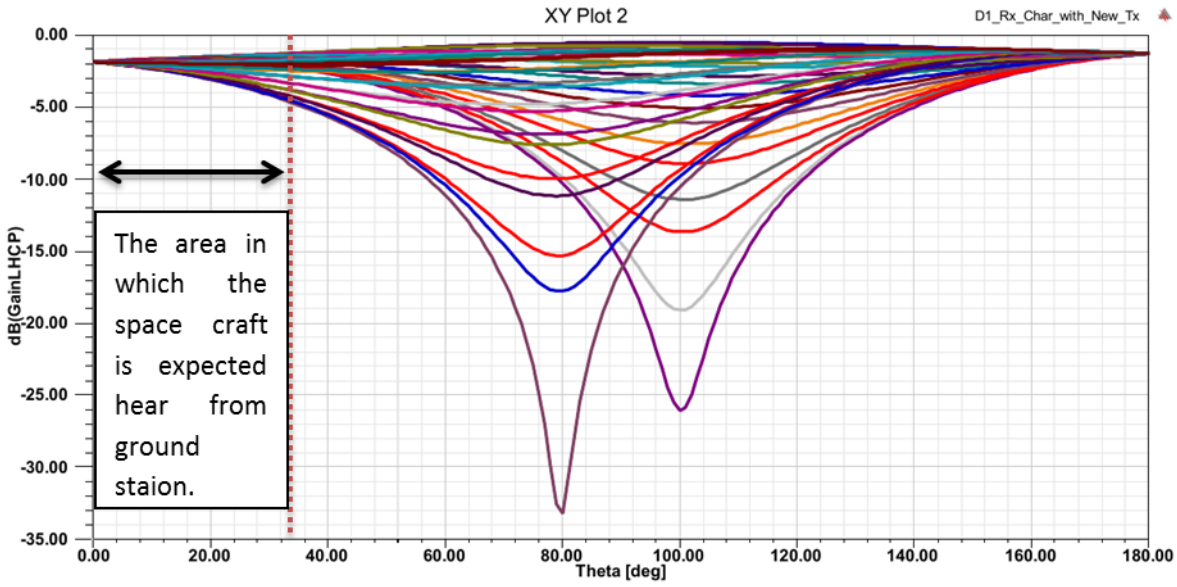

Figure 2.17.: Rx antenna LHCP gain

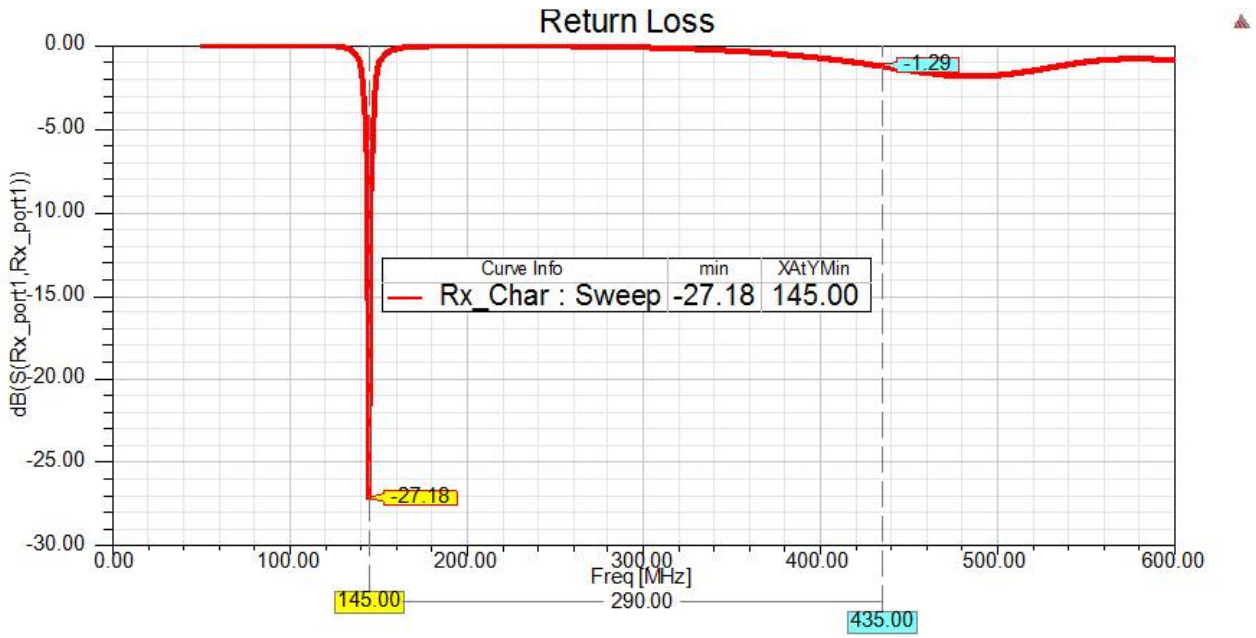

Figure 2.18.: Negative Return Loss (S_{22}) curves of Rx antenna

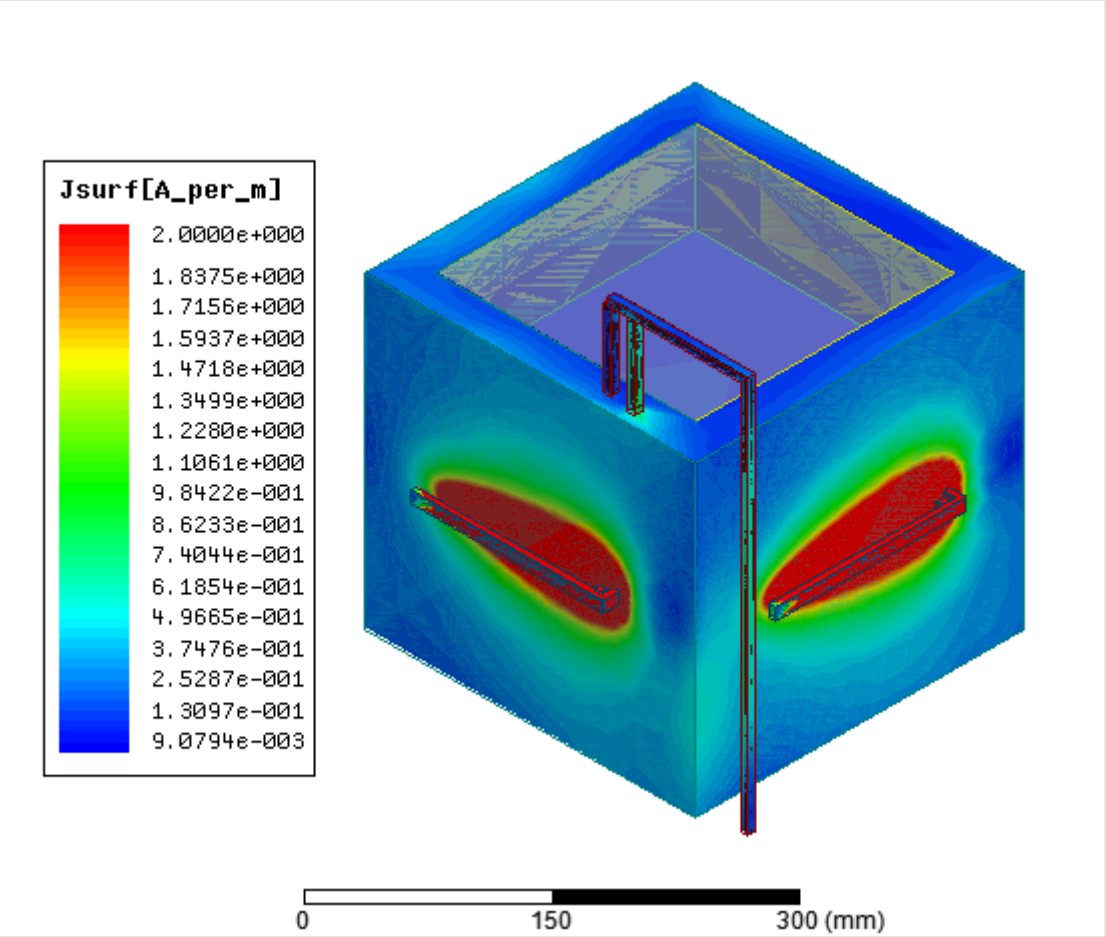

Figure 2.19.: Surface currents on the structure

3. Polarization Diversity System (PDS)

3.1. Overview

The Tx radiation pattern has different sense of polarizations spatially. In other words, it has significant cross polarization. Also, it is observed that the sense of polarization itself changes in a single pass through the ground station. Hence, there is a requirement to have polariztion diversity system at the ground station to overcome communication line losses due to polariztion losses.

3.2. The polariztion diversity system

The ground station that controls the XaTcobeo spacecraft has implemented the polariztion diversity system[8]. This system aims to minimize communications link losses caused by unpredictabe variations of the radiation pattern of the antenna in spacecraft that spin freely. It is based on the combination of multiple signals orthogonally polarized.

In cases where signal transimtted by the spacecraft may become problematic, this system permits the reception of most of the data by using the imformation obtained from signals orthogonally polarized at the same time.

3.3. Typical Ground Station antenna configurations

The hadware typically used in cubesat mission ground stations areFig. 3.1:

- One or more antennas for each band.
- a preamplifier for conditioning the signal to be received.
- a transceiver for down-converting the RF signal to AF signal and up-converting the AF signal to RF signal
- A modem for demodulating the downlink signal and modulating the up-link signal.

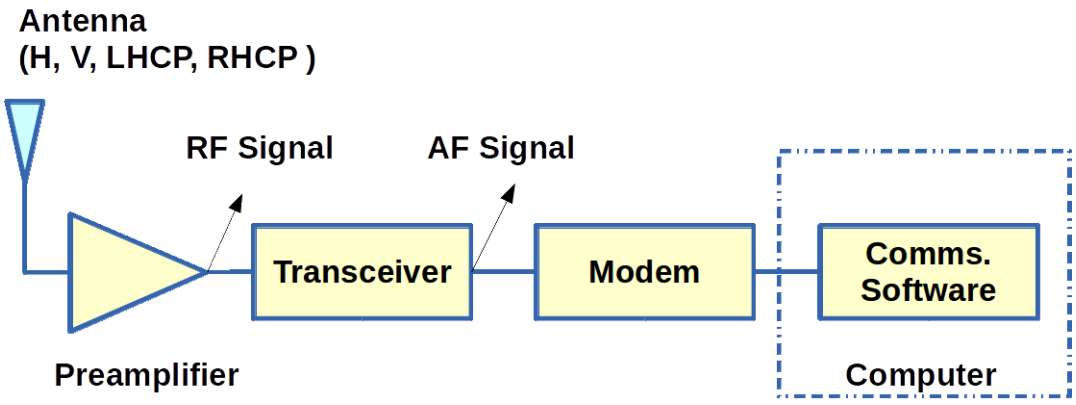

Figure 3.1.: Typical configuration of Ground Station

- A computer with custom communications software that implements the communications protocol and the software for commanding the spacecraft.

These ground stations for cubesats mostly use crossed Yagi for VHF and UHF bands, which consists of two Yagis orthogonally placed in the same boom. This antenna configuration permits the selection of the following polarizations at its output.

1. Fixed circular polarization: This is achieved by combining the outputs of the Yagis with a phasing harness. This antenna configuration cannot receive waves polarized orthogonal to the designed polarization.

2. Fixed linear polarization: This option involves 3 dB polarization loss if the signal being received is circular. If the received signal is linear, the loss depends on the alignment of both teh polarizations.

3.4. Implemetation

Simultaneously utilizing information from several polarizations need a modification of the typical design for the ground station. Possible designs for the the polarization diversity system are presented in [8].

Possible PDS configurations are:

3.4.1. RF Signal Polarization Diversity

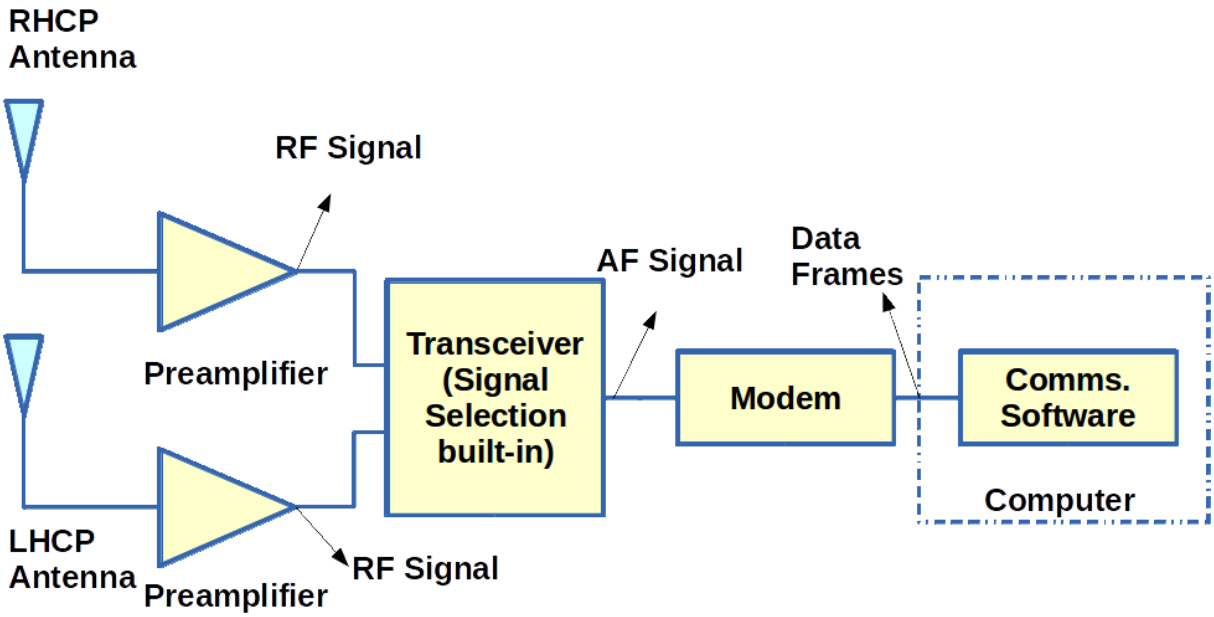

Figure 3.2.: RF signal Polarization Diversity

A transceiver with built-in signal selection capabilities is used for switching among the signals from both preamplifiersFig. 3.2. This device selects teh input with the highest signal strength and demodulates it. Only one branch is demodulated at a time. For the transmission, this transceiver would have to select the most suitable branch and switch the transmitter output to it.

If the polarization changes during the reception of a frame, while the transceiver switches from one input to the other, its output will only be a noisy signal, which involves the loss of the ongoing frame.

3.4.2. AF Signal Polarization Diversity

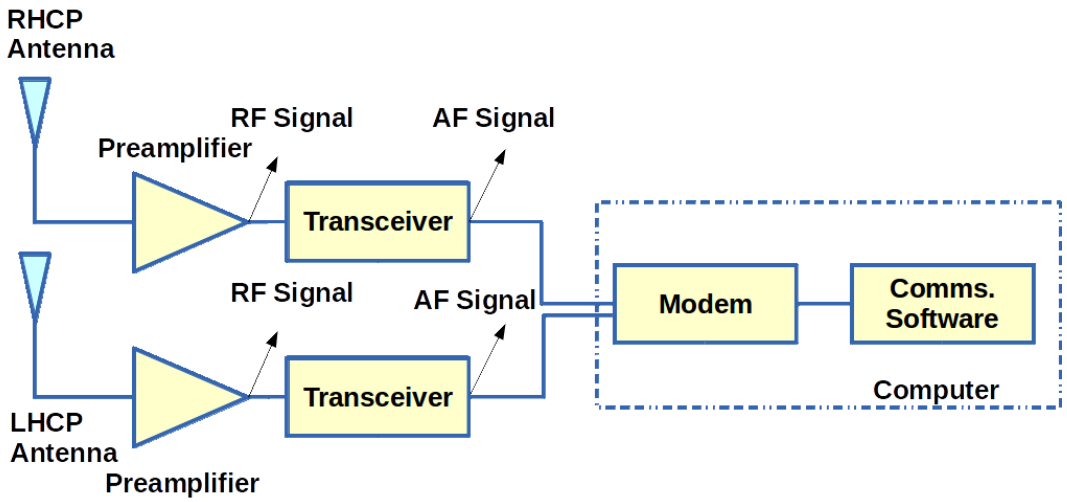

Figure 3.3.: AF signal Polarization Diversity

In this approach, AF signals obtained from both the transcievers are sent to a software modemFig. 3.3. This software modem combines both AF signals through signal processing techniques, giving preference to the one with a higher SNR. This brings the AF sigal ready to be demodulated.

3.4.3. Data Frames Polarization Diversity

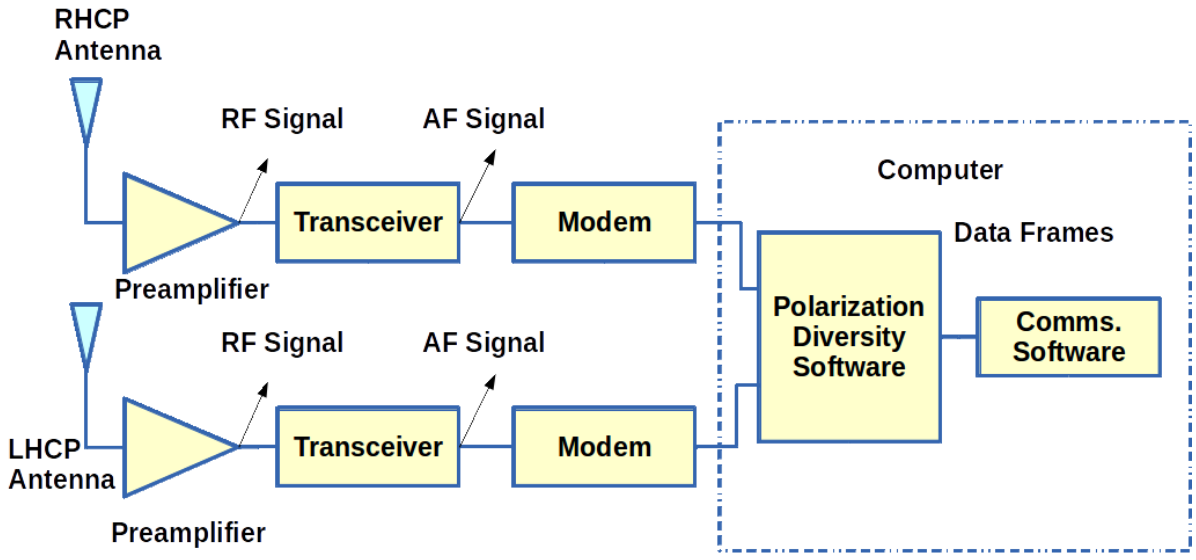

Figure 3.4.: Data Frames signal Polarization Diversity

In this case the whole chain has to be duplicated as shown in Fig. 3.4. The new element is a software component receives up to two frames (one from each polarization frame) and selects the one whose redundancy check is correct. Moreover, this software can be used to record both the input data frames for further offline processing.

In a nutshell, the equipment of the communications chain from the antenna up to the point at which the modification is performed has to be duplicated for each polarization.

4. F Antenna

4.1. Overview

The analysis of the F-antennas used as the Tx antennas is presented in this section. Though the F antenna seems to be a wire antenna, its behaviour is similar to that of a quarter wave patch antenna.

The designed F-antenna in shown in the figure Fig. 4.1

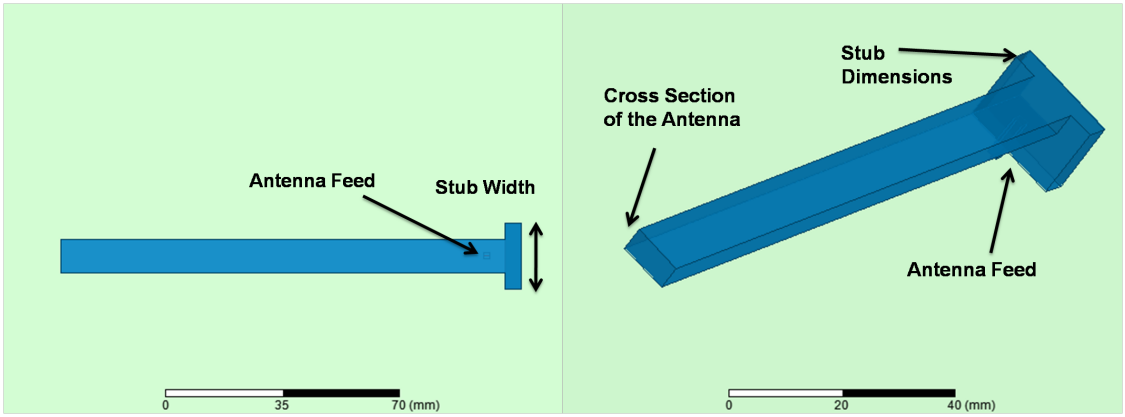

Figure 4.1.: Top view and isometric of the F-antenna

4.2. The microstrip line

Fig. 4.2 shows the cross section of the microstrip line with the descriptive dimensions w, h, t. The characteristic impedance or wave resistance of such a line are analysed in [9].

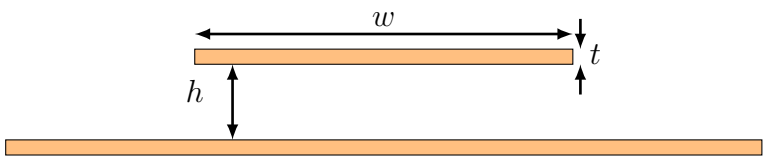

Figure 4.2.: Microstip line

The dimesions of the antenna in our case are $w = 10\,mm$, $h = 10\,mm$, $t = 5mm$.

The equation for the characteristic impedance for a square cross section wire above the plane from [9] is

$$R_1 = 60 \ln \left[\left(\frac{h}{0.59w} + 1.1 \right) - 0.5 + \sqrt{\left(\frac{h}{0.59w} + 1.1 \right)^2 - 1.05} \right]$$

For $w = 10\,mm$, $h = 10\,mm$ the characteristic impedance is $R_1 = 95.29\,\Omega$.

The equation for the characteristic impedance for a thin strip above the plane from [9] is

$$R_2 = 60 \ln \left[\frac{8h}{w} + 1.73 \left(\frac{w}{8h} \right) \right]$$

For $w = 10\,mm$, $h = 10\,mm$ the characteristic impedance is $R_2 = 126.3\,\Omega$.

As the antenna has a rectangular cross section, let the characteristic impedance be the average, $R = 110\,\Omega$.

4.3. Rectangular Microstrip Antennas

4.3.1. The Transmission Line Model

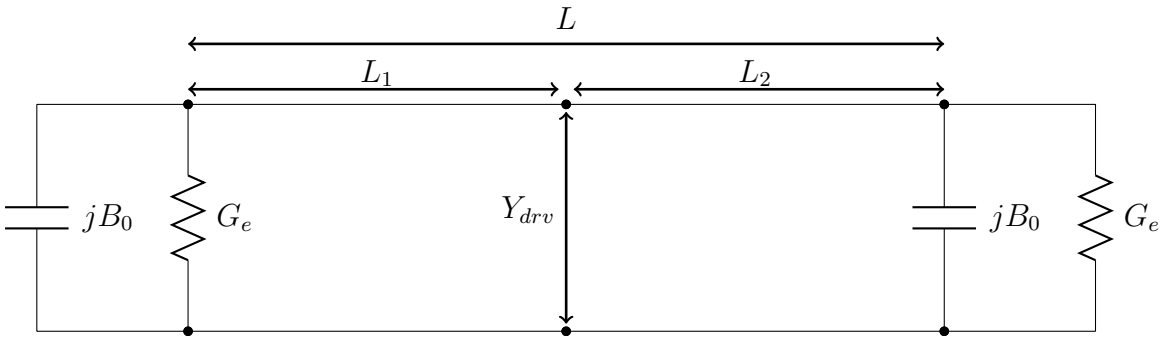

Figure 4.3.: Microstip line

The transmission line model provides a conceptual picture of the simplest implementation of a rectangular microstrip antenna. In this model, the antenna consists of a microstrip transmission line with a pair of loads at either end. The resistive loads

at each end of the transmission line represent loss due to radiation. At resonance, the imaginary components of the input impedance seen at the driving point cancel, and therefore the driving point impedance becomes exclusively real.

The driving point impedance at a driving point between the two radiating edges is represented as

$$Y_{drv} = Y_0 \left[\frac{Y_e + jY_0 tan\left(\beta L_1\right)}{Y_0 + jY_e tan\left(\beta L_1\right)} + \frac{Y_e + jY_0 tan\left(\beta L_2\right)}{Y_0 + jY_e tan\left(\beta L_2\right)} \right]$$

Y_e is the complex admittance at each radiating edge, which consists of an edge conductance G_e and edge susceptance B_e.

$$Y_e = G_e + jB_e$$

Approximate values of G_e and B_e are given by [10]:

$$G_e = 0.00836 \frac{w}{\lambda_0}$$

$$B_e = 0.01668 \frac{\Delta l}{h} \frac{w}{\lambda_0}$$

The value Δl is the line extension due to the electric field fringing at the edge of the patch antenna. The fringing field extension normalized to the substrate thickness h is

$$\frac{\Delta l}{h} = 0.412 \frac{\left(\varepsilon + 0.3\right)\left(w/h + 0.264\right)}{\left(\varepsilon - 0.258\right)\left(w/h + 0.8\right)}$$

4.4. The Quarter-wave Rectangular Microstrip Antenna

The electric field distribution under a rectangular microstrip antenna which is fed to excite the TM_{01} mode exclusively, a virtual short-circuit plane exists in the centred between the two radiating edges and also parallel to them. This virtual shorting plane when replaced with a physical metal shorting plane creates a rectangular microstrip antenna half its original length (approximately $\lambda/4$). This design is known as quarter-wave microstrip patch.

4.4.1. The Transmission line model

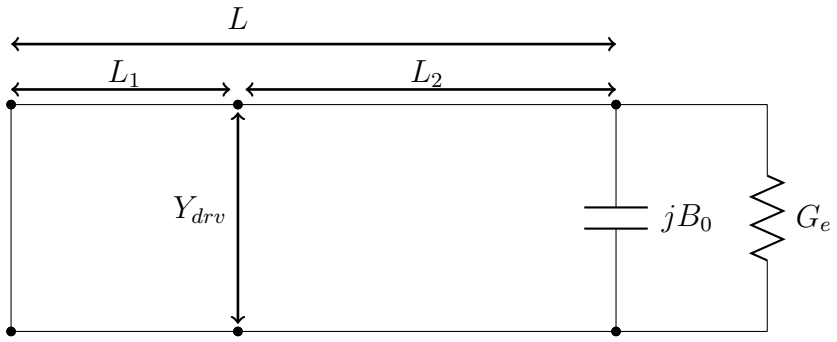

Figure 4.4.: Microstip line

The transmission line model of the design descirbed above in shown in Fig. 4.4 .

Here we have a short on one side and the feed is located to attain port mathcing condition.

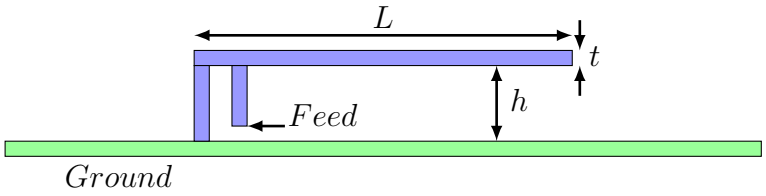

Figure 4.5.: Quarterwave antenna Sideview

A per sec. 4.2 and sec. 4.3.1the antenna can be analysec for the port impedance as Fig. 4.6.

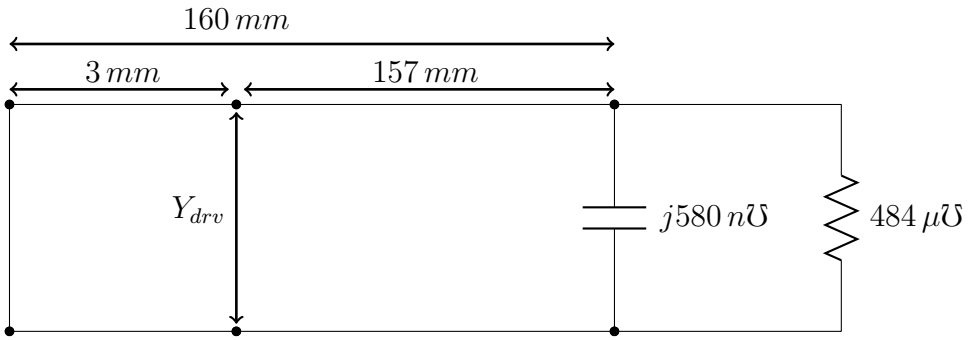

Figure 4.6.: Microstip line

Hence the port impedance will be

$$Y_{drv} = Y_0 \left[-j \cot(\beta L_1) + \frac{Y_e + jY_0 tan(\beta L_2)}{Y_0 + jY_e tan(\beta L_2)} \right]$$

4.5. F antenna - Patch Antenna

By applying the results associated with the pathc antenna, improvements were achieved in the F-antenna structure and its properties.

4.5.1. Reducing the height of the antenna

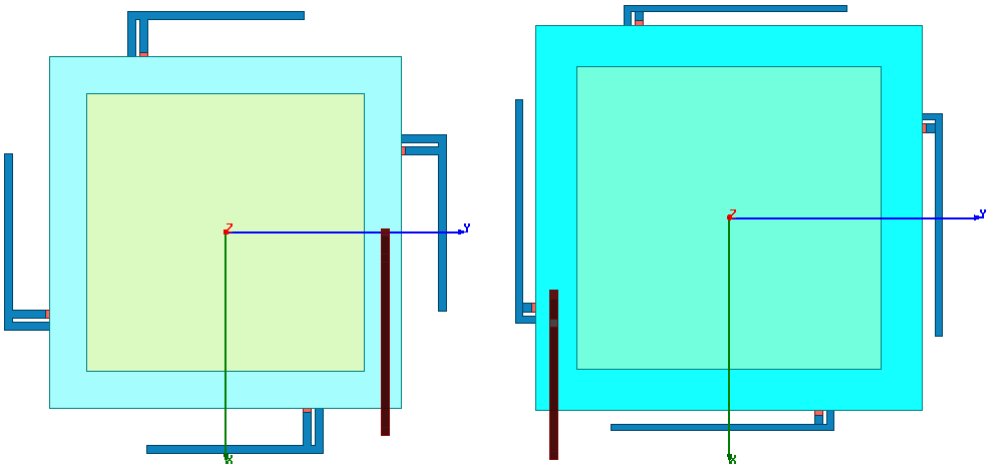

Figure 4.7.: Reduction in height of the antenna

The mechanical vibrations associated with the antennas can be minimized by making them more compact. By applying the results associated with the patch antenna, which relates the width of the patch to the return loss characteristics, improvements were achieved in the F-antenna structure and its properties.

An antenna with the dimensions shown in has been arrived at whose results are presented in sec. 2.3.

The Tx antenna dimensions are as described in Fig. 4.8 .

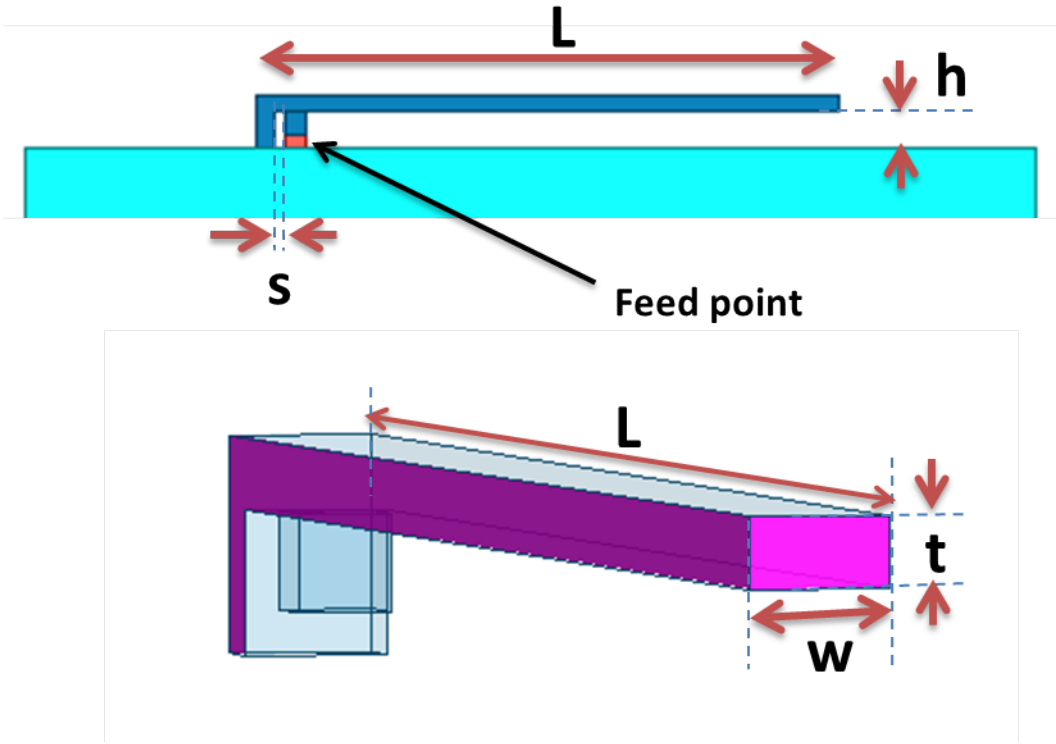

Figure 4.8.: Tx antenna Dimensions

Parameter	L	h	s	t	W
Value (mm)	162	10	3	5	10

Table 4.1.: Tx antenna dimensions

5. Antenna Test Results

5.1. Introduction

After the first version of the antennas were fabricated, their return loss characteristics were probed on VNA. The Rx and Tx characteristics respectively are shown in the following pictures.

The Tx antenna whose length was slightly more than that needed had $40\,dB$ return loss at $417\,MHz$ (lower than intended $435\,MHz$), which was satisfactory. The Rx antenna had a return loss of $18\,dB$ at $121\,MHz$, which was also satisfactory.

After these the antenna were put for test on the terace of the Department building to see whether there is enough radiation.

While working with the antennas, it was observed that the single antenna on a single side wall has same return loss characteristics to that of the antenna on the satellite structure as shown in Fig. 5.1.

So, two F-antenna on plates have been used as receiver and transmitter side for the test. The source was a simple RF source, with no modulation applied at $400\,MHz$ which was connected to the antenna through a SMA cable and the received signal was fed to a spectrum analyzer.

The transmitter and receiver were put on the top of two adjacent buildings facing each other. This setup was chosen to reduce the ground reflections. For a power of $10\,dBm$ fed to the Tx antenna, the received power was around $-40\,dBm$. This established that basically the antennas were radiating. This was the preliminary test done and this prompted for further pattern tests.

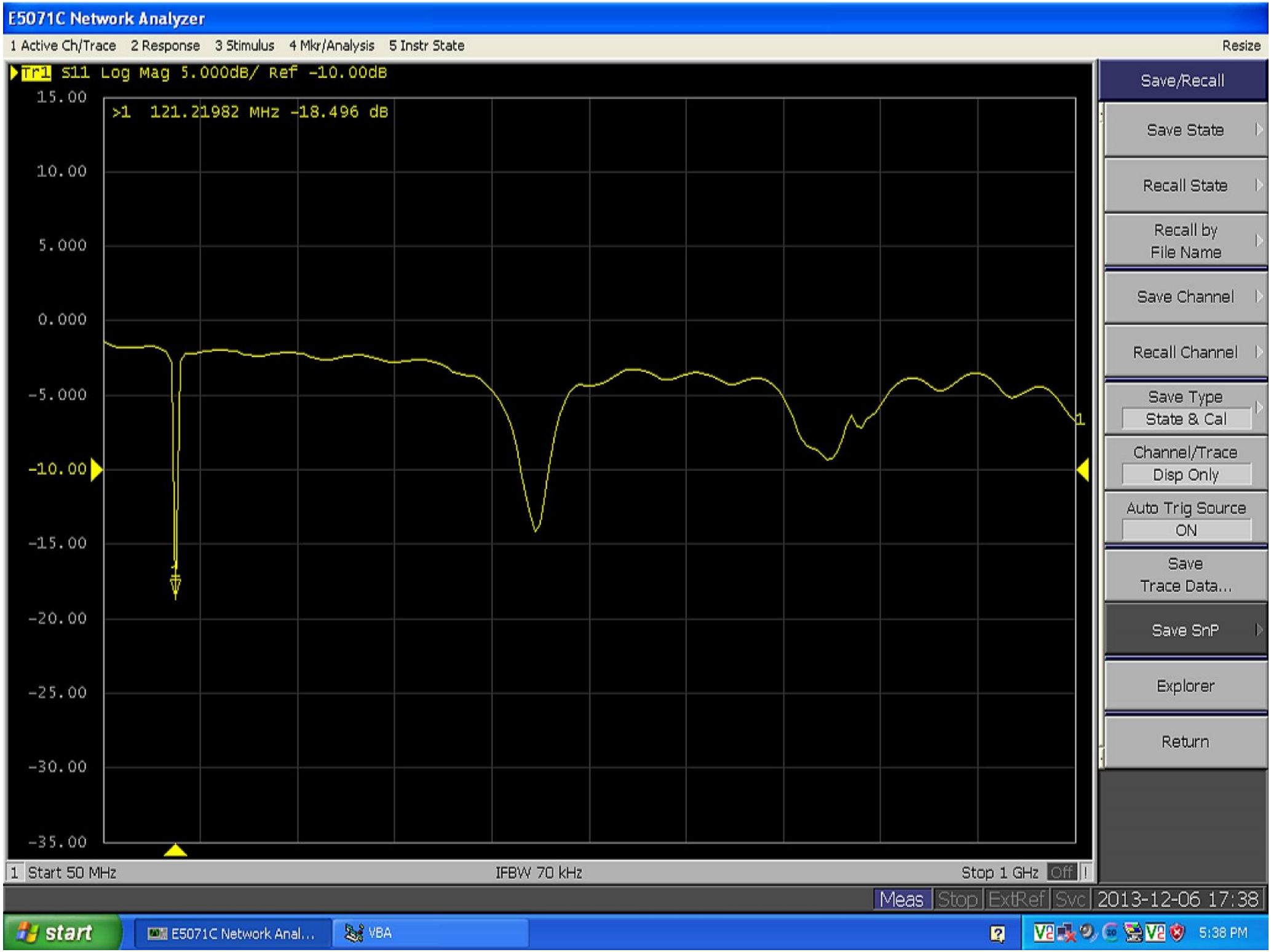
E5071C Network Analyzer
1 Active Ch/Trace 2 Response 3 Stimulus 4 Mkr/Analysis 5 Instr State
Resize
Tr1 S11 Log Mag 5.000dB/ Ref -10.00dB
>1 121.21982 MHz -18.496 dB
15.00
10.00
5.000
0.000
-5.000
-10.00
-15.00
-20.00
-25.00
-30.00
-35.00
1 Start 50 MHz
IFBW 70 kHz
Stop 1 GHz
Off
Save/Recall
Save State
Recall State
Recall by File Name
Save Channel
Recall Channel
Save Type
State & Cal
Channel/Trace
Disp Only
Auto Trig Source
ON
Save Trace Data...
Save SnP
Explorer
Return
Meas
Stop
ExtRef
Svc
2013-12-06 17:38
start
E5071C Network Anal...
VBA
5:38 PM

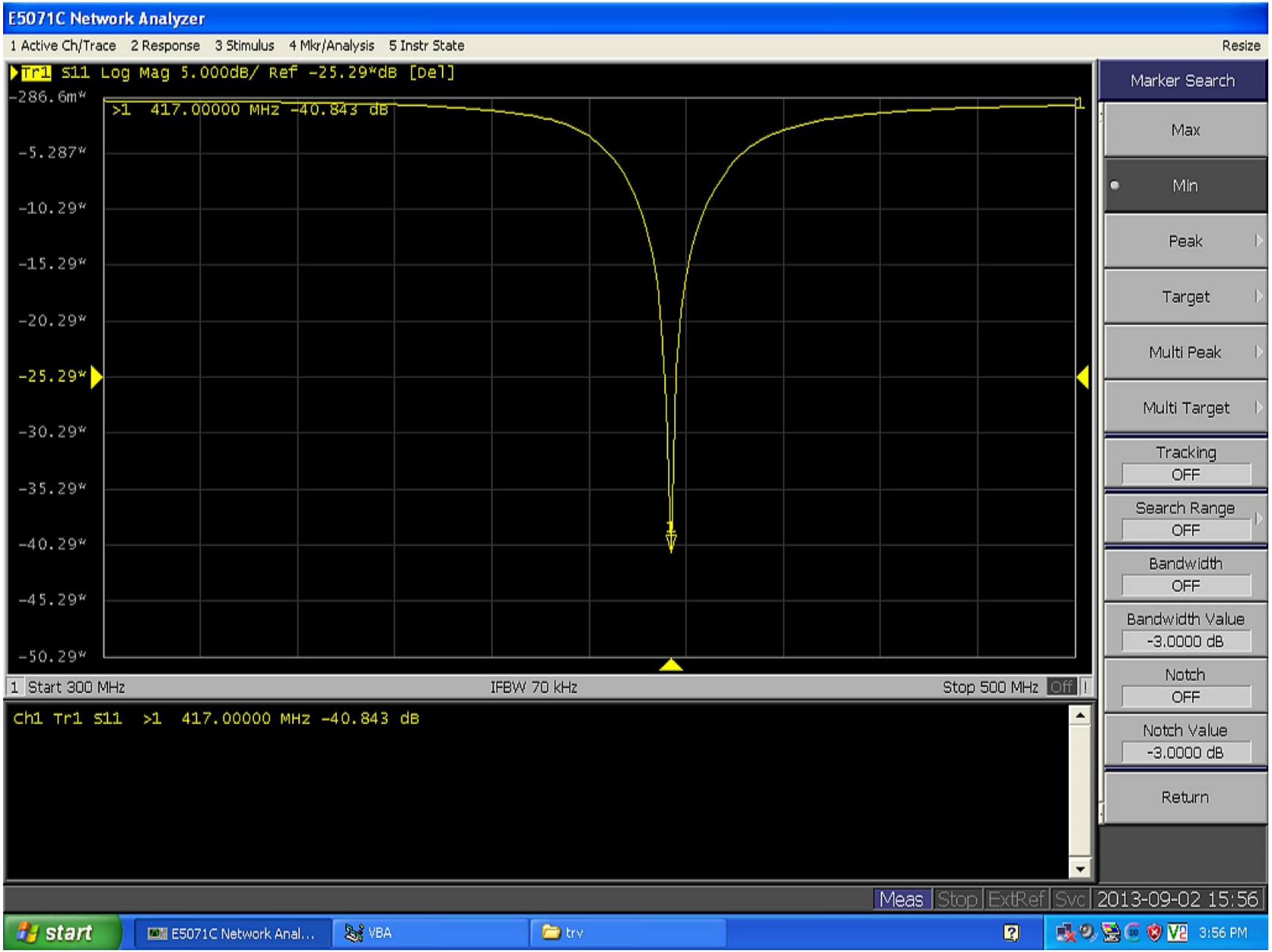
E5071C Network Analyzer
1 Active Ch/Trace 2 Response 3 Stimulus 4 Mkr/Analysis 5 Instr State
Resize
Tr1 S11 Log Mag 5.000dB/ Ref -25.29*dB [Del]
-286.6m*
-5.287*
-10.29*
-15.29*
-20.29*
-25.29*
-30.29*
-35.29*
-40.29*
-45.29*
-50.29*
>1 417.00000 MHz -40.843 dB
1 Start 300 MHz
IFBW 70 kHz
Stop 500 MHz
Off
Ch1 Tr1 S11 >1 417.00000 MHz -40.843 dB
Marker Search
Max
Min
Peak
Target
Multi Peak
Multi Target
Tracking
OFF
Search Range
OFF
Bandwidth
OFF
Bandwidth Value
-3.0000 dB
Notch
OFF
Notch Value
-3.0000 dB
Return
Meas
Stop
ExtRef
Svc
2013-09-02 15:56
start
E5071C Network Anal...
VBA
trv
3:56 PM

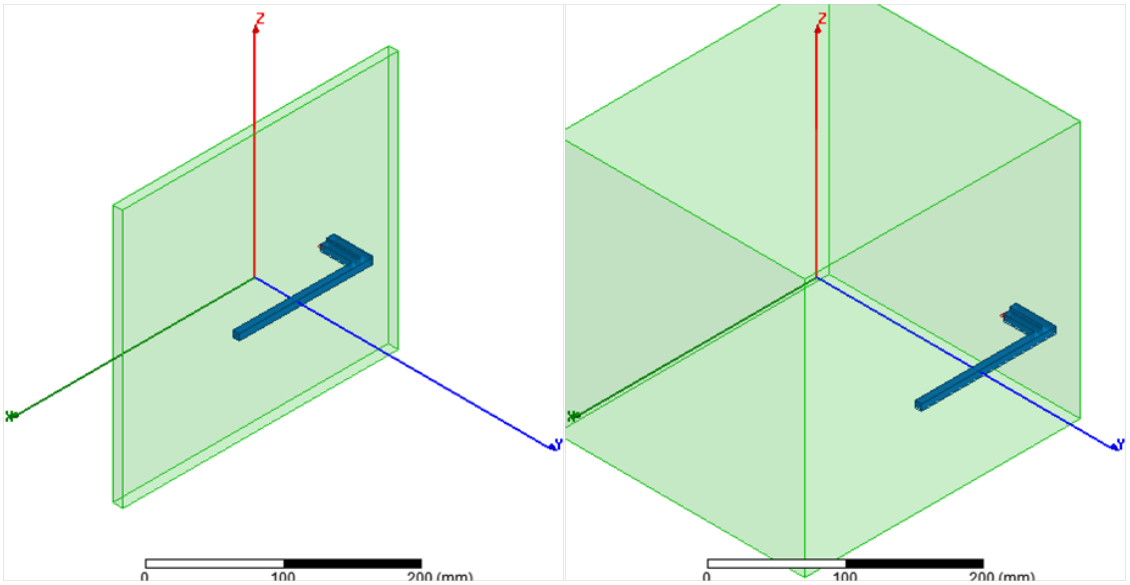

Figure 5.1.: F-antenna on a plate and Cube

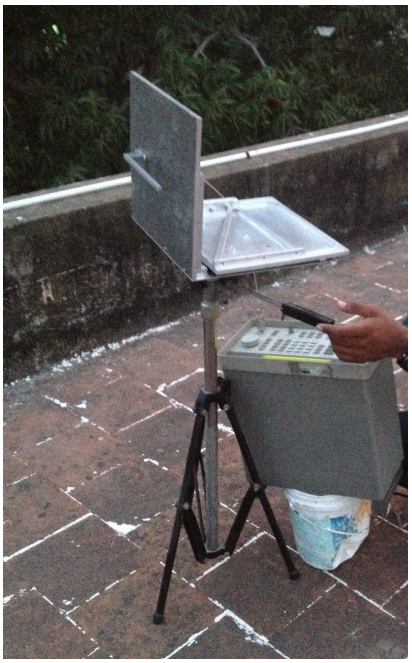

Figure 5.2.: Antenna testing on the terrace

5.2. The Test Setup at VSSC

The UHF and VHF antennas are tested at the test range of VSSC, Trivandrum. The setup of the test range in referred to as Slant Range [11]. Here the source antenna

is located close to the ground and the Antenna Under Test (AUT) is mounted on a tower. The source antenna is fixed, but the AUT is manoeuvred using a robotic arm which has 2-axis independence.

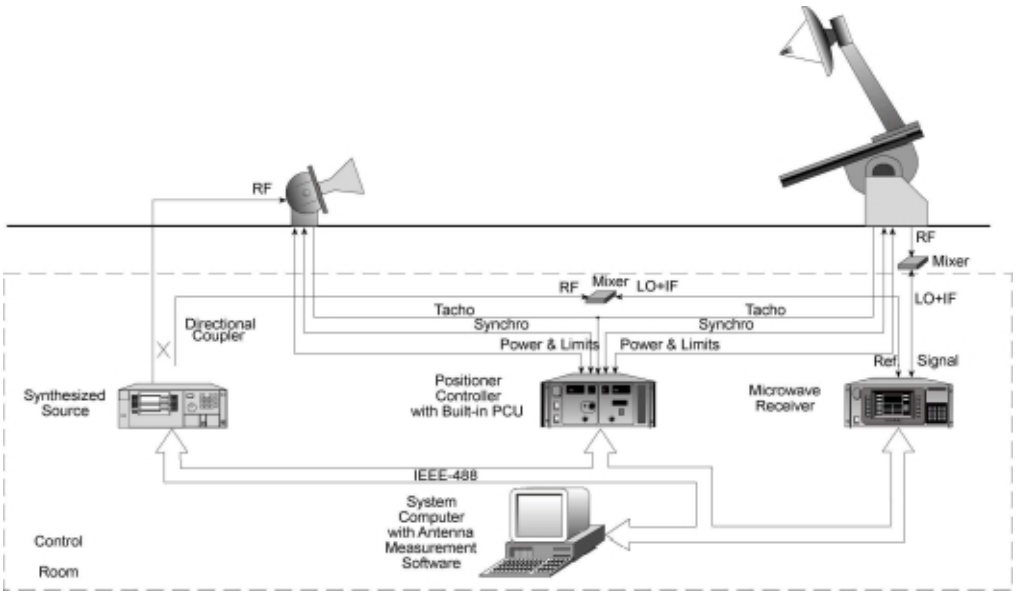

Figure 5.3.: Antenna Test Setup

The source antenna is a crossed log-periodic antenna with the provision of selecting vertical, horizontal, RHCP or LHCP polarizations. In our case only horizontal and vertical polarizations were used.

The radiation pattern measurements are done in receive mode where the satellite structure is the receiver.

5.2.1. Far Field

Far field is often defined as the region where the pointing vector is real (only radiating fields). In this region the fields decay as $\frac{1}{r}$ and radiation pattern is independent of r.

The region beyond $r > \frac{2D^2}{\lambda}$ can be regarded as far field, where D is the largest dimension of the AUT and λ the wavelength and assuming the source radiating spherical waves.

For $D = 60\,cm$,

In the test range, the distance between the two antennas was $45\,m$.[12]

Frequency	Far-field
435 MHz	> 1 m
145 MHz	> 0.34 m

Table 5.1.: Far-field regions

5.3. Gain Measurement

The method used for Gain measurement is Gain Comparision Method[13]. This requires an antenna whose gain is exactly known (called gain standard) and a transmitting antenna whose gain does not need to be known. Two sets of measurements are performed.

1) The gain standard is in receiving mode, and its receved power P_{GS} is measured.

2) The test antenna is in receiving mode in exactly the same arrangement (the distance R and the transmitted power P_0 are kept the same), and its received power P_{AUT} is measured.

In both measurements the receiving antennas are matched to their loads (the receiver).

The Friss transmission equation is

$$\frac{P_r}{P_t} = \left(\frac{\lambda}{4\pi R}\right)^2 G_t G_r$$

The above two measurements lead to (taking log on both sides)

$$G_{AUT\,dB} + G_{0\,dB} = 20\log_{10}\left(\frac{4\pi R}{\lambda}\right) + 10\log_{10}\left(\frac{P_{AUT}}{P_0}\right)$$

$$G_{GS\,dB} + G_{0\,dB} = 20\log_{10}\left(\frac{4\pi R}{\lambda}\right) + 10\log_{10}\left(\frac{P_{GS}}{P_0}\right)$$

Here,

$G_{AUT\,dB}$ is the gain of the test antenna

$G_{GS\,dB}$ is the gain of the standard antenna

$G_{AUT\,dB}$ is the gain of the transmitting antenna

The above two equations lead to

$$G_{AUT\,dB} = G_{GS\,dB} + 10\log_{10}\left(\frac{P_{AUT}}{P_{GS}}\right)$$

If the test antenna is circulary of elliptically polarized, two orthogonal linearly polarized gain standards must be used in order to obtain the partial gains corresponding to each polarized component. The total gain of the test antenna will be

$$G_{AUT\,dB} = 10\log_{10}\left(G_{AUTv} + G_{AUTh}\right)$$

5.4. Polarization Measurements

A complete description of the antenna polarization is given by the polarization ellipse (the axial ratio and the tilt angle), as well as the sense of rotation (clockwise, or counter-clockwise).

The polarization of an antenna in given direction is defined as the polarization of the electric field vecor **E** in the far field, radiated by the antenna in that direction.

Different methods employed to measure polarization are

1. polariztion-pattern method
2. rotaing - source method
3. multiple-amplitude-component method
4. phase-amplitude method

5.5. The Test results

The test results are available in the Appendix chapter 1.

6. Link Budget and SNR

6.1. Downlink Budget

For the link budget analysis for downlink is presented in this section.

Downlink Propagation Loss				Units
Downlink Frequency	435			MHz
Orbit Altitude	900			km
Elevation Angle	0	13	90	deg
Distance to the satellite	3074	1960	900	km
Free Space Loss L_{fs}	155	151	144.3	dB
Satellite Antenna Gain G_{tx}	13	7	2	dB
Satellite Losses L_{sat}	1	1	1	dB
Transmit Power P_t	0	0	0	dBW
Transmit EIRP P_{EIRP}	14	8	1	dBW
Atmospheric Losses L_{atm}	0.35	0.35	0.35	dB
Ionospheric Losses L_{ion}	0.40	0.40	0.40	dB
GS Pointing Error	3	3	3	deg
Pointing Loss L_{point}	3.0	3.0	3.0	dB
Polarization Mismatch L_{pol}	3.0	3.0	3.0	dB
Total Propagation Loss L_{prop}	161.7	157.7	151.0	dB

Table 6.1.: Downlink total propagation loss

- The satellite's orbit is assumed to a Low Earth Orbit (LEO) with and altitude of 900 km.
- The distance between the satellite and groundsation varies with the position of the satellite. It is farthest for elevation angle of 0° and closest for 90° independent of the azimuth angle, which represent the worst and best case.
- The 13° elevation is the case where the downlink margin is approximately $+6\,dB$, which is of interest. The downlink observations of cubesats presented in [14] show that the received power is about $6\,dB$ less than the estimated values.

Downlink Propagation Loss				Units
Downlink Frequency	435			MHz
Orbit Altitude	900			km
Elevation Angle	0	13	90	deg
Distance to the satellite	3074	1960	900	km
Free Space Loss L_{fs}	155	151	144.3	dB
Satellite Antenna Gain G_{tx}	13	7	2	dB
Satellite Losses L_{sat}	1	1	1	dB
Transmit Power P_t	0	0	0	dBW
Transmit EIRP P_{EIRP}	14	8	1	dBW
Atmospheric Losses L_{atm}	0.35	0.35	0.35	dB
Ionospheric Losses L_{ion}	0.40	0.40	0.40	dB
GS Pointing Error	3	3	3	deg
Pointing Loss L_{point}	3.0	3.0	3.0	dB
Polarization Mismatch L_{pol}	3.0	3.0	3.0	dB
Total Propagation Loss L_{prop}	161.7	157.7	151.0	dB

Table 6.2.: Downlink total propagation loss

- The porpagation loss is calculated using the Friis transimission equation 6.1.in which d is the distance in meters and $\lambda_0 = 0.69\,m$ is the free space wavelength corresponding to $435\,MHz$ frequency.

$$L_{fs} = 10\log\left(\frac{4\pi d}{\lambda_0}\right)^2 [dB] \tag{6.1}$$

- The satellite antenna gain values G_{tx} are as per the gain pattern obotained in the simulations.

- The satellite loss L_{sat} is an approximate values. This includes connector losses, cable losses, filter losses and divider losses.

- The radio will be programmed to deliver and output power of $P_t = 1\,W$ $(= 0\,dBW)$.

- The Equivalent Isotropically Radiated Power P_{EIRP} is

$$P_{EIRP} = P_t + L_{sat} + G_{tx}$$

- The atmospheric and ionospheric losses are approximate values as per [15]. These values seem to be overestimated values as per [16].

Downlink Propagation Loss				Units
Downlink Frequency	435			MHz
Orbit Altitude	900			km
Elevation Angle	0	13	90	deg
Distance to the satellite	3074	1960	900	km
Free Space Loss L_{fs}	155	151	144.3	dB
Satellite Antenna Gain G_{tx}	13	7	2	dB
Satellite Losses L_{sat}	1	1	1	dB
Transmit Power P_t	0	0	0	dBW
Transmit EIRP P_{EIRP}	14	8	1	dBW
Atmospheric Losses L_{atm}	0.35	0.35	0.35	dB
Ionospheric Losses L_{ion}	0.40	0.40	0.40	dB
GS Pointing Error	3	3	3	deg
Pointing Loss L_{point}	3.0	3.0	3.0	dB
Polarization Mismatch L_{pol}	3.0	3.0	3.0	dB
Total Propagation Loss L_{prop}	**161.7**	**157.7**	**151.0**	**dB**

Table 6.3.: Downlink total propagation loss

- The the antenna system witht the rotors at ground station are prone to some pointing error. [14] reported a systematic pointing error of 7° which is avoidable. The error may also occur due to inaccurate/unupdated TLE data [17] and other factors like refraction due to temeperature and pressure variations along the path of propagation.
- The typical HPBW of the Yagi antenna with gain of $18\,dB$ used in ground stations is about 5° . Accordingly the pointing loss is taken as $3\,dB$.
- Polarization mismatch loss calculations are presented in sec. 1.8.
- The total propagation loss is

$$L_{prop} = L_{fs} + L_{atm} + L_{ion} + L_{pol} + L_{point}$$

Downlink Margin				Units
Elevation Angle	0	13	90	deg
Total Propagation Loss L_{prop}	161.7	157.7	151.0	dB
Rx Antenna Gain G_{Rx}	18.0	18.0	18.0	dBi
Rx component noise temp T_{Rx}	94.0	94.0	94.0	K
Rx input noise temp T_A	300.0	300.0	300.0	K
System noise temp T_{sys}	394.0	394.0	394.0	K
Rx Noise Bandwidth B	20.0	20.0	20.0	kHz
Rx Isotropic Power P_{iso}	-175.7	-165.5	-150.0	dBW
Rx Power P_{Rx}	-157.7	-147.5	-132.0	dBW
Rx Noise Power P_{noise}	-159.6	-159.6	-159.6	dB
SNR SNR	1.85	12.05	27.55	dB
Modulation Scheme	GMSK	GMSK	GMSK	
Data Rate R_b	9600	9600	9600	bps
Eb/No Received	5.03	15.24	30.70	dB
Eb/No threshold for 1e-5	8.20	8.20	8.20	dB
Downlink Margin	-3.1	7.0	22.5	dB

Table 6.4.: Downlink Margin

- The Yagi antenna 436CP42UG from M2 Antennas [18] has specified gain of 18.9 dB. Deducting the possible line losses, gain is taken as 18 dB.
- The calculations of Rx component noise temp T_{Rx} and antenna noise temp T_A are taken from [19], in which the link budget analysis for IITMSAT is presented.

$$T_{sys} = T_A + T_{Rx}$$

- B is the noise bandwidth of the receiving system.
- The isotropic power at the receiver P_{iso} and power at the recevier antenna P_{Rx} are $P_{iso} = P_{EIRP} - L_{prop}$ and $P_{Rx} = P_{iso} + G_{Rx}$.
- The noise power at the receiver is

$$P_{noise} = k + T_{sys} + B \ \ [dB]$$

  where k is the Boltzmann constant $k = 1.38 \times 10^{-23}\, m^2\, kg\, s^{-2}\, K^{-1}$
- $SNR = P_{Rx} - P_{noise}$ and $\frac{E_b}{N_o} = SNR + 10\log(B) - 10\log(R_b)$
- The modulation scheme used and data rates are adapted from [19].

6.2. Uplink Budget

The uplink budget calculations involve similar calculations as that of downlink budget. The uplink budget is presented below.

Uplink Propagation Loss			Units
Downlink Frequency	145		MHz
Orbit Altitude	900		km
Elevation Angle	5	40	deg
Distance to the satellite	3000	1072	km
Free Space Loss L_{fs}	145.2	136.3	dB
Transmitter Antenna Gain G_{tx}	16	16	dB
Ground Station Losses L_{GS}	6	6	dB
Transmit Power P_t	14	14	dBW
Transmit EIRP P_{EIRP}	24	24	dBW
Atmospheric Losses L_{atm}	0.2	0.2	dB
Ionospheric Losses L_{ion}	0.7	0.7	dB
Pointing Error (GS)	3	3	deg
Pointing Loss L_{point}	3	3	dB
Polarization Mismatch L_{pol}	0	0	dB
Total Propagation Loss	149.1	140.2	dB

Table 6.5.: Uplink Propagation Losses

- The atmospheric and ionospheric losses are approximate values as per [15]. These values seem to be overestimated values as per [16].
- The polarization mismatch loss in this case is zero, as the transmitting antenna at ground station is assumed to transmit and LHCP wave and also the LHCP gain of the onboard receiver antenna is considered for the calculations.
- The ground station loss of $6\,dB$ has been reported in [20].

Uplink Margin			Units
Elevation Angle	5	40	deg
Total Propagation Loss L_{prop}	149.1	140.2	dB
Rx Antenna Gain G_{Rx}	-2	-5	dB
System noise temp T_{sys}	500	500	K
Rx Noise Bandwidth B	10	10	kHz
Rx Isotropic Power P_{iso}	-125.1	-116.2	dBW
Rx Power P_{Rx}	-128.1	-122.2	dBW
Rx Noise Power P_{noise}	-161.6	-161.6	dB
SNR SNR	33.5	39.4	dB
Modulation Scheme	FSK	FSK	
Channel Data Rate R_b	1200	1200	bps
Eb/No Received	42.7	48.6	dB
Eb/No Threshold for 1e-5	13.8	13.8	dB
Uplink Margin	28.9	34.8	dB

Table 6.6.: Uplink Margin

- The Rx antenna gain is as per the LHCP gain pattern in Fig. 2.6.
- This shows a comfortable uplink margin.

6.3. Signal to Noise Ratio (SNR)

In the downlink and uplink budgets presented in previous sections, the factors varying with elevation are the propagation loss and antenna gain. In this context the SNR can be represented as function of elevation and azimuth angles.

6.3.1. Propagation loss

Typical skytrack of LEO satellites with respect to the ground station is shown in fig Fig. 6.1. This has been obtained using the software GPredict [21].

The propagation loss is only a function of elevation. For a satellite with mean orbit altitude of 900 km, the distance to the satellite as a function of elevation angle α can be expressed as

$$d = \frac{7100}{\cos(\alpha)} \cos\left(\alpha \arcsin\left(\frac{64}{71}\cos(\alpha)\right)\right)$$

(taking Earth's radius as 6400 km)

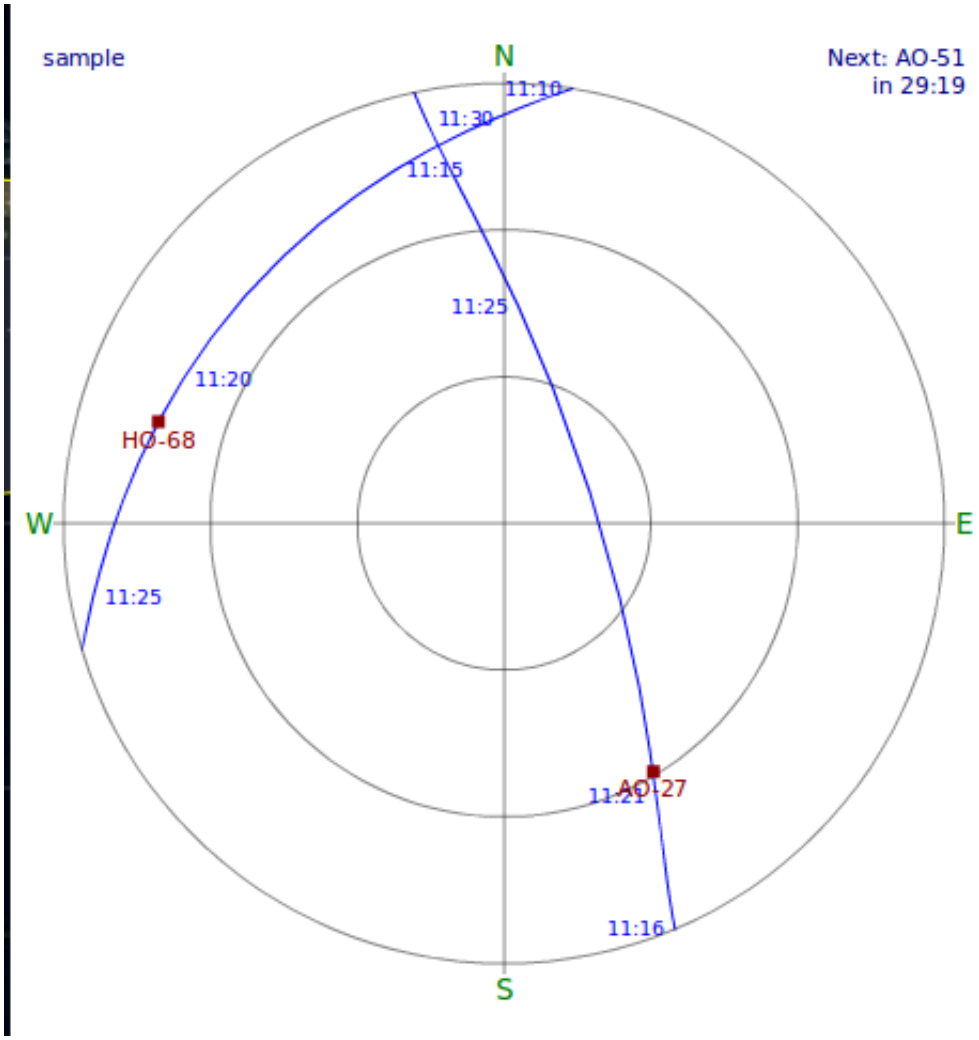

Figure 6.1.: Typical skytrack of LEO satellites

The propagation loss can be calculated using Friss equation 6.1. The downlink and uplink propagation losses is represented in Fig. 6.3 & Fig. 6.4.

As per the constraints of the mission sec. 1.6, the satellites payload axis always points the magnetic field, which dictates the satellite's attitude towards ground station. Taking this into account the SNR and Link Margin values for uplink and downlink can be represented as .

6.4. Simple monopole - A comparision.

A simple design, monopole on the metallic cube Fig. 6.7, is presented here for comparision.

The gain pattern of this design is in Fig. 6.8. The SNR characteristics are .

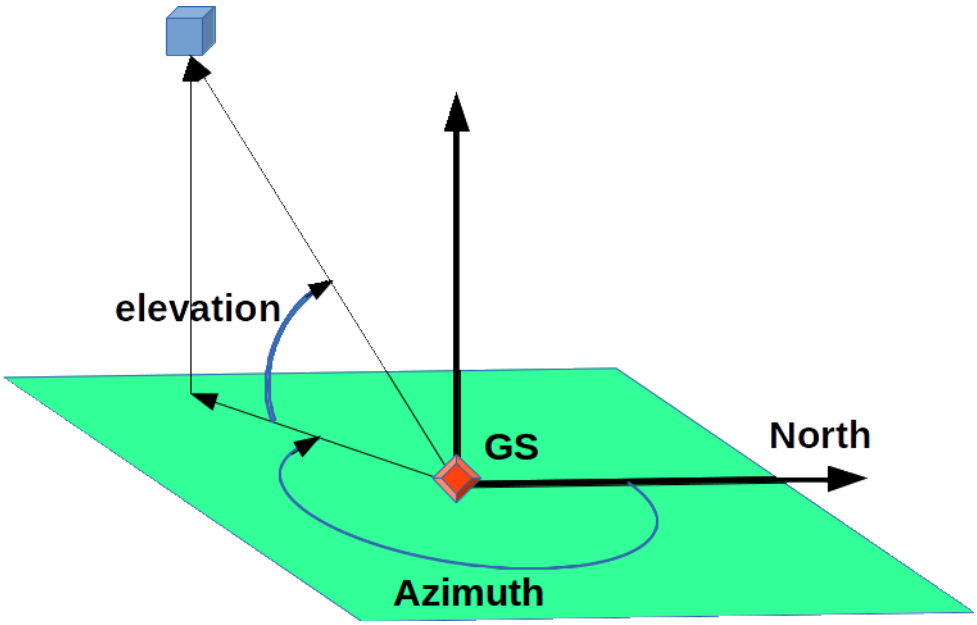

Figure 6.2.: Azimuth and elevation angles description

This design has met the downlink margin requirements. As explained in sec. 1.6 the antenna placement on the satellite body has many constraints. One of them is that antennas cannot be placed on the top face (payload face). So, this design does not suit the mission requirements.

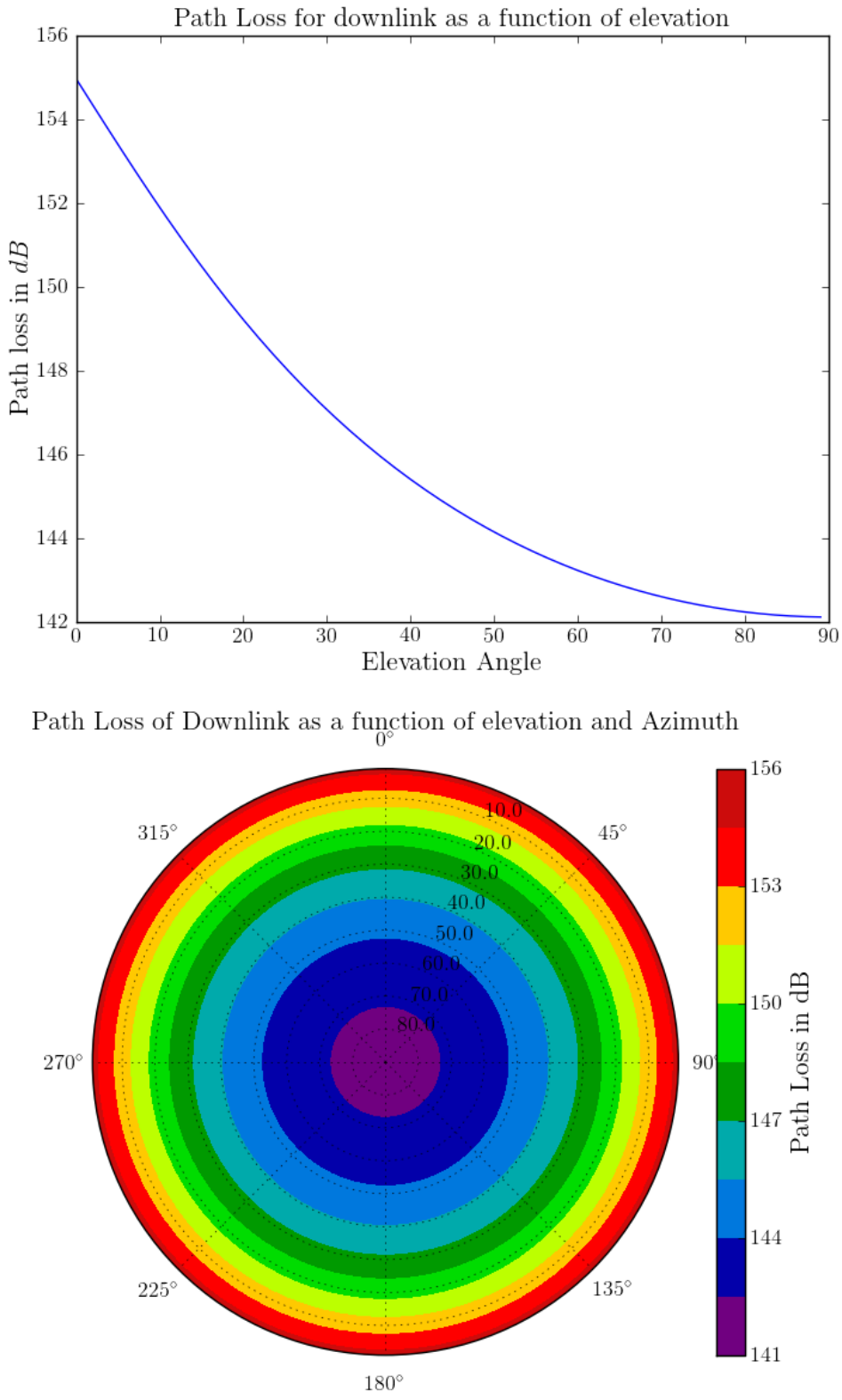

Figure 6.3.: Downlink Path Loss

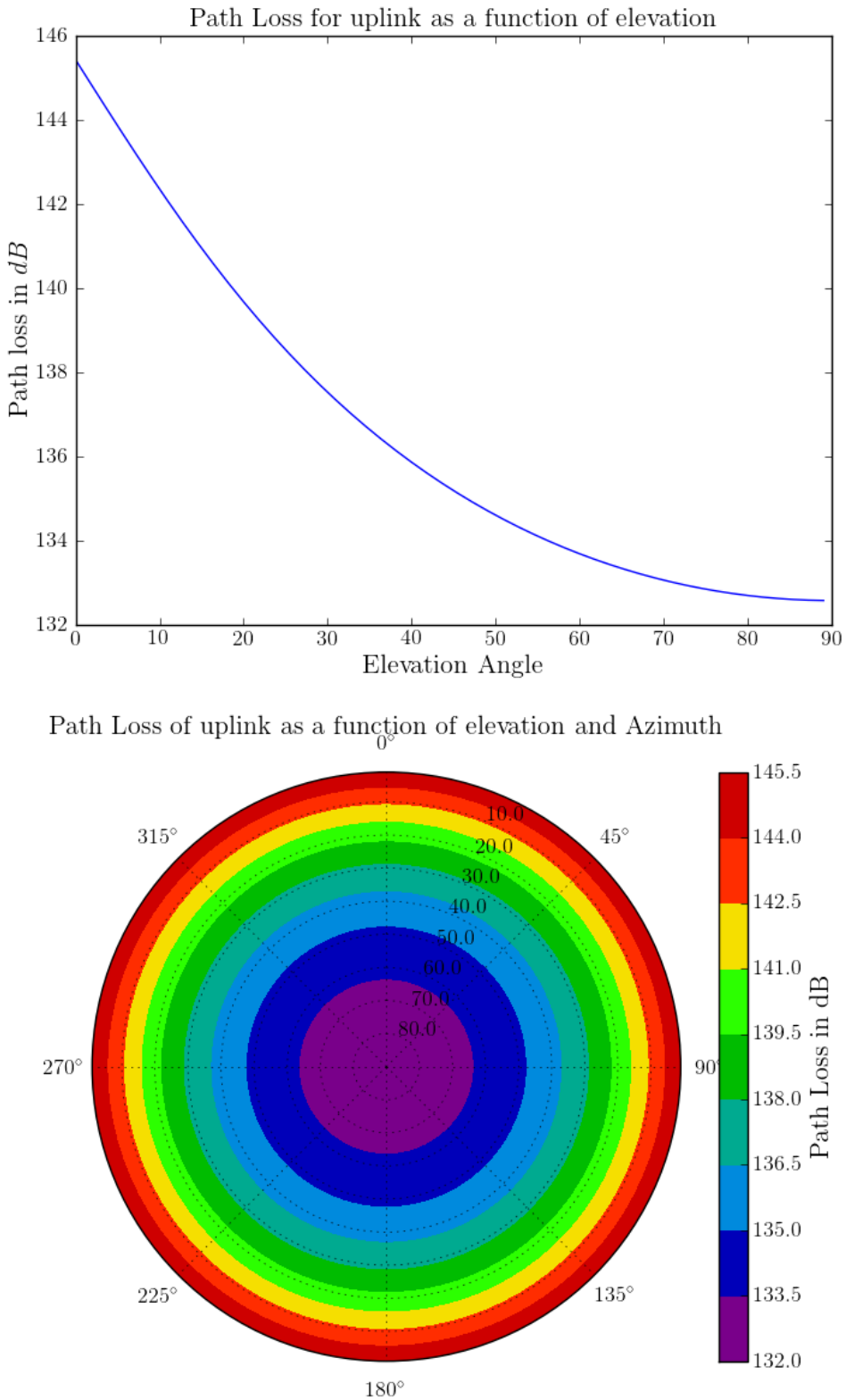

Figure 6.4.: Uplink Path Loss

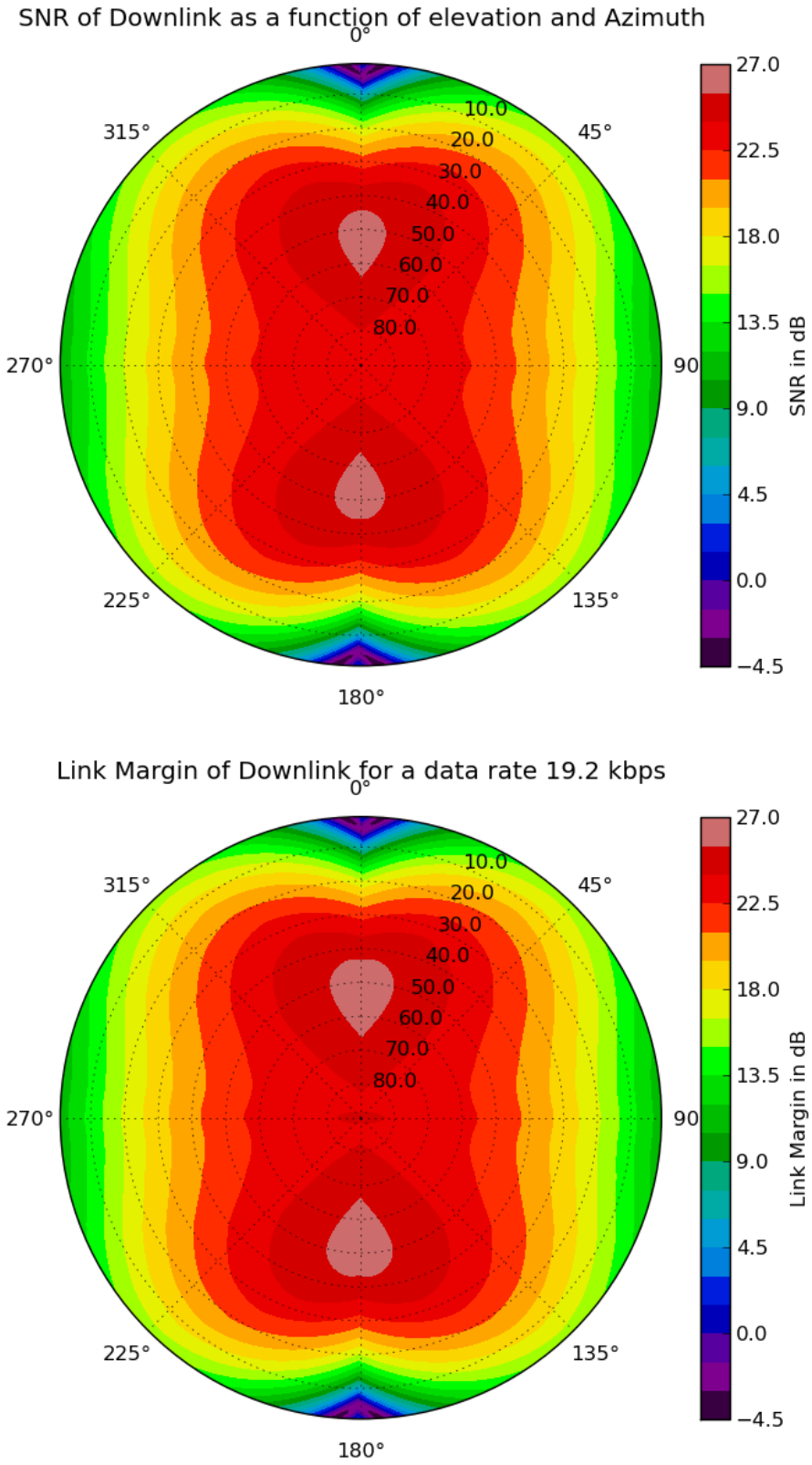

Figure 6.5.: Downlink SNR and Link Margin for the antennas designed

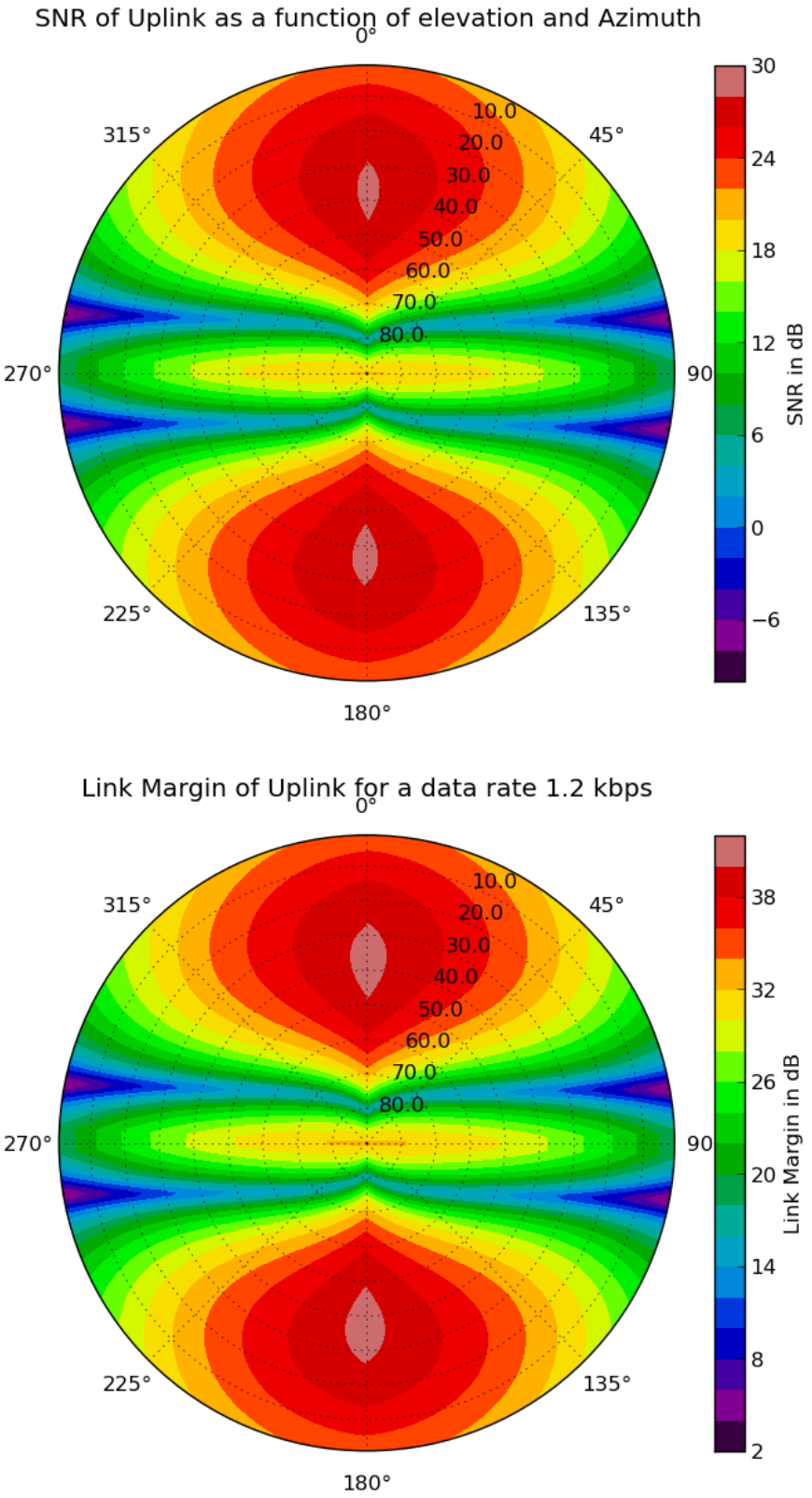

Figure 6.6.: Uplink SNR and Link Margin for the antennas designed

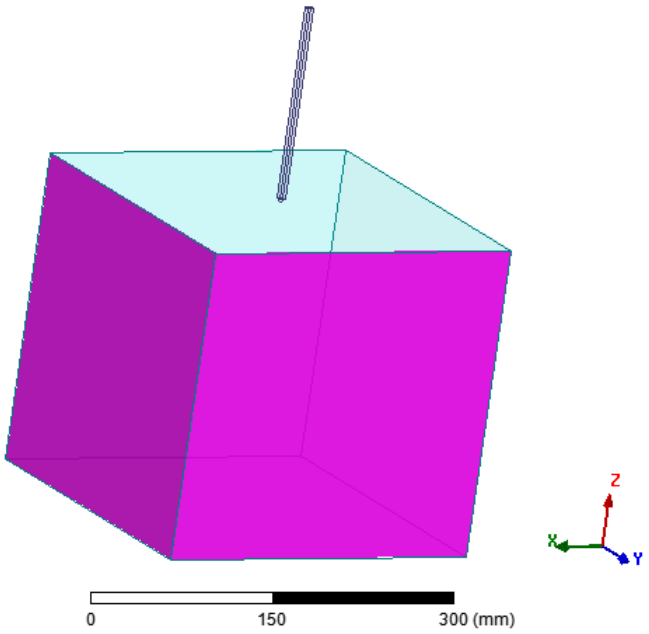

Figure 6.7.: Simple monopole on Metallic cube

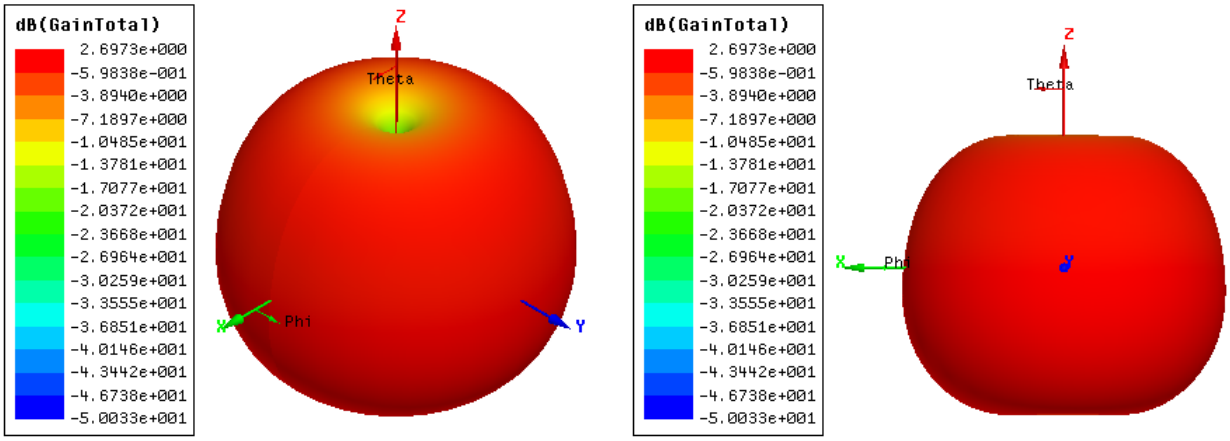

Figure 6.8.: Gain pattern of the monopole

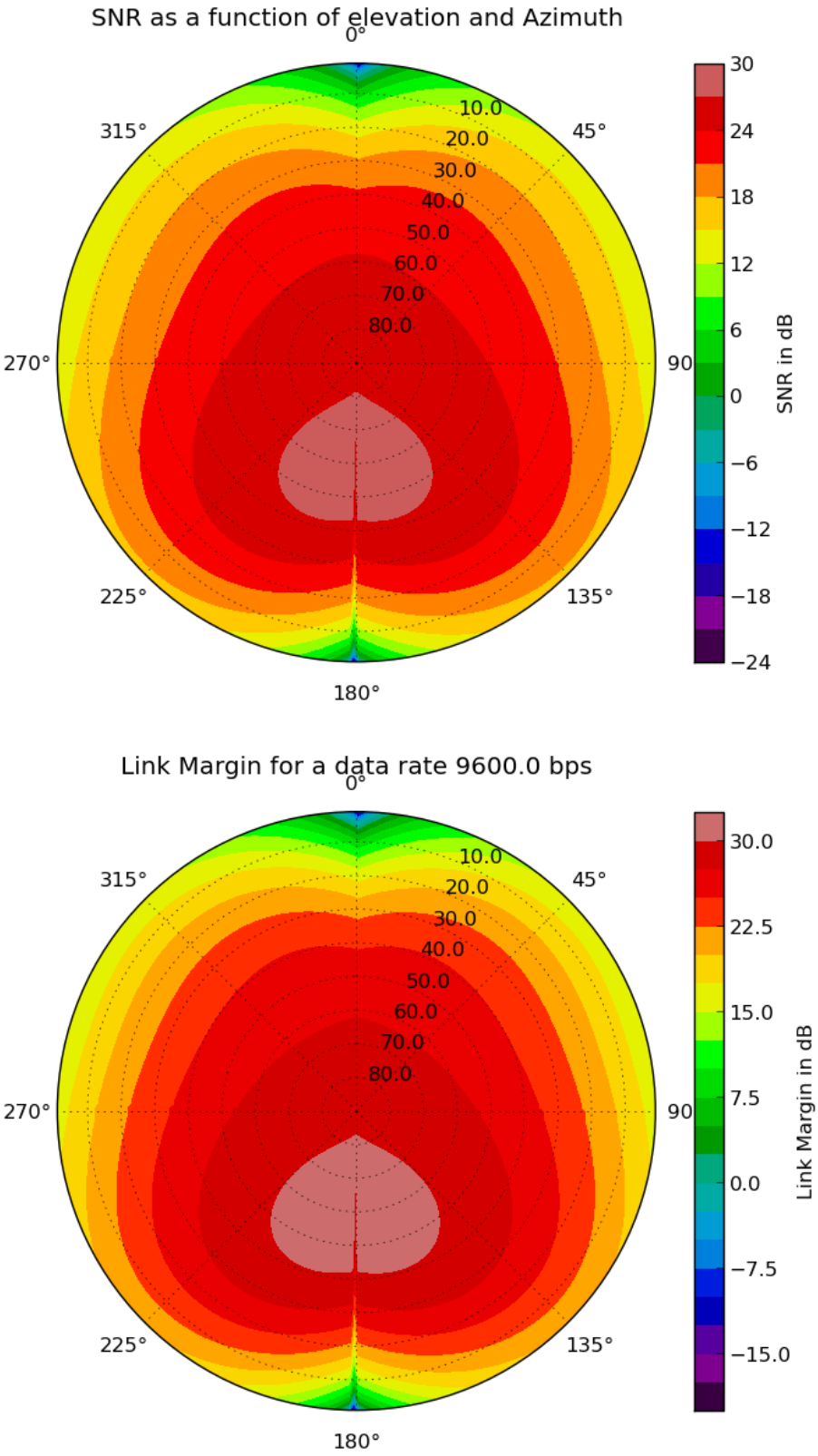

Figure 6.9.: SNR and Link Margin calculations for monopole design

Conclusion

The form factor of the onboard antennas have been reduced. This ensures mechanical stability of the structure. These antennas are rigidly bind to the structure and there is no need of any complex deploying mechanism.

The approach of treating the F-antenna has resulted in tweaking with the antenna parameters.

The receiver antenna is a novel design, which would be not possible without the simulation tools. Though the working principle of the antenna is not very clear, it characteristics are satisfactory.

The surprising aspect of the antennas is the gain pattern whose polarization characteristics are strange. To tackle this issue, Polarization Diversity System is planned in the ground station system.

The effect of the solar panels on the antenna performance has be to analysed.

A. Antenna gain pattern measurement results.

The antenna measurements were done at VSSC, Trivandrum.

The Tx antennas were fabricated with extra length (5mm), so that the antennas can be trimmed down to get the desired resonant frequency. The antenna were resonant at $422\,MHz$ and they could not be modified in time to have desired resonant frequency of $435\,MHz$, hence the gain pattern measurements were done at $422\,MHz$ for Tx antennas.

Also the Rx antenna had high return loss at $150\,MHz$ than at the desired frequency $145\,MHz$. The gain pattern measurements for Rx antennas were done for $150\,MHz$.

The plots in the following pages show the linear polarization measurements compared to that of the HFSS simulations.

The Tx gain patterns seem to match the simulation results. Offsets observed in the readings correspond to the actual offset of the structure placement on the robotic arm at the test range.

The Rx gain patterns seem unconformal with the simulation results. This may be due to the fact that at the frequency of $150\,MHz$ (wavelength of $2\,m$) the structure on which the satellite is placed comparable to the wavelength. Hence scattering may be one of the reasons for the deviation.

A.1. Tx Gain Patterns

Vertical Pol
Seaside Roll

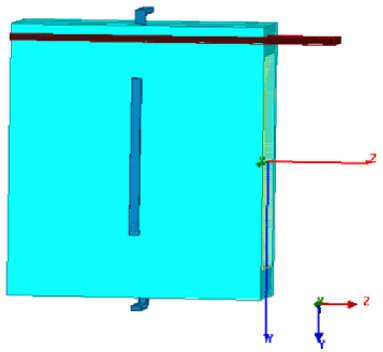

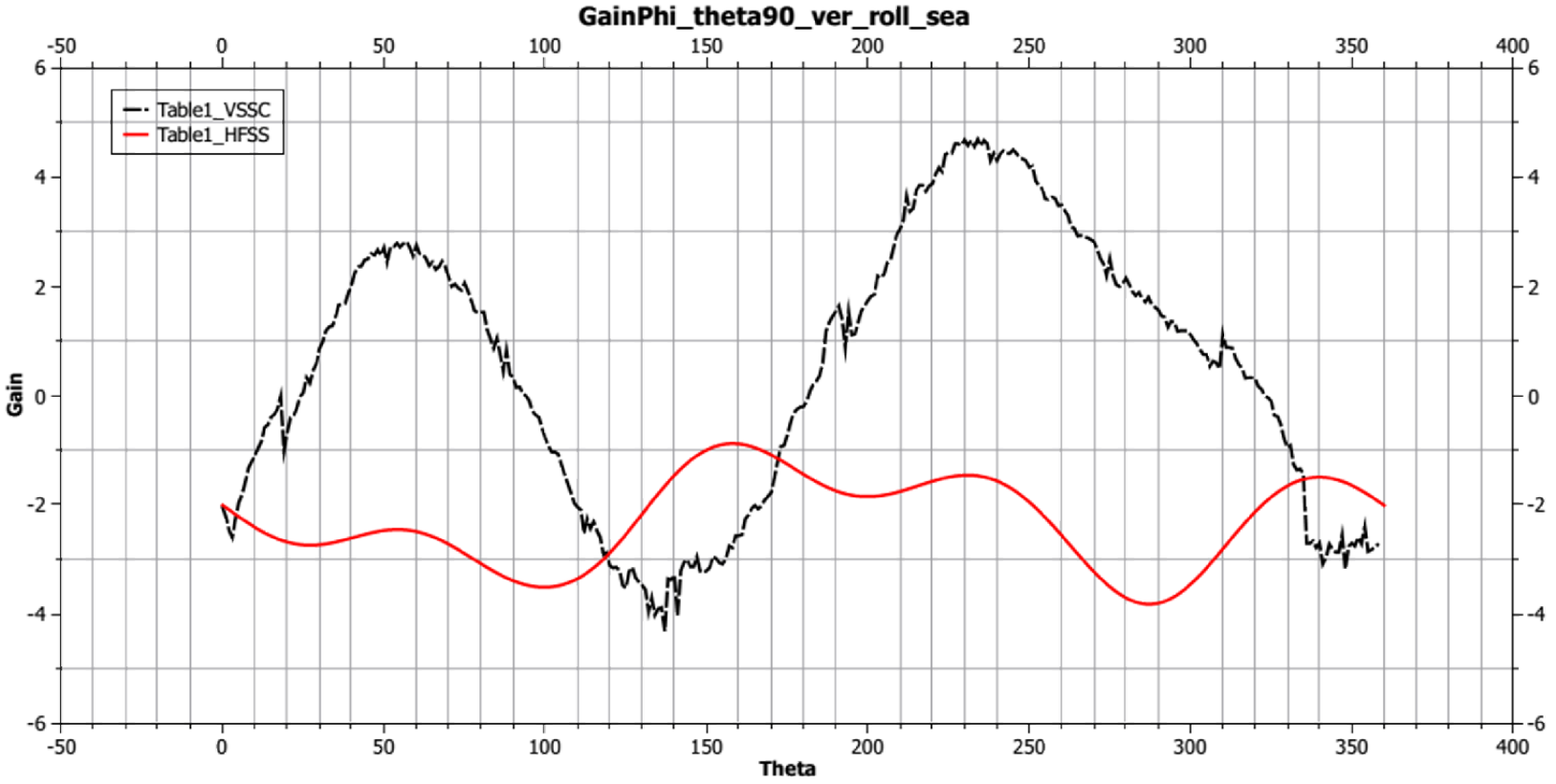

Rotate about z axis

Horizontal Pol
Seaside Roll

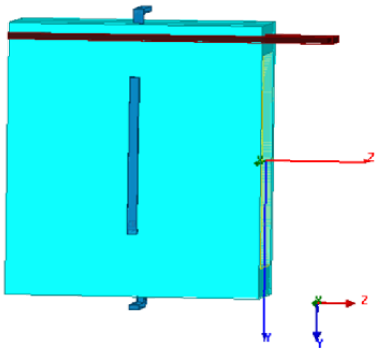

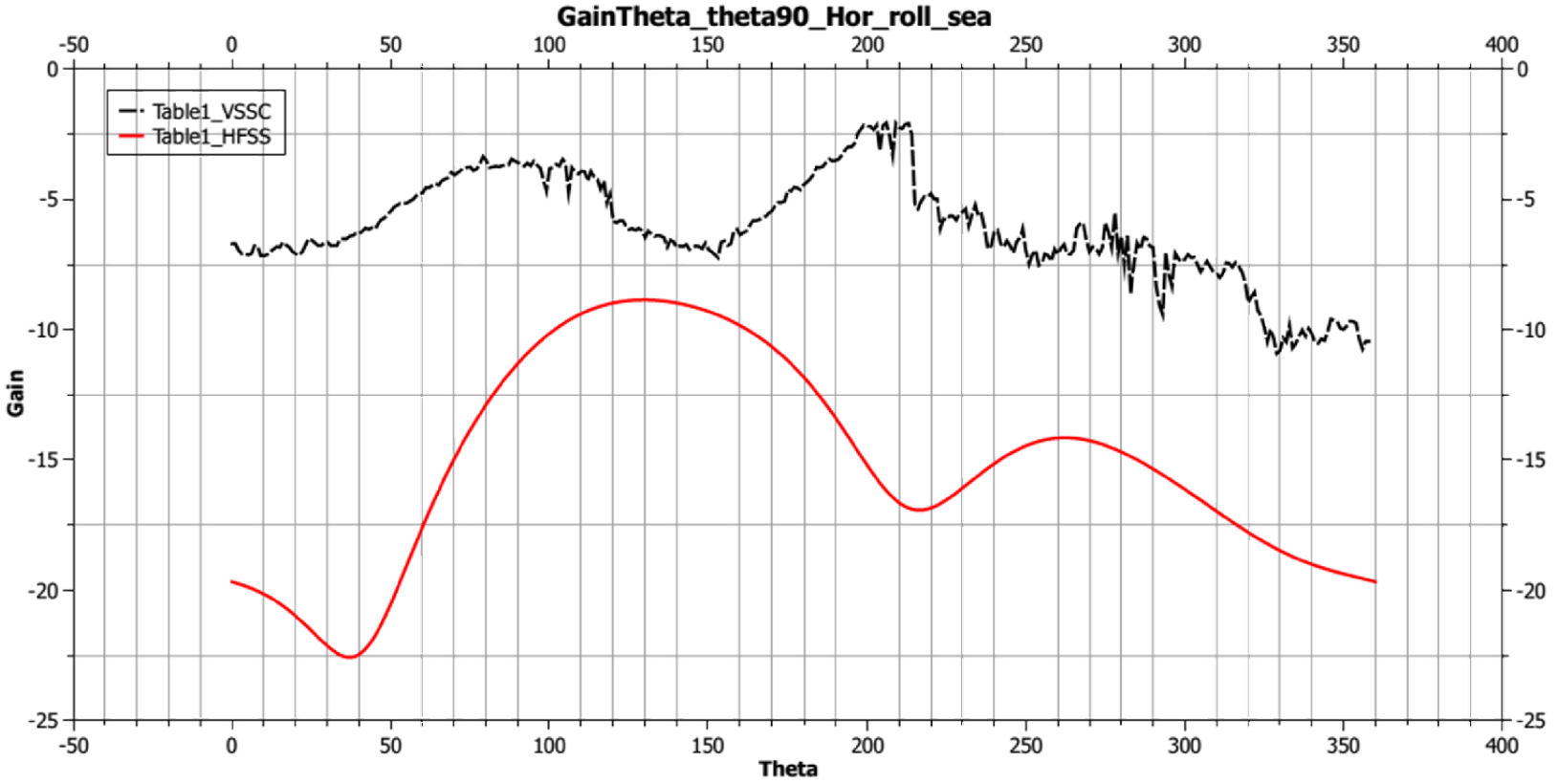

Rotate about z axis

Vertical Pol
Azimuth
Phi 0 deg

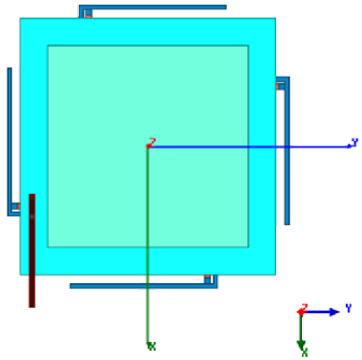

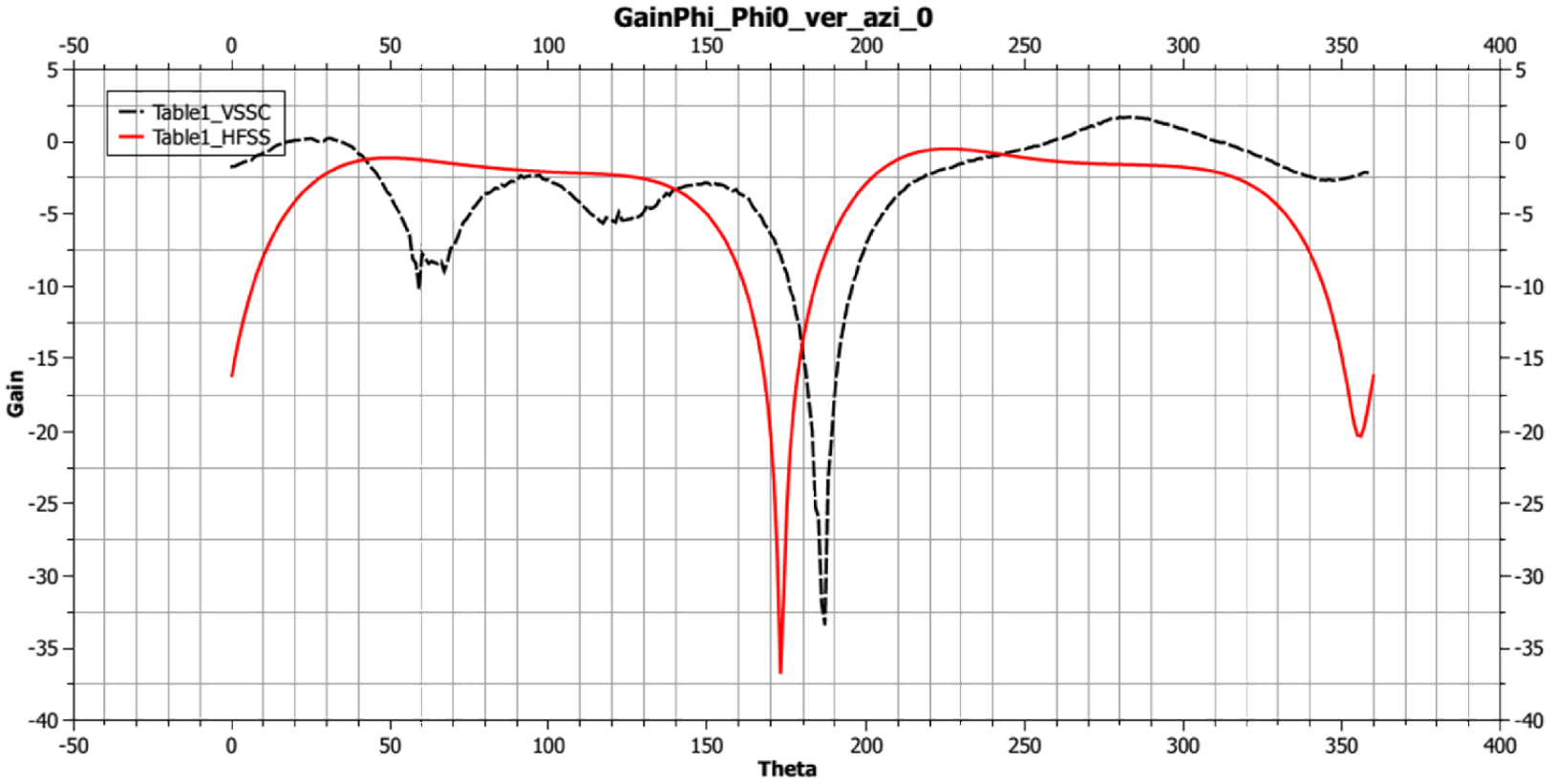

Rotate about x axis

Vertical Pol
Azimuth
Phi 90 deg

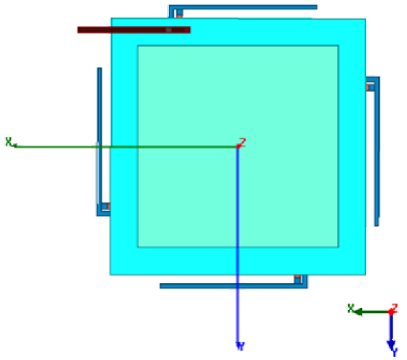

Rotate about y axis

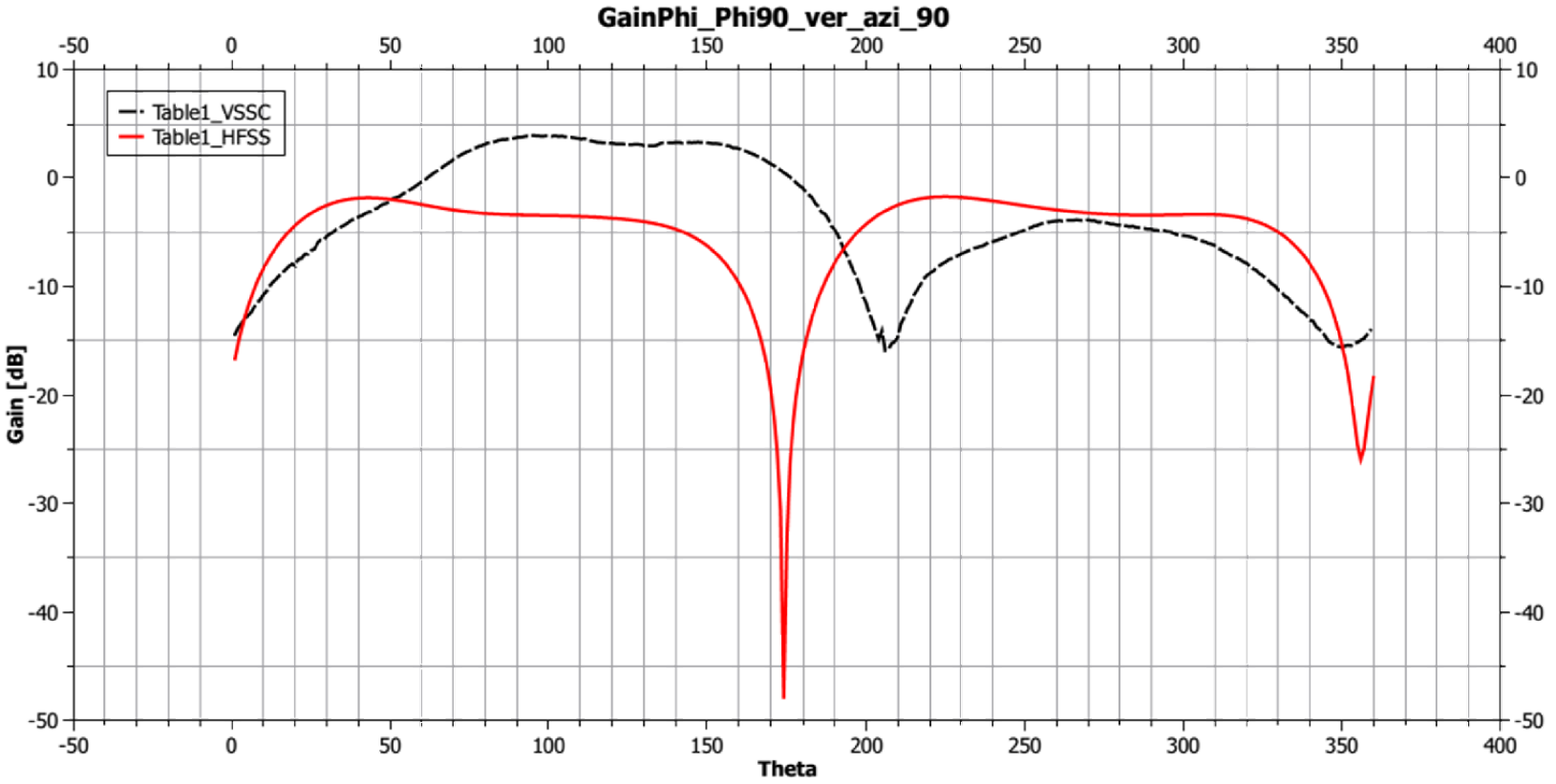

Horizontal Pol
Azimuth
Phi 0 deg

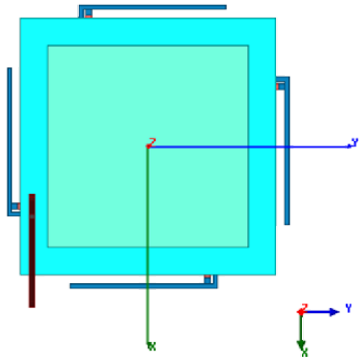

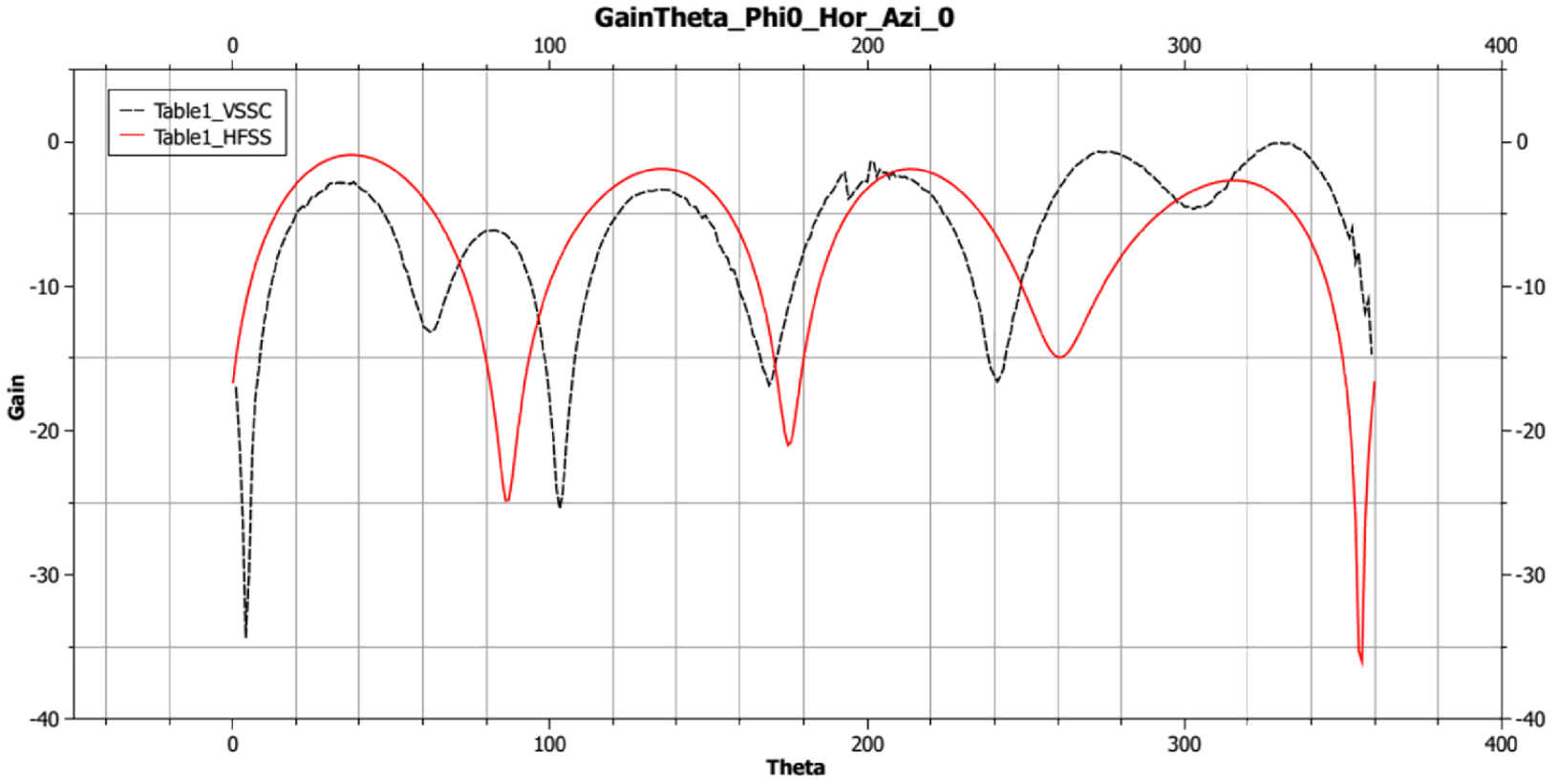

Rotate about x axis

Horizontal Pol
Azimuth
Phi 90 deg

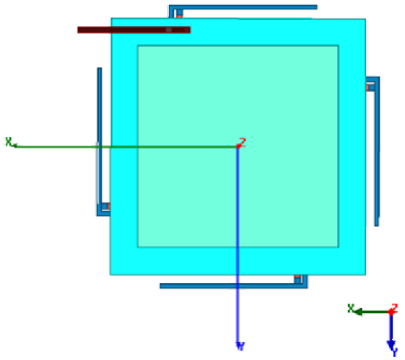

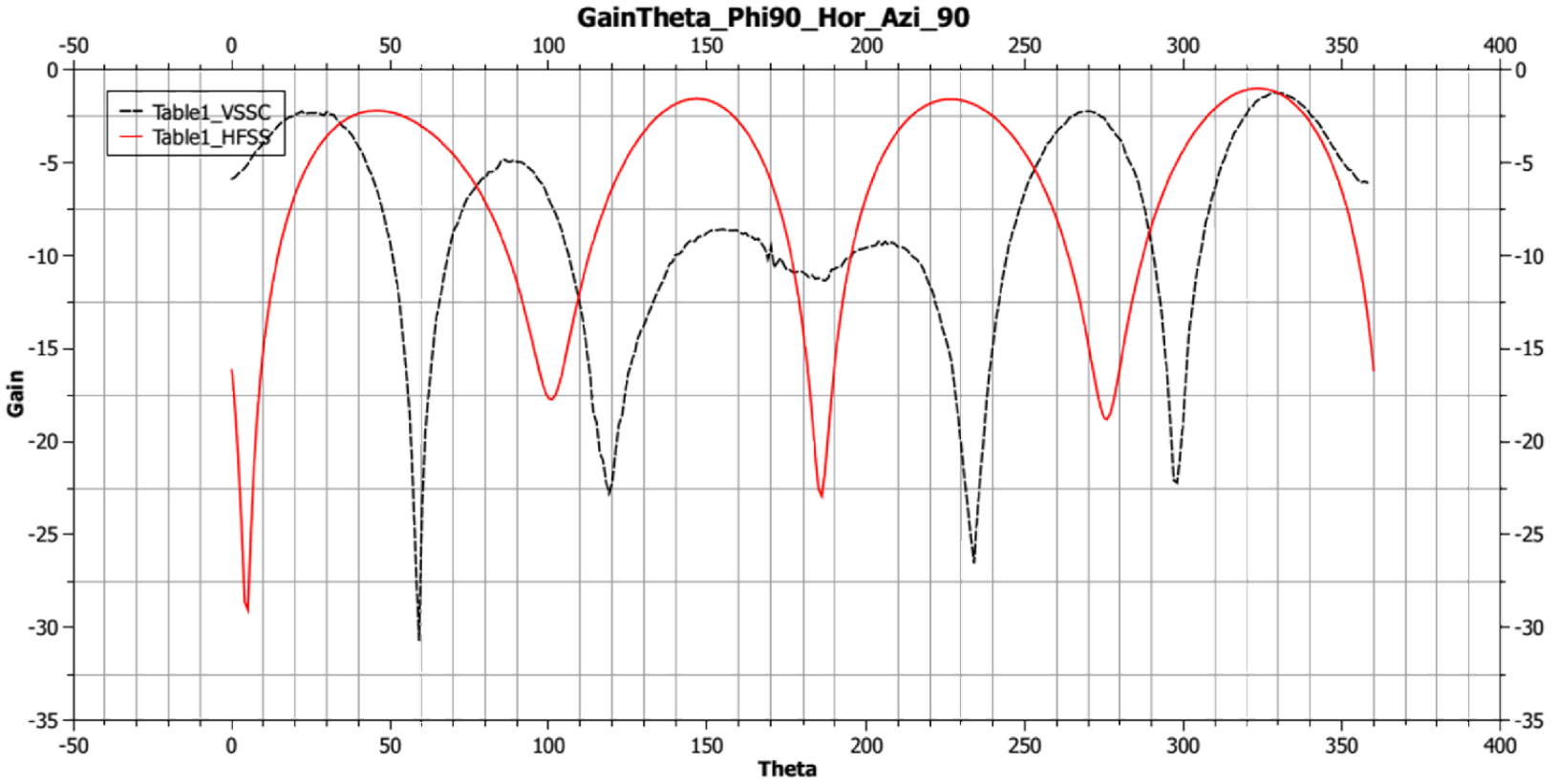

Rotate about y axis

A.2. Rx Gain Patterns

Vertical Pol
Seaside Roll

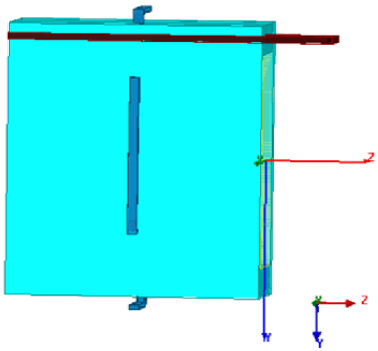

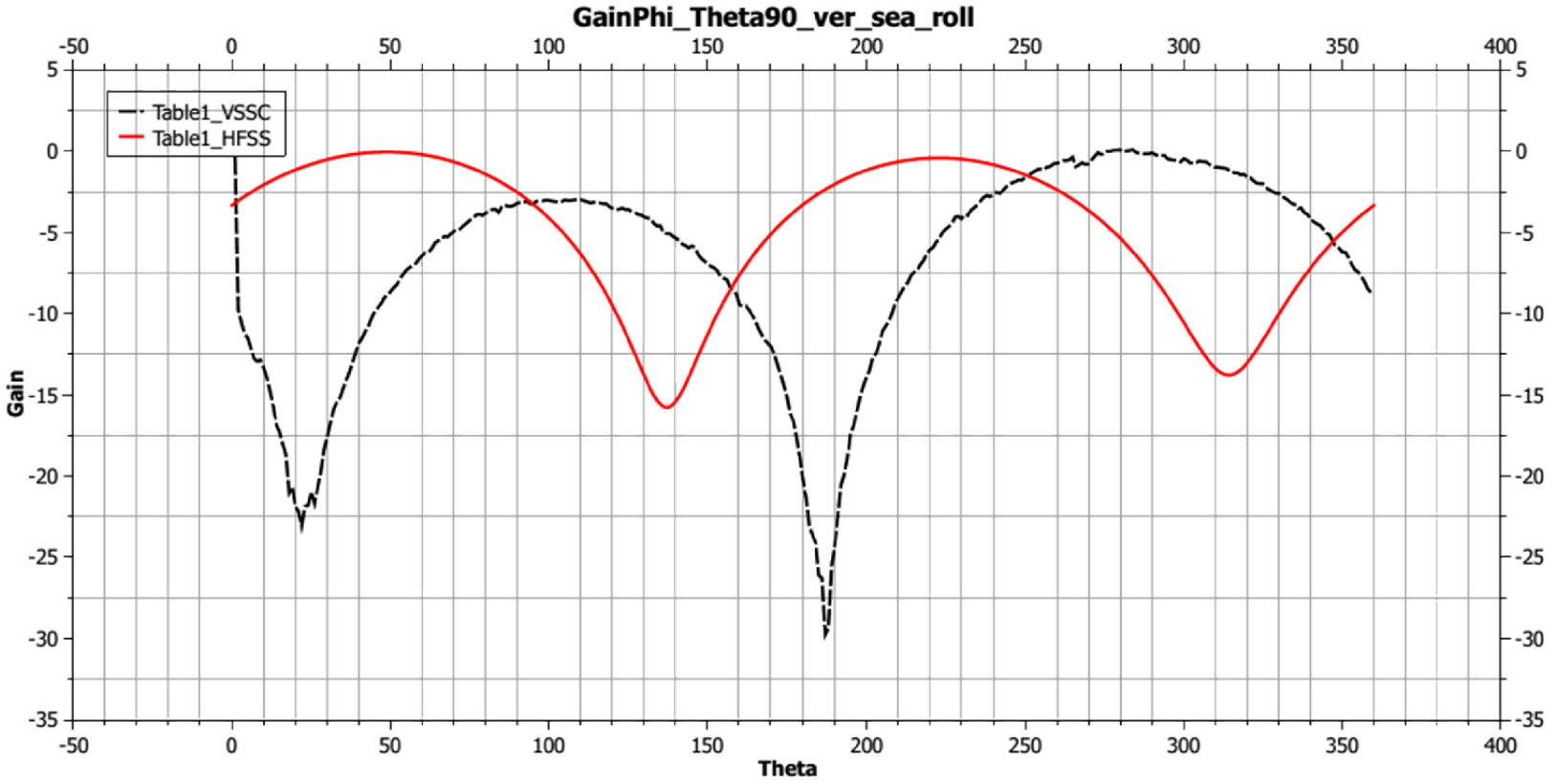

Rotate about z axis

Horizontal Pol
Seaside Roll

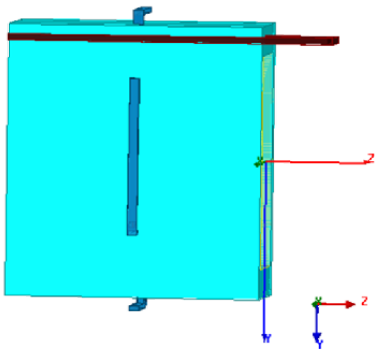

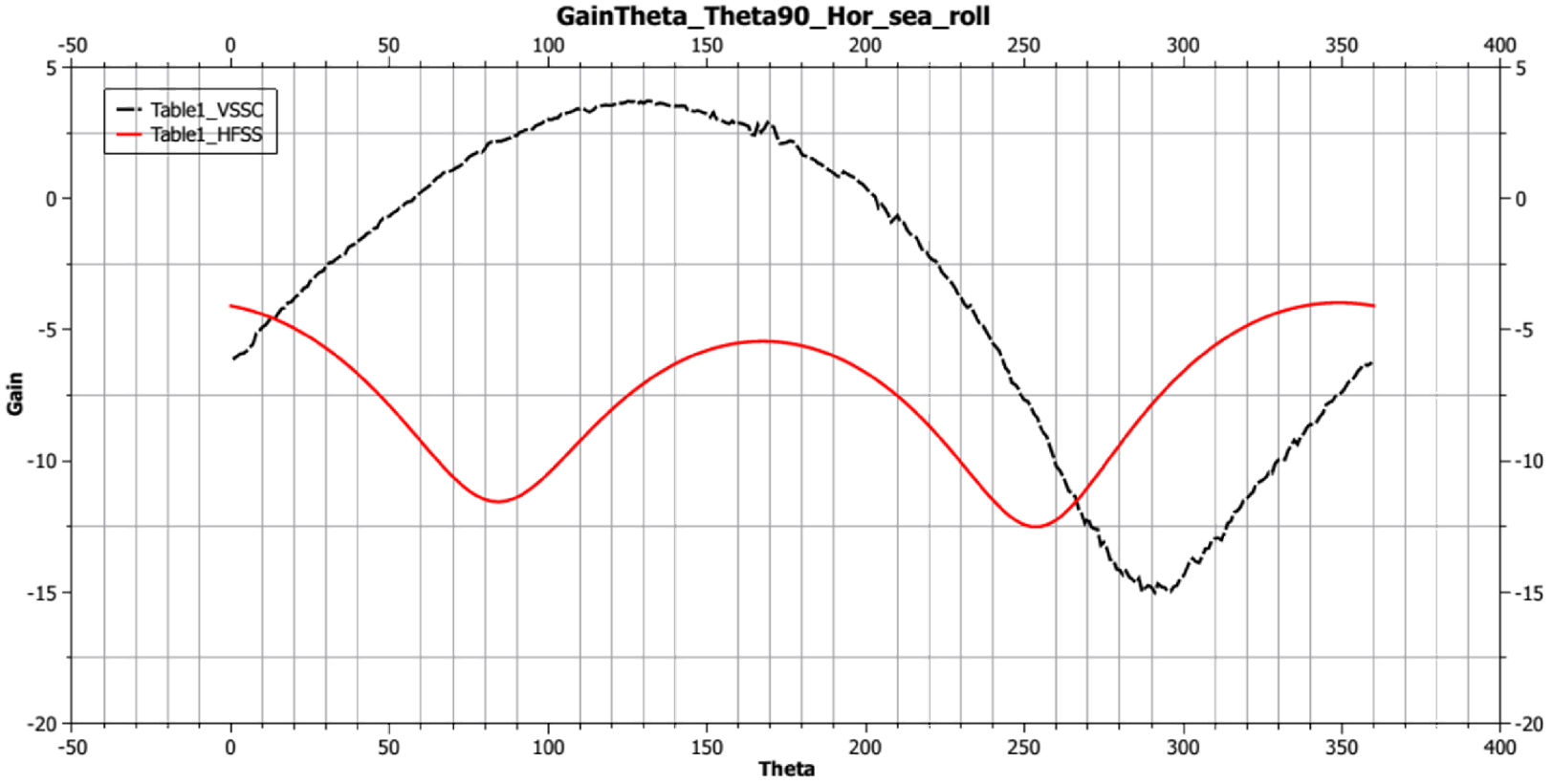

Rotate about z axis

Vertical Pol
Azimuth
Phi 0 deg

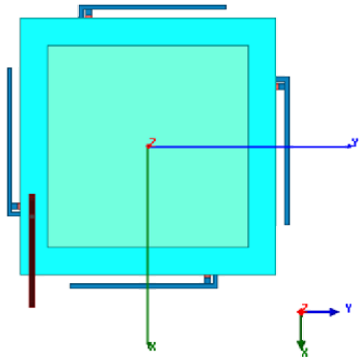

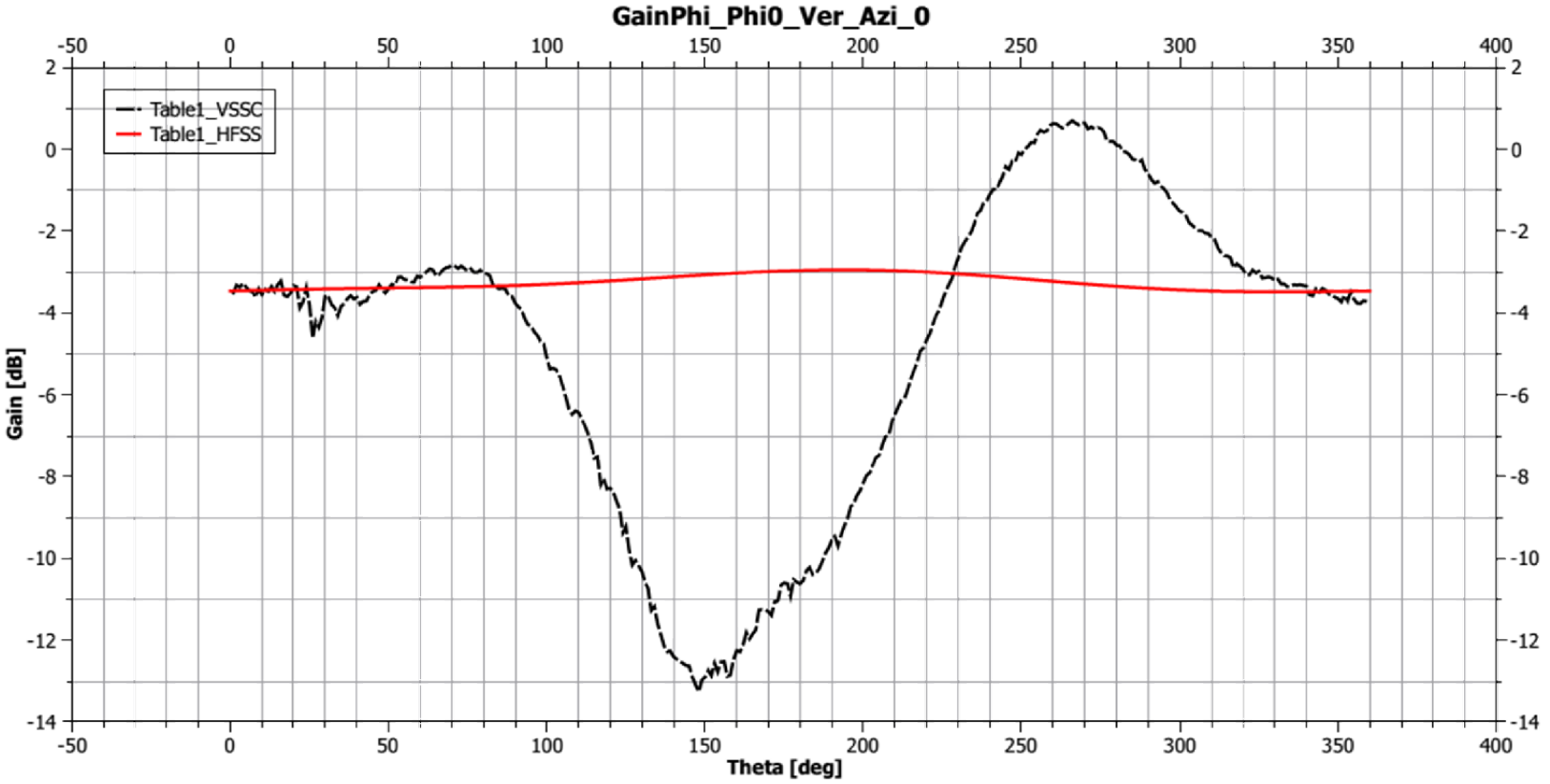

Rotate about x axis

Vertical Pol
Azimuth
Phi 90 deg

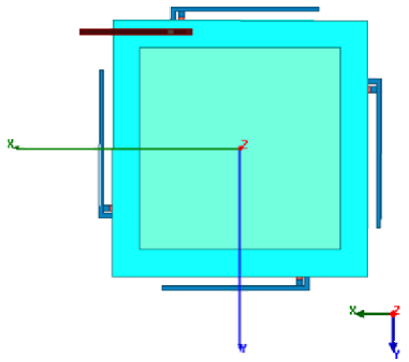

Rotate about y axis

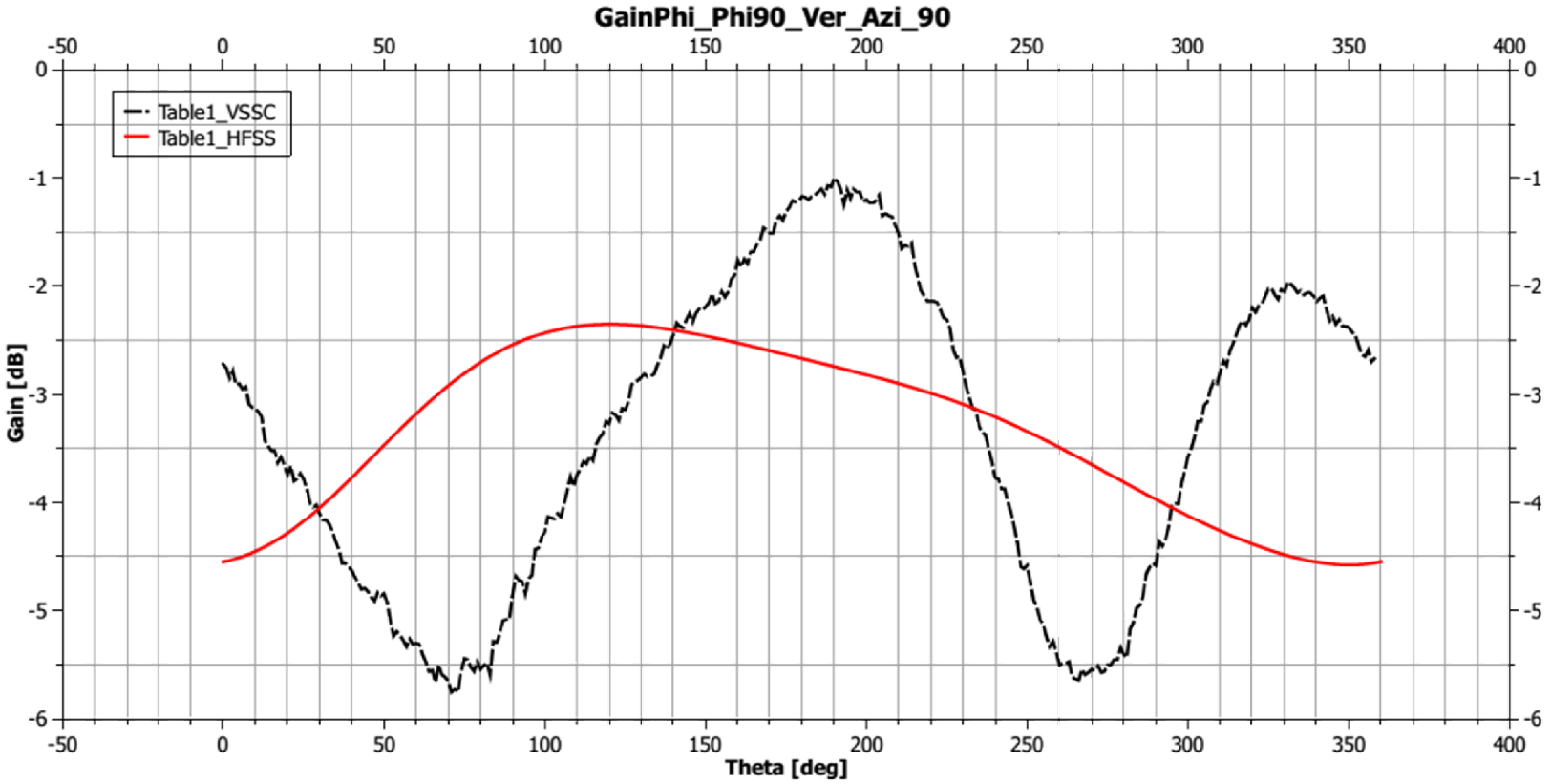

Horizontal Pol
Azimuth
Phi 0 deg

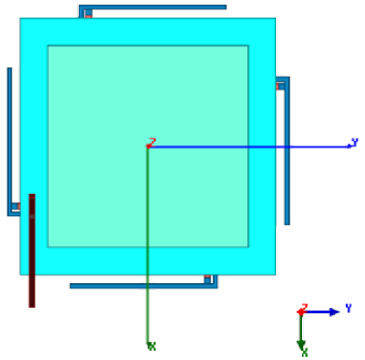

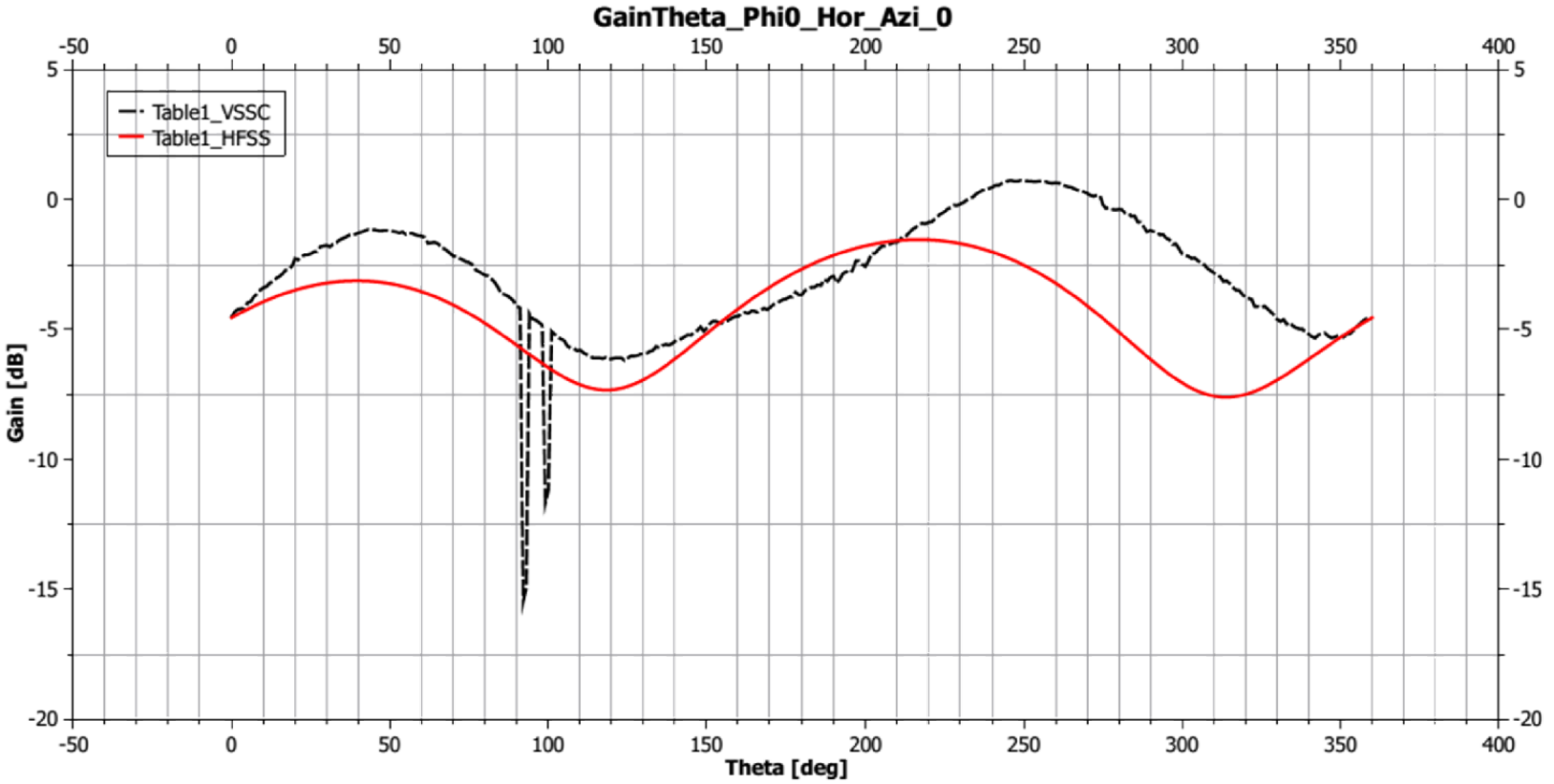

Rotate about x axis

Horizontal Pol
Azimuth
Phi 90 deg

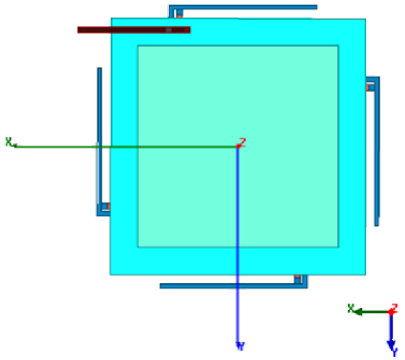

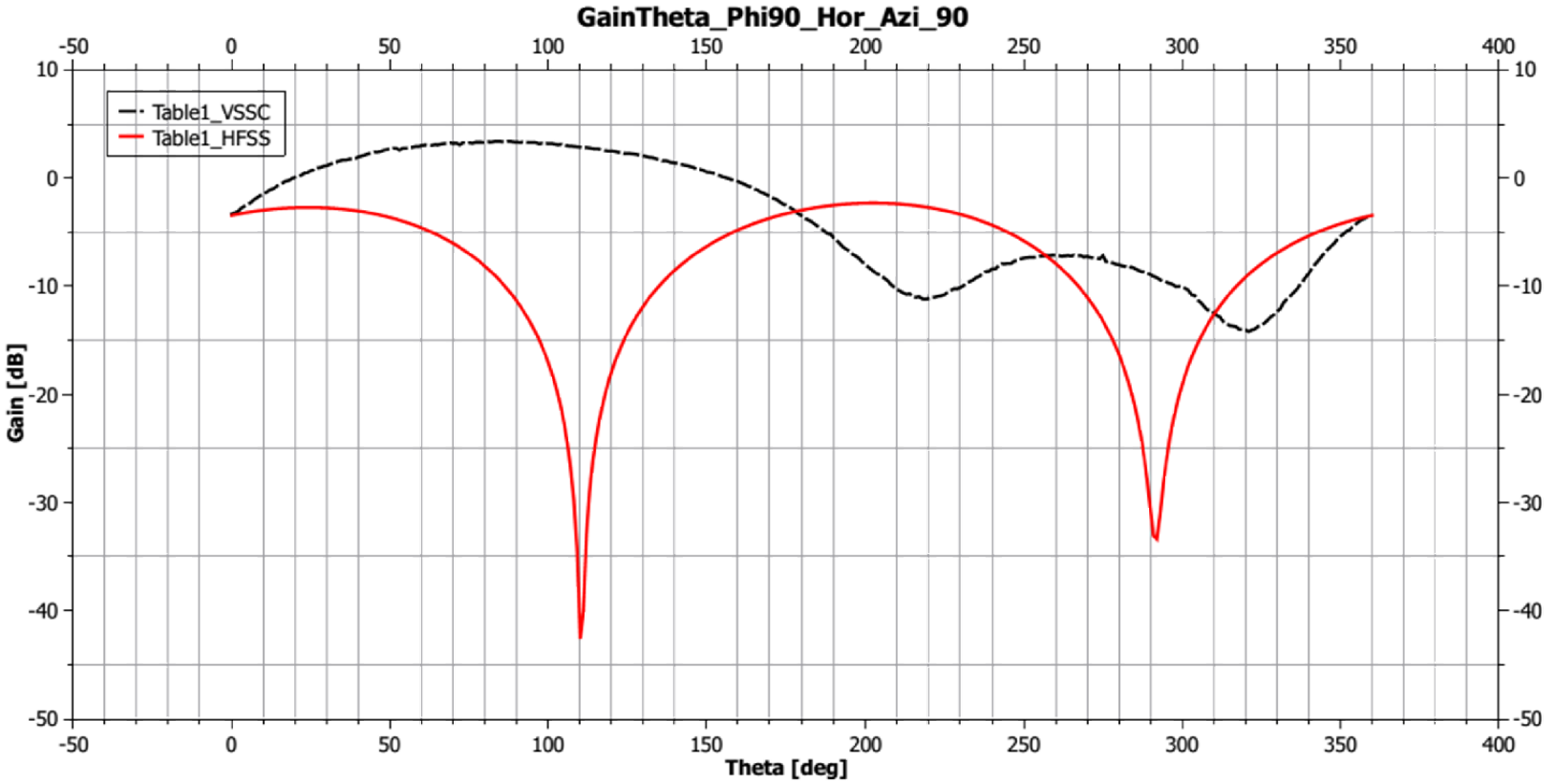

Rotate about y axis

B. CST Microwave Studio simulations

The CST microwave studio with educational license was used to simulate the antennas. These severed towards validating the results obtained in HFSS. The gain patterns for a structure with single Tx and Rx antenna compared to that of the HFSS simulation results are presented in the following figures.

- Rx_Radiation_pattern

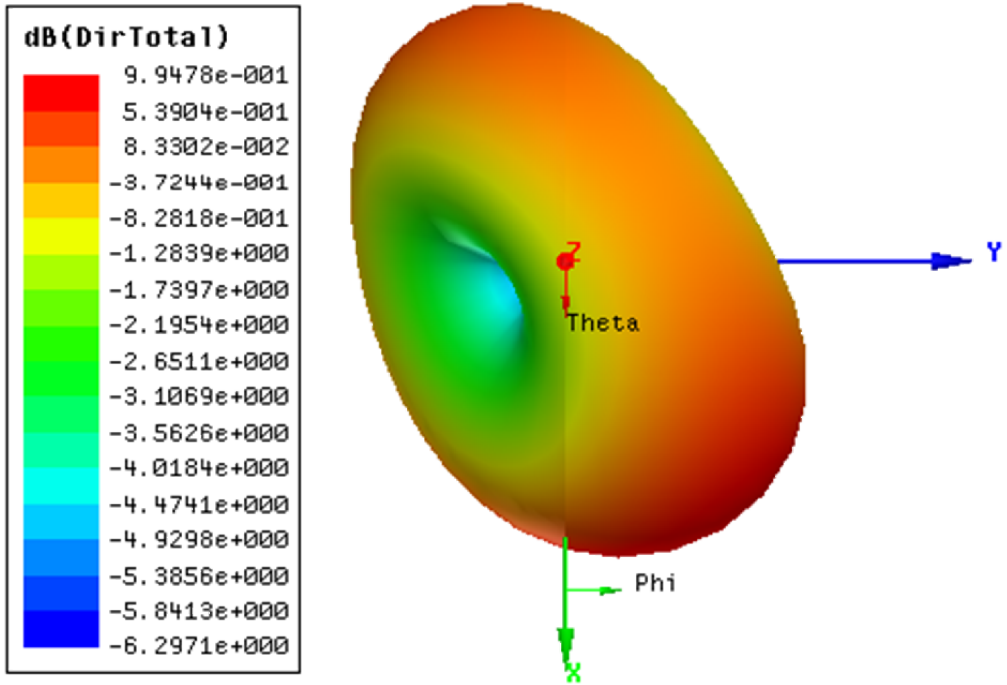

- HFSS

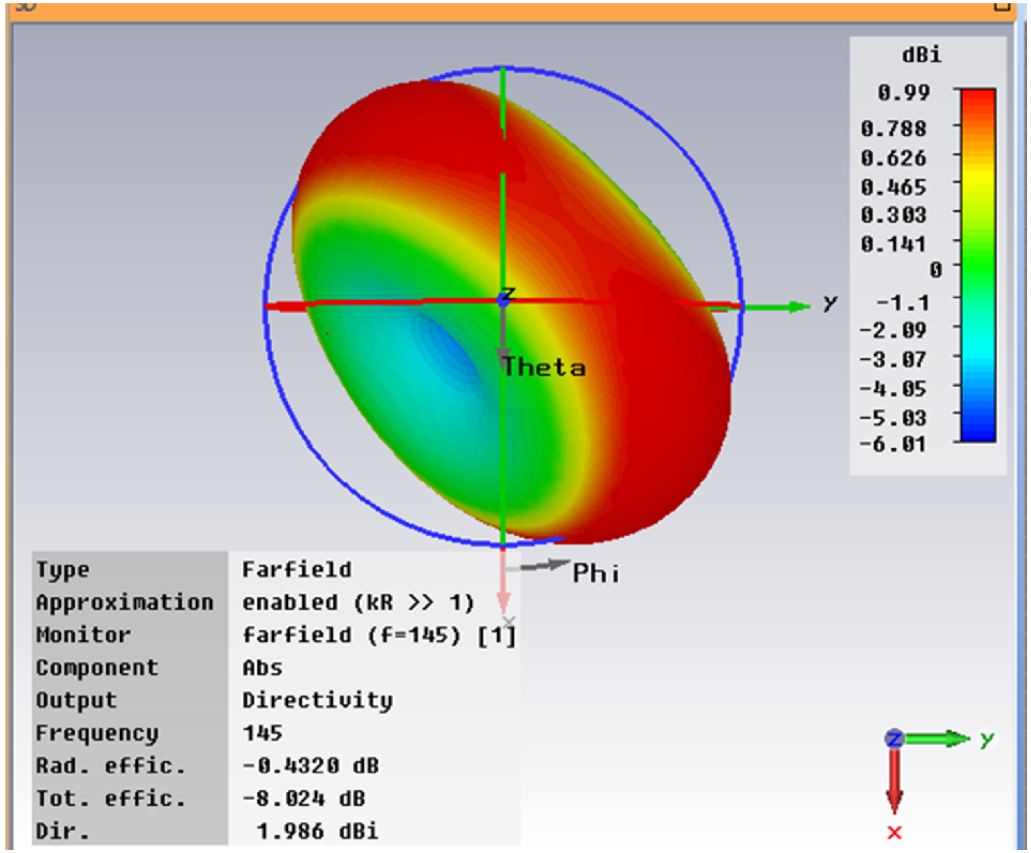

- CST

- Tx_Radiation_pattern

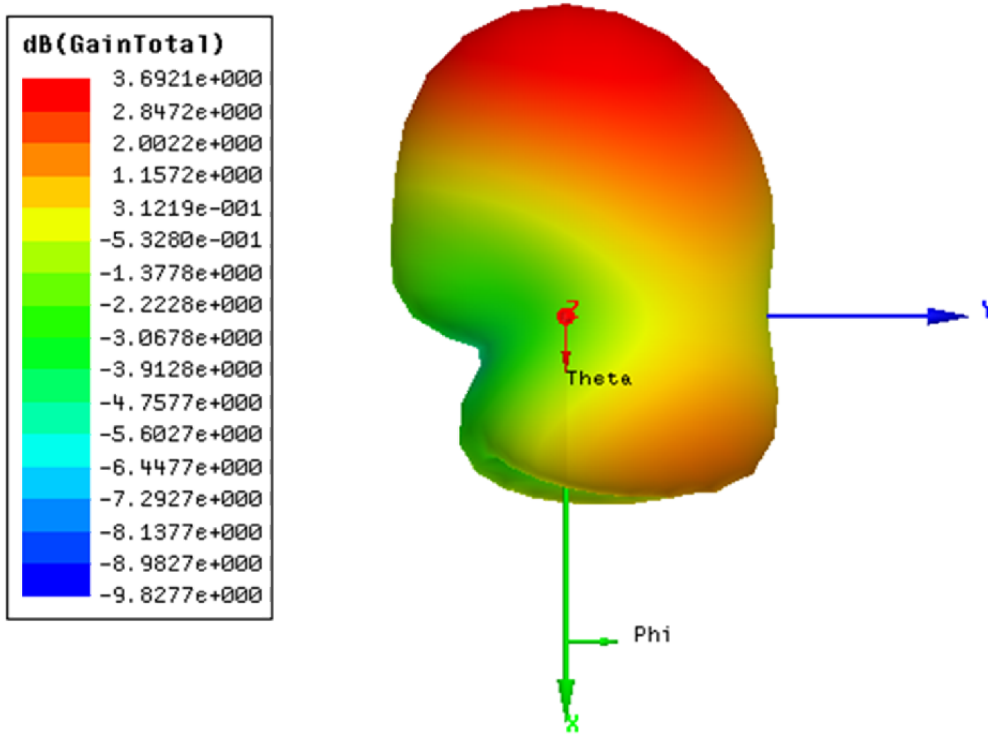

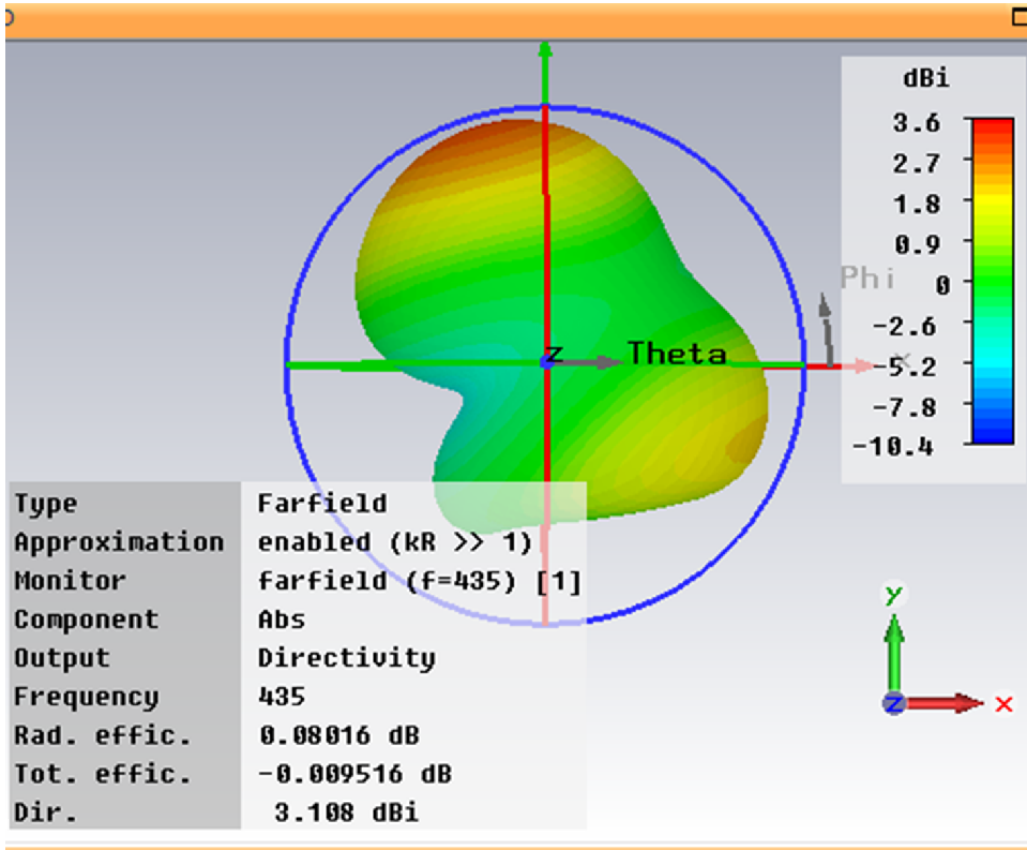

- HFSS
- CST

Bibliography

[1] S.Gao, "Antennas for modern small satellites," *IEEE Antennas and Propagation Magazine*, vol. 51, no. 4, pp. 40–56, August 2009.

[2] S. H. A. MD, "Design of iitmsat onboard antennas," Master's thesis, Dept of EE, IIT Madras, June 2013.

[3] IITMSAT, "Iit madras student satellite project." [Online]. Available: http://iitmsat.iitm.ac.in/

[4] EOPortal. Last visited Apr 2014. [Online]. Available: https://directory.eoportal.org/web/eoportal/satellite-missions

[5] H. Schrank, "Polarization loss in a link budget when using measured circular-polarization gains of antennas," *IEEE ANTENNAS AND PROPAGATION Magazine*, vol. 38, no. 1, February 1996.

[6] Ludwig chart. [Online]. Available: http://antennadesigner.org/ludwig_chart.html

[7] GOMSPACE. Uhf turnstile antenna. [Online]. Available: http://gomspace.com/index.php?p=products-ant430

[8] A. J. Vazquez-Alvarez, "Design of polarization diversity system for ground stations of cubesat space systems," *IEEE ANTENNAS AND WIRELESS PROPAGATION LETTERS*, vol. 11, pp. 917–920, 2012.

[9] H. A. Wheeler, "Transmission-line properties of a strip on a dielectric sheet on a plane," *IEEE Trans. Microwave Theory Tech*, vol. MTT-25, p. No.8, 1977.

[10] R. Bancroft, *Microstrip and Printed Antenna Design.* Scitech Publishing, Inc., 2009.

[11] AGILENT, "Antenna measurement theory." [Online]. Available: http://www.home.agilent.com/upload/cmc_upload/All/?&cc=IN&lc=eng

[12] MILLITECH, "Wave calculator suite." [Online]. Available: http://www.millitech.com/Calculators.htm

[13] A. S. Committee, *IEEE Standard Test Procedures for Antennas*, IEEE Std. IEEE Std 149-1979, Rev. 2008.

[14] K. Voormansik, "Satellite signal strength measurements with the international space university ground station and the university of tartu ground station," Master's thesis, UNIVERSITY OF TARTU Faculty of Science and Technology Institute of Physics, 2009.

[15] Z. J. Leffke, "Distributed ground station network for cubesat communications," Master's thesis, Virginia Polytechnic Institute and State University, 2013.

[16] D. L. J. Ippolito, *Propagation Effects Handbook for Satellite Systems Design, Section 2.* Stanford Telecom, 1999.

[17] T.-L.-E. Data. [Online]. Available: http://www.celestrak.com/NORAD/elements/

[18] M. Antennas. [Online]. Available: http://www.m2inc.com/index.php?ax=amateur&pg=107

[19] J. M. MEVADA, "Design and implementation of communication subsystem for leo satellites," Master's thesis, DEPT of EE, INDIAN INSTITUTE OF TECHNOLOGY MADRAS.

[20] P. E. Thoppay, "Design of rf system for cubesat," EPFL - SWISSCUBE, Tech. Rep. [Online]. Available: http://ctsgepc7.epfl.ch/07%20-%20Telecommunications/

[21] GPredict. [Online]. Available: http://gpredict.oz9aec.net/

Nomenclature

ACS	Attitude Control System
AUT	Antenna Under Test
CDMS	Command and Data Management System
COM	Communication Subsystem
EPS	Electrical Power System
LEO	Low Earth Orbit
PIFAs	Printed Inverted-F-shaped Antennas
SAM	Structure and Mechanisms
SPEED	Space based Proton and Electron Energy Detector
TCS	Thermal Control System.
VNA	Vector Network Analyzer
VSSC	Vikram Sarabhai Space Center